IKE Institut für Kernenergetik
und Energiesysteme

Modelling of Fast Neutron Transients in an Accelerator Driven System

Cristian Rabiti

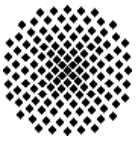

Universität Stuttgart

IKE 6-202

MODELLING OF FAST NEUTRON TRANSIENTS IN AN ACCELERATOR DRIVEN SYSTEM

Von der Fakultät für Maschinenbau der Universität Stuttgart zur

Erlangung der Würde eines

Doktor-Ingenieurs (Dr.-Ing.) genehmigte Abhandlung

vorgelegt von

Cristian Rabiti

aus Forlì (FC), Italien

Hauptberichter: Prof. G. Lohnert, Ph. D.

Mitberichter: Frau Prof. Dr. rer. nat. B. Wohlmuth

Tag der mündlichen Prüfung: 10. November 2006

Institut für Kernenergetik und Energiesysteme der Universität Stuttgart

2007

Acknowledgment

The number of people I wish to thank is very large. This tells me that I was fortunate in my professional life to meet such good people. I wish to start with my thesis from which everything has originated which significant credit is due to Dr. Richard Sanchez. From my discussions with him I attribute my passion for applied mathematics in the field of neutron transport where by I would not be at this point, thus I thank Dr. Sanchez.
After my graduation, I took a doctoral position in Germany. In Germany I met with Dr. Werner Maschek who believed in me and accepted me in his team. Sometimes I think that he still estimates me more than I do and even if I am not for sure the best worker: forgetting meetings, being late at deadlines is one of my specialties, his door was always open for any help and suggestions: thanks Werner.
Now it comes the time of the person that, of course after me, has the greatest responsibility in this thesis: Dr. Andrei Rineiski. He has made the choice of the subject and he lead me during these three years by means of long discussions, I believe that not a day passed without I knocked at his door, may be just to say everything is going on. But this is not the place only for technical thanks therefore a special thank to Andrei because he was always able to bring me back to calm when the code was not running and I got no other explanation that some kind of evil magic.
There is another unforgettable person: Dr. Edgar Kiefhaber; first of all I should apologize to him about not having been able to read all the articles and references he gave me. Discussing with him was always a pleasure and not only about work but also about historical aspects of nuclear technology. Thanks also for having spent so much time correcting my presentations and papers, I believe that when I would have finished he would have felt eased too, forgive me again and thank Edgar.
Now, even when I was always speaking about how it is possible to divide the 'world' in even and odd functions but only in time scales with so many zeros after the comma that a normal engineer would laugh about, one person in Stuttgart decided that I could get a Ph.D. in mechanical engineering anyway. Thanks Professor Günter Lohnert: it was a pleasure being one of your students. I have to say that I always appreciated your comments. I got the feeling that every paper approved by you was a step towards the final goal and this was for me important.
I want to thank all the 'Partition and transmutation' team at Forschungszentrum Karlsruhe. It, was a lovely place where to work, I felt well with you all; you helped me with the German language (especially Claudia), and also how to forget the smoker community: no one is without if someone has some.
Thanks also to Dr. Thomas Schulenberg, director of the Institute for Nuclear and Energy Technologies, and to the Forschungszentrum Karlsruhe for offering me the opportunity of performing this thesis work.
I wish to thank also Dr. Michael A. Smith who helped me reviewing this work especially the English correctness.
There is a person that followed me since a long time. When we met for the first time, neutrons were not yet in my life, but she followed me when ever possible, and allowed me to go around in Europe for my job and passion. I cannot imagine a better support for me and I know that it was not always easy at all sharing me with my work. Thanks Anna, you have a great part.
There is also a lady that probably is still wondering if she has done a good job growing me up, for the moment it seems yes even if it means that I am always far from her and she misses me; thanks for all, dear mother.
Now I have to carry out a reverential duty that I'm glad to be able to fulfill: this thesis is dedicated to my father that I lost too early but he is of course part of me.

CONTENTS

Abstract

There are several alternatives under consideration for energy production aiming at reducing the dependence upon oil, coal, and natural gas. The underlying goal of course is a future in which oil, coal, and natural gas will play a far less important role in energy supply. One such alternative is nuclear energy derived from nuclear fission. This power source, similar to oil, coal, and natural gas is backed up by years of engineering experience. Increasing its role should increase its public acceptance, especially in Europe, where its use is strongly under discussion. The key factor that will decide the role of nuclear power in the future lies in the proof of a safe way to handle nuclear waste. For this reason, several alternative approaches for treating nuclear waste have been proposed and are investigated. Every idea proposed is, of course, a trade off between the public acceptance, costs, and technological capabilities. One of the most challenging approaches, from the technological point of view, is the strategy based on burning the most dangerous part of nuclear waste in dedicated reactors such as the one studied in this work. This alternative introduces a new class of reactor behavior which needs to be carefully studied. The analysis work inevitably relies upon high precision simulation using numerical codes. This thesis is primarily focused upon the simulation of transients in the neutron density of the reactor resulting from transients of the amplitude of an external neutron source. The VARIANT-KIN3D was used as the starting point of this thesis work. VARIANT is a code that solves the steady state neutron transport equation using a hybrid finite element method coupled with an even-parity spherical harmonics approximation. KIN3D simulates the time-dependence of the reactor system by transforming the time dependent problem into a set of pseudo steady state ones. The KIN3D code can therefore make use of the steady state VARIANT solutions to model the reactor behavior in time. In order to transform the time dependent problem into a set of steady state ones, a time discretization scheme is needed. It is in this thesis, that the time discretization scheme has been strongly improved, thereby overcoming many of the preceding difficulties encountered when coupling the KIN3D and VARIANT codes. The first newly introduced time integration scheme is a first order backward Euler method combined with a reduction scheme. This first new discretization scheme has been validated against an analytic benchmark showing its accuracy and robustness. Several others tests have shown that its feasibility in application to realistic problems appears unlikely due to its high computational cost. This difficulty has been successfully overcome by introducing an adaptive time step control scheme. This variable time step approach was implemented only after considerable analytic analysis of the influence of such a feature on the order of precision achieved by the time integration scheme. In this work it is proven that the adoption of variable time step requires an increase in the order of the Euler scheme to avoid a loss of the structure of the equations in their time discrete form. The final scheme implemented in this thesis is a non linear second order mixed backward-centered Euler combined with a reduction scheme. Several benchmark problems have been solved using both of the two new schemes in order to compare the differences with the previous approach and to investigate the influence of the discretization of the angular variable on the time spatial behavior of the neutron density. The coupling between VARIANT and KIN3D based upon these new time discretization schemes has been implemented for all the spatial (XYZ, HEX-Z) and angular discretizations available inside the VARIANT code. The final version of the VARIANT-KIN3D code is a very powerful tool which can be used for the analysis of all types of transients that occur in a nuclear reactor. The specific achievement is the capability to deal with very difficult ones such as the short time scale transients induced by an external source and with others transients that occur on much longer time scales. This great flexibility was achieved without requiring a substantial increase in the computation time.

Kurzfassung

Zur Verminderung der Abhängigkeit von fossilen Brennstoffen wie Öl, Kohle und Erdgas werden verschiedene Alternativen zur Energieerzeugung betrachtet. Das Hauptziel ist natürlich eine Zukunft, in der die fossilen Brennstoffe eine wesentlich geringere Rolle bei der Energiebereitstellung spielen werden. Eine der Alternativen ist die Kernenergie aus der Kernspaltung. Ähnlich wie bei den fossilen Brennstoffen kann diese Energiequelle auf langjährige Betriebserfahrungen zurückgreifen. Ein Anwachsen Ihrer Rolle sollte auch zu einer erhöhten Akzeptanz in der Öffentlichkeit führen, speziell in Europa, wo ihr Einsatz unter erheblichen Vorbehalten steht. Ein entscheidender Faktor für die zukünftige Rolle der Kernenergie liegt im Nachweis der sicheren Handhabung des nuklearen Abfalls. Aus diesem Grund wurden mehrere verschiedenartige Vorgehensweisen vorgeschlagen, die auch weiterhin untersucht werden. Jedes vorgeschlagene Konzept ist ein Kompromiss zwischen öffentlicher Akzeptanz, den Kosten und den technologischen Gegebenheiten. Einer der herausforderndsten Vorschläge, unter technologischen Gesichtspunkten, besteht in der Strategie, den gefährlichsten Teil des nuklearen Abfalls in gezielt dafür ausgelegten Reaktoren zu verbrennen, wie sie in dieser Arbeit behandelt werden. Dieser besondere Reaktortyp, ein Beschleuniger getriebenes System mit externer Neutronenquelle (ADS = Accelerator Driven System), hat spezielle dynamische Eigenschaften, die näher untersucht werden müssen. Die Dissertation beschäftigt sich hauptsächlich mit der Simulation von Transienten, insbesondere mit der Veränderung der Neutronendichteverteilung des Reaktors, die durch eine zeitliche Änderung der Amplitude einer externen Neutronenquelle verursacht wird. Das Rechenprogrammpaket VARIANT-KIN3D bildet den Ausgangspunkt für die hier beschriebenen Untersuchungen. VARIANT löst die stationäre dreidimensionale Neutronentransportgleichung unter Benutzung einer hybriden Finite-Elementmethode, gekoppelt mit einer Kugelflächenfunktionen- Näherung gerade Ordnung. KIN3D simuliert die Zeitabhängigkeit der gesuchten Lösung für das Reaktorverhalten indem es das zeitabhängige Problem in einen Satz von pseudo-stationären Gleichungen transformiert. KIN3D kann daher die stationären Lösungen von VARIANT direkt benutzen, um das zeitabhängige Problem zu beschreiben. Für die Transformation des zeitabhängigen Problems in einen Satz von stationären Problemen wird eine Zeitdiskretisierung benötigt. In dieser Arbeit wurde das Zeitdiskretisierungs-Schema wesentlich verbessert und damit zahlreiche vorher festgestellte Schwierigkeiten in der Kopplung zwischen KIN3D und VARIANT beseitigt. Das erste neu implementierte Zeitintegrationsschema ist ein Rückwärts-Euler-Verfahren erster Ordnung kombiniert mit einem Reduktionsverfahren. Dieses neue Schema wurde an einem analytischen Benchmark überprüft und seine Genauigkeit und Robustheit nachgewiesen. Das Verfahren ist allerdings mit hohen Rechenzeiten verbunden, was seine Anwendung bei praktischen Problemen einschränkt. Diese Schwierigkeit konnte mit einem neuen adaptiven Verfahren für die Zeitschrittkontrolle überwunden werden. Dieses Vorgehen mit variablen Zeitschritten wurde erst nach umfangreichen analytischen Untersuchungen zu seinem Einfluss auf die Genauigkeits-Ordnung des Codes implementiert. In der Arbeit wird der Nachweis geführt, dass die Verwendung variabler Zeitschritte eine Erhöhung der Ordnung des Euler-Schemas erfordert, um einen Verlust der Struktur der Gleichungen in ihrer zeit-diskretisierten Form zu vermeiden. Das letztendlich in der Arbeit angewandte Verfahren besteht aus einem nichtlinearen gemischten rückwärts-zentrierten Euler-Schema zweiter Ordnung kombiniert mit einem Reduktionsverfahren. Mehrere Benchmark-Probleme wurden mit den beiden neuen Verfahren gelöst. Dabei wurden die Unterschiede gegenüber dem früher verwendeten Verfahren verglichen und der Einfluss der Diskretisierung der Winkelvariablen auf das räumlich-zeitliche Verhalten der Neutronendichte untersucht. Die Kopplung zwischen VARIANT und KIN3D wurde für diese neuen Zeit-Diskretisierungs-Methoden vollständig implementiert, also für alle räumlichen (XYZ, HEX-Z) und Winkel-Diskretisierungen, die in VARIANT verfügbar sind. Die endgültige Fassung des Programmpaketes VARIANT- KIN3D stellt ein sehr leistungsfähiges Werkzeug dar, das für die Analyse aller Arten von Transienten, die in einem Kernreaktor auftreten könnten, eingesetzt werden kann. Das herausragende

Merkmal ist die Fähigkeit des Codes, auch sehr schwierige Fälle zu behandeln, wie ultra-kurze Transienten, hervorgerufen durch schnelle Änderungen der externen Quelle (in einem ADS) sowie andere Transienten, deren Verlauf sich über längere Zeitskalen erstreckt. Diese große Flexibilität konnte ohne wesentliche Erhöhung der Rechenzeiten erzielt werden.

Chapter I. INTRODUCTION

I.1. Background

Public acceptance of a peaceful use of nuclear technologies is strictly connected to the problems associated with nuclear waste management. By now, two main strategies have been proposed: 1) direct permanent storage of spent fuel and 2) partition and transmutation. The second approach has the advantage of destroying most of the nuclear waste but at the same time it is a more difficult technological challenge.

The partition and transmutation of nuclear waste is difficult because it implicitly requires reactions induced by neutrons. The most suitable place for performing this process is within a nuclear reactor. Unfortunately the introduction of this waste into traditional reactors, leads to significant safety problems and a general deterioration in the neutronic safety parameters is observed. These include: a decreasing Doppler feedback coefficient, a positive and large magnitude coolant void reactivity worth and a strong reduction in the fraction of delayed neutrons all of which complicate the dynamic control of reactors in case of incident and for hypothetical accident scenarios, and thus decrease the safety margins.

For these reasons, a new reactor concept called Accelerator Driven System (ADS) has been proposed [7 to 11]. The distinguishing characteristic of an ADS is that the nuclear reactor is configured such that it is never critical (does not possess the ability to have a self-sustained fission reaction) and therefore an external neutron source is needed to maintain a steady state neutronic population and correlated power generation.

Figure 1 shows an example ADS proposed by the JAERI Company [12] within the 5th European Framework Project. The external source of neutrons is derived from a proton spallation reaction at the center of the core. Protons, accelerated by a LINAC (Linear

Accelerator), are directed to the center of the core via a beam tube. The external neutrons are produced within a fairly small target region close to the center of the core (in this project the target is a melted lead bismuth eutectic mixture). The spallation process occurs due to the high energy protons impacting upon the target thereby causing a cascade of reactions which provide the neutrons needed to maintain the fission reaction.

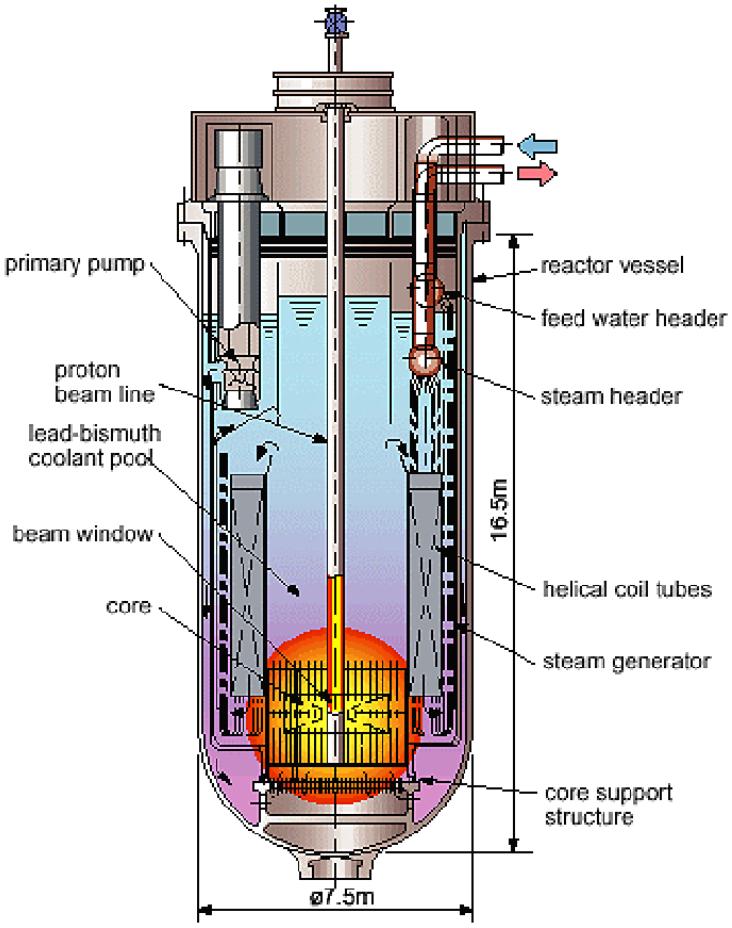

Figure 1: JAERI's design of a lead-bismuth cooled ADS.

The fundamental parameter used to describe the steady state condition of a reactor is k_{eff}, which is sometimes referred to as the fundamental eigenvalue. K_{eff} is the main parameter describing in time [1-4] (on a time scale over which fuel depletion is considered to be negligible) the evolution of the neutron density. There are two approaches to define k_{eff} for a reactor. The first, termed k'_{eff}, is derived from a physical point of view while the second one, termed k_{eff}, is

derived from a purely mathematics one. Consider the neutron density present in a reactor at time zero, which is referred to as the zeroth generation. Let us assume that there are no unstable nuclides and thus no spontaneous neutron emissions. When all the neutrons belonging to the zeroth generation have disappeared from the system (by absorption or leakage) the total number of neutrons created directly by the zeroth generation represent the first generation. Even if there is not an exact correspondence between time and generations, by means of the definition of the *mean generation time* it is possible to cast the generation process into a time frame. Thus, it is natural to describe the evolution in time of the average number of neutrons in the system as a function of the ratio between the number of neutrons in two subsequent generations that is exactly the physical (first) definition of the k'_{eff}:

$$k'_{eff} = \frac{\text{neutron population at generation n+1}}{\text{neutron population at generation n}}. \tag{1.1}$$

Of course the ratio between neutrons at two sequential generations can be expressed as the ratio between the reactions that add and subtract neutrons from the reactor:

$$k'_{eff} = \frac{\text{neutrons produced by fission + neutrons produced by external source}}{\text{neutrons lost by leakage + neutrons absorbed in medium}}. \tag{1.2}$$

Mathematically, k_{eff} is defined as the fundamental eigenvalue (the highest in mode) of the mathematical operator describing the steady state neutron transport phenomena inside the reactor core. From this definition, one integrates the steady state transport equation over its phase space (position, energy, and angle) yielding an eigenvalue problem with an expression for k_{eff} of

$$k_{eff} = \frac{\text{fission production (in the fundamental mode)}}{\text{(leakage + absorbtion in medium)(in the fundamental mode)}}, \tag{1.3}$$

where the fundamental mode is the eigenfunction corresponding to the fundamental eigenvalue.

The numerical interpretation of these numbers is clear which can be described succinctly using

- Sub-critical reactor : $k_{eff} < 1$
- Critical reactor : $k_{eff} = 1$
- Super-critical reactor : $k_{eff} > 1$

If k'_{eff} is equal to 1, the reactor is in a steady state mode and if k_{eff} is equal to 1 the reactor is able to sustain the nuclear fission chain. For an ADS, the external source of neutrons provides the neutrons needed to maintain a stable neutron fission chain (i.e. $k'_{eff} = 1$) even if the reactor is sub-critical (i.e. $k_{eff} < 1$). Without this external neutron source the neutron density will tend to zero with time. In this work only the mathematical definition of the k_{eff} is considered because it is not dependent upon the time behavior of the external source thus it is bounded only by the material composition and geometry of the reactor.

I.2. Motivations

Several numerical analyses [8-10] have indicated that a high concentration of fuel derived from nuclear waste loaded inside of a present-day nuclear reactor could lead to fuel failure during standard accident scenarios. In some cases an unacceptable super-critical state of the reactor system was predicted. Under these circumstances, the power can increase exponentially [4] on a time scale of less than 10^{-6}s [5, 6]. The main idea behind the ADS is the ability to operate in a regime where k_{eff} is never greater than 1. Of course this could not be possible without the presence of the external source. The design value of k_{eff} in an ADS becomes a balance of economics and safety.

The upper limit is determined by the fact that no accident scenarios should result in a supercritical reactor configuration. As the eigenvalue is decreased from this upper limit, the number of external neutrons required to maintain a certain power level increases. Consequently, the efficiency of the plant that is coupled to the power dedicated to produce the external neutrons decreases. A secondary problem associated with a decreasing eigenvalue is an increasing concentration of the neutron density near the beam target. This peaks the

temperature distribution at the center of the reactor and thus the reactor must operate at a lower power level. As one would expect, the margin of sub-criticality (i.e. how much the eigenvalue is below unity) is a key issue to the feasibility of an ADS. This margin must be measured during operation and several methods have been proposed to do it, such as the PND (Prompt Neutron Decay) [13] and the SPJ (Source Prompt Jump) [14] methods. Both are based upon reconstructing the eigenvalue by measuring the response of neutron detectors to a fast amplitude change of the external source during reactor operation. These procedures should of course be validated in a wide range of potential ADS operations (k_{eff} between 0.9 and 1). Currently, experiments in zero power reactors have been performed and more are planned in the future.

These experiments are monetarily expensive and can require a substantial amount of time and analysis. It is also unrealistic to assume that these experiments can exactly simulate those situations expected to be present in an ADS, e.g. those related to temperature feedback effects and thus the full range of operating conditions of an ADS may not be tested completely. Given this last problem, it is imperative to confirm validation with numerical codes. These codes must be capable of modeling and reproducing the available experimental results from standard reactor systems along with simulating the unique operational characteristics of an ADS.

One of the most widely used neutronics codes applied for the analysis of fast reactors is the ERANOS platform [15, 16]. Given the properties of the ADS (i.e. neutronic spectrum) the ERANOS code is well suited as a starting point for developing an analysis tool appropriate for an ADS. The ability of the ERANOS code to simulate the transient neutron flux in a sub-critical system has been tested in the framework of the MUSE (Multiplication d'Une Source Externe) experiment [17, 18]. Figure 2 shows a layout of the experimental device.

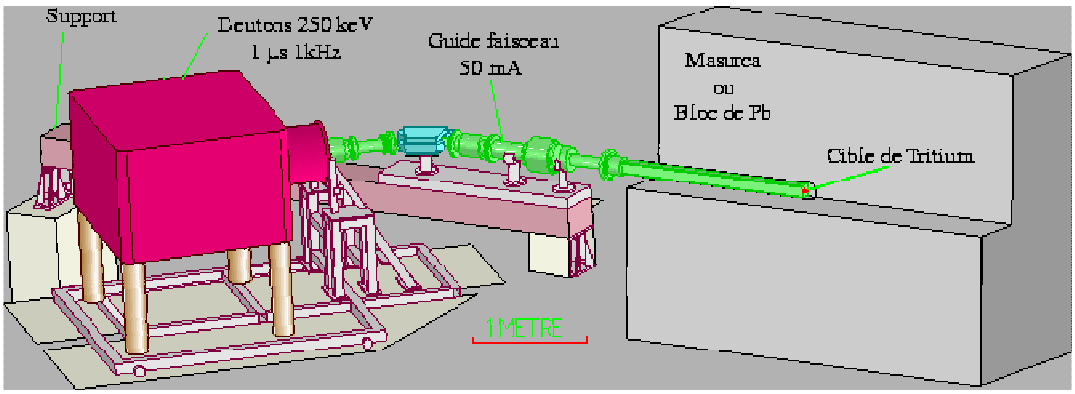

Figure 2: MUSE experiment.

In the MUSE experiments, a proton accelerator (GENEPI) produced a beam of deuterons directed towards a tritium target. The deuterium-tritium reaction yields 14 MeV neutrons which are scattered and moderated by a lead blanket surrounding the target. The blanket is situated in the center of the MASURCA core as is the target. The reactor fuel is composed of Pu-U (metal, oxide) fuel with a 24% plutonium enriched fuel. The plutonium is essentially composed of 76% Pu-239 and 18% Pu-240. The reflector surrounding the core is composed of 75% steel and 25% Sodium (volume fractions).

In the MASURCA core several U-235 based neutron detectors are inserted at various locations to measure the time behavior of the neutron density during (deuteron) source pulses.

The simulation results achieved by ERANOS for one experiment are shown in Figure 3 where it is noted that KIN3D is the component of ERANOS that performed the time dependent analysis. The four different ERANOS results were obtained using different cross section data evaluations (material property describing neutron interaction with core materials) [19]. As can be seen, the agreement between experiment and simulation is quite good, but clearly not exact. As it turns out, these simulations cannot be used to validate methodologies for the online

monitoring of the eigenvalue since the uncertainty in the result amounts to several percent which are not acceptable given the narrow range of acceptable eigenvalue for the ADS.

Errors in simulating these transients arise from several factors which can be separated into two components: errors in evaluation of the cross sections, and numerical error connected to the discretization of the mathematical model.

Unfortunately it is not simple to separate the errors arising from the two different sources. Nevertheless, Figure 3 shows that even with different cross section libraries there are notable similarities such as the underestimation of the flux before 20 μs. Such a behavior suggests that numerical modeling of the problem is in part causing the discrepancies in the experimental and numerical results.

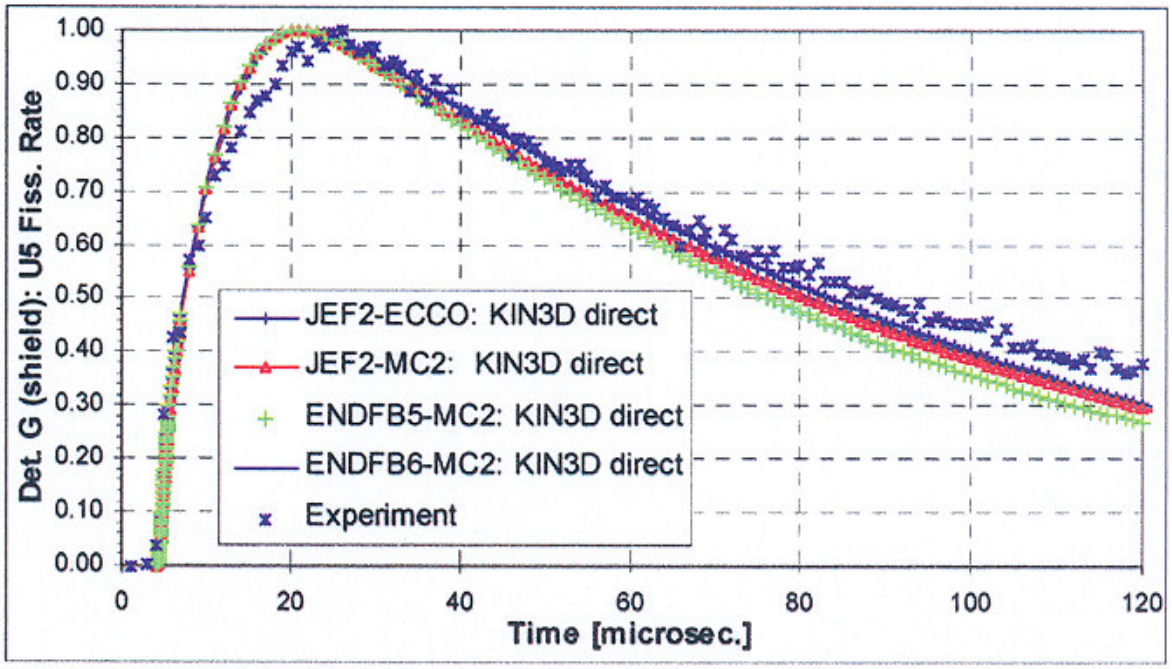

Figure 3: Response after 1μs source pulse: experimental data and code result with different cross section

I.3. The Neutron Transport Equation

The transport equation is a statistical description of the neutral particle-matter interaction [1-4]. The particle density is fully described by this distribution function in phase space (position $\vec{r}$ [cm], velocity $\vec{u}$ [cm s^{-1}]) and time t [s]): $n(\vec{r},\vec{u},t)$.

Being a statistical description two hypothesis should be satisfied:

- The differential volume in the phase space $d\vec{r}d\vec{u}$ should be small enough to consider the distribution function constant.
- The differential volume in the phase space $d\vec{r}d\vec{u}$ should contain enough particles to allow a statistical description.

- $n(\vec{r},\vec{u},t)d\vec{r}d\vec{u}$ *: = probability for a particle to be within the element* $d\vec{r}d\vec{u}$ *surrounding* $\vec{r},\vec{u}$ *at time t.*

If N_0 is the total number of neutrons in the systems it is possible to define the density function associated to the distribution n: $N(\vec{r},\vec{u},t) = N_0 n(\vec{r},\vec{u},t)$.

- $N(\vec{r},\vec{u},t)d\vec{r}d\vec{u}$ *: = expected number of neutrons within the element* $d\vec{r}d\vec{u}$ *surrounding* $\vec{r},\vec{u}$ *at time t.*

In the Boltzmann equation the following hypothesis are also assumed to be valid:

- The distribution function at the time and spatial scale at which collisions happen can be considered constant.
- Collisions are only binaries.
- Before collisions, particles are not correlated.

Focusing on the neutrons population inside a nuclear reactor, some additional simplifying hypotheses are possible:

- The fraction of neutrons that undergo spontaneous decay is negligible in the time scale of interest for the evolution of the distribution function.
- Neutron-neutron collisions are negligible with respect to neutron-matter collisions.

- No other forces, except the one arising from collisions, affect neutrons (for example the effect of gravity is negligible).
- The matter could be considered at rest.

For practical reasons, the neutron angular flux defined as follows: $\varphi(\vec{r},\vec{u},t)=|\vec{u}|N(\vec{r},\vec{u},t)$, is preferred over the neutron density.

It is also common practice to make a change of variables and define the angular flux with respect to the space $(\vec{r},\vec{\Omega},E)$ rather than $(\vec{r},\vec{u})$. The new coordinate system is defined by:

$$\begin{cases}\vec{\Omega}=\vec{u}/|\vec{u}| & \text{Direction,}\\ E=1/2m|\vec{u}|^2 & \text{Neutron Energy.}\end{cases} \tag{1.4}$$

Note that this coordinate system change is done taken in account the fact that φ is not a point function but a distribution over $(\vec{r},\vec{u})$ and, accordingly, over $(\vec{r},\vec{\Omega},E)$.

After the variable change $\varphi(\vec{r},\vec{\Omega},E,t)$ is measured in [$eV^{-1}cm^{-2}s^{-1}$] with the following physical interpretation:

- $\varphi(\vec{r},\vec{\Omega},E,t)dEd\vec{\Omega}$*: = the expected number of neutrons per unit area and time crossing the surface centered at* $\vec{r}$ *with energy E in dE and direction* $\vec{\Omega}$ *in* $d\vec{\Omega}$.

Next a mathematical model of the physical interaction between neutrons and matter is introduced. The main processes important for neutrons in a nuclear reactor are: capture, inelastic and elastic scattering, and fission (n-2n reactions are considered to be negligible in this analysis for simplicity). The total cross section encompasses all of the interactions that move or remove a neutron from its position in the phase space which is represented as:

- $\Sigma_T(\vec{r},\vec{\Omega},E,t)$*: = total effective cross section* [cm^{-1}]*: probability of interaction per unit distance of neutron travel.*

The different kinds of interactions can be divided into processes that remove neutrons from the systems and those that simply move and eventually multiply neutrons.

- $\Sigma_{TRANS}(\vec{r},\vec{\Omega}\leftarrow\vec{\Omega}',E\leftarrow E',t)dEd\vec{\Omega}$*: = total effective transfer cross section* [$eV^{-1}cm^{-1}$]*: probability, per unit distance of neutron travel, of having an interaction that will move*

(or multiply), in the phase space, the neutron from $\left(\vec{r},\vec{\Omega}',E'\right)$ *to* $dEd\vec{\Omega}$ *centered in* $\left(\vec{r},\vec{\Omega},E\right)$.

- $\Sigma_A\left(\vec{r},\vec{\Omega},E,t\right)$*: = effective absorption cross section* [cm^{-1}]*: probability of neutron loss by absorption per unit distance of neutron travel.*

The relation between the above defined cross sections is:

$$\Sigma_T\left(\vec{r},\vec{\Omega},E,t\right)=\int_{4\pi}d\vec{\Omega}'\int_0^{+\infty}dE'\Sigma_{TRANS}\left(\vec{r},\vec{\Omega}'\leftarrow\vec{\Omega},E'\leftarrow E,t\right)+\Sigma_A\left(\vec{r},\vec{\Omega},E,t\right). \qquad (1.5)$$

The total transfer cross section is usually split in two pieces: the scattering transfer cross-section and the fission transfer cross-section. This is primarily done based upon the different properties exhibited by these two components:

- $\Sigma_s\left(\vec{r},\vec{\Omega}\leftarrow\vec{\Omega}',E\leftarrow E',t\right)dEd\vec{\Omega}$ *:= effective scattering transfer cross section* [eV^{-1} cm^{-1}]*: probability of interaction of scattering type per unit distance of neutron travel that will move, in the phase space, the neutron from* $\left(\vec{r},\vec{\Omega}',E'\right)$ *to* $dEd\vec{\Omega}$ *centered in* $\left(\vec{r},\vec{\Omega},E\right)$.
- $\Sigma_f\left(\vec{r},\vec{\Omega}\leftarrow\vec{\Omega}',E\leftarrow E',t\right)dEd\vec{\Omega}$*: = effective fission transfer cross section* [$eV^{-1}cm^{-1}$]*: probability of interaction of fission type per unit distance of neutron travel that will move (multiplication is also possible), in the phase space, the neutron from* $\left(\vec{r},\vec{\Omega}',E'\right)$ *to* $dEd\vec{\Omega}$ *centered in* $\left(\vec{r},\vec{\Omega},E\right)$.

In general the composition of a nuclear reactor is such that the matter can always be considered isotropic in the space scale of interest for φ variations. Consequently, the effective total and absorption cross-sections become angularly independent.

$$\begin{aligned}\Sigma_T\left(\vec{r},\vec{\Omega},E,t\right)\cong\Sigma_T\left(\vec{r},E,t\right)&=\frac{1}{4\pi}\int_{4\pi}d\vec{\Omega}\int_{4\pi}d\vec{\Omega}'\int_0^{+\infty}dE'\Sigma_{TRANS}\left(\vec{r},\vec{\Omega}'\leftarrow\vec{\Omega},E'\leftarrow E,t\right)\\&\quad+\Sigma_A\left(\vec{r},E,t\right), \qquad (1.6)\\ \Sigma_A\left(\vec{r},\vec{\Omega},E,t\right)\cong\Sigma_A\left(\vec{r},E,t\right)&=\frac{1}{4\pi}\int_{4\pi}d\vec{\Omega}\Sigma_A\left(\vec{r},\vec{\Omega},E,t\right).\end{aligned}$$

Under this hypothesis the scattering transfer cross-section becomes invariant under rotation. This means that the deflection angle, after a scattering, is independent of the incoming direction. In this case the dependence from $\vec{\Omega} \leftarrow \vec{\Omega}'$ could be reduced to the dependence from the cosine between the in-coming and out-going direction. Taking into account the fact that $\vec{\Omega}$ is a unit vector, the cosine can be expressed with the scalar product $\vec{\Omega} \cdot \vec{\Omega}'$, this last expression is the standard approach used to describe the angular dependence of the scattering transfer cross section:

$$\Sigma_s\left(\vec{r}, \vec{\Omega} \leftarrow \vec{\Omega}', E \leftarrow E', t\right) \cong \Sigma_s\left(\vec{r}, \vec{\Omega} \cdot \vec{\Omega}', E \leftarrow E', t\right). \tag{1.7}$$

Also, in the case of the fission cross-section several approximations in the treatment of nuclear reactors are considered to be acceptable. First, given the small contribution from fission induced by very high energy neutrons, it is possible to assume that the direction of neutrons emitted by fission process has no correlation with the incident neutron direction and thus the emission is isotropic with respect to angle. Under this assumption and the hypothesis of an isotropic medium, the angular dependence of the effective fission cross-section is eliminated. We can also assume that the energy of the neutrons produced in a fission reaction is independent to the energy of the neutron initiating the fission reaction thus the cross section can be factorized in energy:

$$\Sigma_f\left(\vec{r}, \vec{\Omega} \leftarrow \vec{\Omega}', E \leftarrow E', t\right) \cong \chi\left(\vec{r}, E, t\right) \nu\left(\vec{r}, E, t\right) \Sigma_f\left(\vec{r}, E', t\right) / 4\pi. \tag{1.8}$$

Where $\chi\left(\vec{r}, E, t\right)$ [eV^{-1}] is known as the effective fission spectrum and $\chi\left(\vec{r}, E, t\right) dE$ expresses the probability for a neutron created by fission to be emitted with energy E in *dE*.

To account for the fact that more than one neutron is produced per fission reaction, an additional parameter is introduced which gives the average number of neutrons produced by the fission reaction: $\nu\left(\vec{r}, E, t\right)$.

The steady state neutron transport equation is a balance equation in the phase space $\left(\vec{r}, \vec{\Omega}, E\right)$. Taking into account all of the physical processes described above and including an external

source $S_{ext}\left(\vec{r},\vec{\Omega},E\right)$, it is possible to achieve the following form of the steady state Boltzmann transport equation for neutrons.

$$\begin{cases}\left(\vec{\Omega}\cdot\vec{\nabla}+\Sigma_T\left(\vec{r},E\right)\right)\varphi\left(\vec{r},\vec{\Omega},E\right)=\int_0^{\infty}dE'\int_{4\pi}d\vec{\Omega}'\Sigma_s\left(\vec{r},\vec{\Omega}\cdot\vec{\Omega}',E\leftarrow E'\right)\varphi\left(\vec{r},\vec{\Omega}',E'\right)+\\ \chi\left(\vec{r},E\right)\int_0^{\infty}dE'\nu\left(\vec{r},E'\right)\Sigma_f\left(\vec{r},E'\right)\int_{4\pi}d\vec{\Omega}'\varphi\left(\vec{r},\vec{\Omega}',E'\right)+S_{ext}\left(\vec{r},\vec{\Omega},E\right),\\ \vec{r}\in V\subseteq R^3,\ \vec{\Omega}\in\left[-\frac{\pi}{2},\frac{\pi}{2}\right]\times[0,2\pi],\ E\in[0,+\infty];\\ \varphi\left(\vec{r},\vec{\Omega},E\right)=\varphi_0\left(\vec{r},\vec{\Omega},E\right)+\int_{\partial V}dS\int_{\substack{2\pi^+\\ \vec{\Omega}\cdot\hat{n}_+>0}}d\vec{\Omega}'\int_0^{+\infty}dE'\mathrm{A}\left(\vec{r}'\to\vec{r},\vec{\Omega}'\to\vec{\Omega},E'\to E\right)\varphi\left(\vec{r}',\vec{\Omega}',E'\right),\\ \vec{r}\in\partial V\subseteq R^2,\ \vec{\Omega}\cdot\hat{n}_+<0,\ E\in[0,+\infty];\end{cases}$$

(1.9)

$\hat{n}_+$ represents the outward normal to the surface ∂V and thus the condition $\vec{\Omega}\cdot\hat{n}_+<0$ or $\vec{\Omega}\cdot\hat{n}_+>0$ indicates all the directions in-coming and out-going in the spatial domain. The albedo operator kernel *A* describes the probability of a neutron with energy *E',* direction $\vec{\Omega}'$ that is escaping from the systems at position $\vec{r}'\in\partial V$ to return to the system with energy *E,* direction $\vec{\Omega}$ and at position $\vec{r}\in\partial V$.

In order to shorten the notation the following operator definitions are used:

$$\int_0^{\infty}dE'\int_{4\pi}d\vec{\Omega}'\Sigma_s\left(\vec{r},\vec{\Omega}\cdot\vec{\Omega}',E\leftarrow E'\right)=H[\ ]\left(\vec{r},\vec{\Omega},E\right):=\quad\text{Scattering operator,}$$

$$\chi\left(\vec{r},E\right)\int_0^{\infty}dE'\nu\left(\vec{r},E'\right)\Sigma_f\left(\vec{r},E'\right)\int_{4\pi}d\vec{\Omega}'=F[\ ]\left(\vec{r},\vec{\Omega},E\right):=\quad\text{Fission operator,}$$

$$\int_{\partial V}dS'\int_{\substack{2\pi^+\\ \vec{\Omega}\cdot\hat{n}_+>0}}d\vec{\Omega}'\int_0^{+\infty}dE\mathrm{A}\left(\vec{r}'\to\vec{r},\vec{\Omega}'\to\vec{\Omega},E'\to E\right)=A[\ ]\left(\vec{r},\vec{\Omega},E\right):=\quad\text{Albedo operator.}$$

(1.10)

Introducing these expressions reduces the transport equation to:

$$\begin{cases} \left(\vec{\Omega}\cdot\vec{\nabla}+\Sigma_T\left(\vec{r},E\right)\right)\varphi\left(\vec{r},\vec{\Omega},E\right)=H\left[\varphi\right]\left(\vec{r},\vec{\Omega},E\right)+ \\ F\left[\varphi\right]\left(\vec{r},\vec{\Omega},E\right)+S_{ext}\left(\vec{r},\vec{\Omega},E\right), \\ \vec{r}\in V\subseteq R^3,\ \ \vec{\Omega}\in\left[-\pi/2,\pi/2\right]\times\left[0,2\pi\right],\ \ E\in\left[0,+\infty\right]; \\ \varphi\left(\vec{r},\vec{\Omega},E\right)=\varphi_0\left(\vec{r},\vec{\Omega},E\right)+A\left[\varphi\right]\left(\vec{r},\vec{\Omega},E\right), \\ \vec{r}\in\partial V\subseteq R^2,\ \ \vec{\Omega}\cdot\hat{n}_+<0,\ \ E\in\left[0,+\infty\right]. \end{cases} \tag{1.11}$$

To describe the time evolution of the angular neutron flux, the fission operator should be split in two components, a prompt one and a delayed one. In fact, part of it acts like a transfer operator in time. To explain the reason of this behavior it may be adequate to recall briefly the fission process dynamics. After a neutron hits a fissionable target, if a fission takes place (it is the most probable event), in a very short time scale (compared with the time scale of the angular flux variations) the original target nuclide splits in two lighter fractions (fission products) releasing practically at the same time neutrons that are usually named *prompt neutrons.* The number of these prompt fission neutrons and kind of individual fission product isotopes are a statistical functions of the target type and of neutron energy. Sometimes, some of the fission products are in a very excited state and go through a decay process that leads to the release of one additional neutron usually named *delayed neutron*. The release of the delayed neutron happens during a time interval that is comparable with the one of the angular flux variation. For this last reason, the fission process that involves the emission of a delayed neutron should be treated as a time transfer operator. The delayed neutrons are not only transferred in time but, in addition, they show a different energy emission spectrum compared to that of the prompt neutrons. Several fission products, so-called precursors, could lead to the emission of delayed neutrons. Each different one is characterized by a particular elapsing time (decay time) between the neutron absorption, by the target nuclide, and the release in the system of the delayed neutrons. Usually, instead of introducing a time transfer operator it is common practice in reactor physics, first, to introduce the spatial density of each different

nuclide that will release a delayed neutron (*precursor concentration*), and then, second, to couple the transport equation with equations describing the time evolution of the precursor concentrations. The number of nuclides releasing delayed fission neutrons is quite high; therefore we have several characteristic precursor decay times. Generally, different precursor concentrations are grouped in 'families' showing a similar decay period. In nuclear reactor theory, classically, only six families of delayed neutrons are used. Now it is possible to introduce the following quantities:

- $:=$ *effective prompt fission emission spectrum* [eV^{-1}]*;*
- $\beta(\vec{r},E,t) :=$ *effective delayed neutron fraction: fraction of delayed neutrons generated in a fission reaction by a neutron of energy E;*
- $\chi_p(\vec{r},E,t)\int_0^\infty dE'\nu(\vec{r},E',t)\left(1-\beta(\vec{r},E',t)\right)\Sigma_f(\vec{r},E')\int_{4\pi} d\vec{\Omega}' = F_p[\ ](\vec{r},\vec{\Omega},E,t):=$
  := Prompt fission operator.

For each family, *i*, the following quantities can be defined

- $C_i(\vec{r},t) :=$ *effective precursor concentration* [cm^{-3}]*: expected density of neutron emission with a decay time of* λ_i*;*
- $\lambda_i :=$ *effective precursor decay constant*[s^{-1}]*;*
- $\chi_i(E,t) :=$*effective emission spectrum* [eV^{-1}]*: probability of neutron emission at energy E;*
- $\beta_i(\vec{r},E,t) :=$ *effective delayed neutron fraction for family i: fraction of delayed neutrons of family i generated in a fission reaction by a neutron of energy E.*

With the above definitions, and the introduction of the initial conditions for the flux and the precursor concentrations, respectively: $\varphi_{T0}(\vec{r},\vec{\Omega},E,0)$ and $C_i|_0$, the time behavior of the angular flux can be described via the following equations. Note that the notation for in-coming and out-going angular flux on the boundary is kept from equation (1.9):

$$
\begin{cases}
\left(u(E)^{-1}\partial_t + \vec{\Omega}\cdot\vec{\nabla} + \Sigma_T(\vec{r},E,t)\right)\varphi(\vec{r},\vec{\Omega},E,t) = H[\varphi](\vec{r},\vec{\Omega},E,t) + \\
F_p[\varphi](\vec{r},\vec{\Omega},E,t) + S_{ext}(\vec{r},\vec{\Omega},E,t) + \sum_{i=1}^{NF}\chi_i(\vec{r},E,t)\lambda_i C_i(\vec{r},t), \\
\varphi(\vec{r},\vec{\Omega},E,0) = \varphi_{T0}(\vec{r},\vec{\Omega},E,0), \\
\partial_t C_i(\vec{r},t) = -\lambda_i C_i(\vec{r},t) + \\
+\beta_i(\vec{r},E,t)\int_0^{\infty} dE'\nu(\vec{r},E',t)\Sigma_f(\vec{r},E',t)\int_{4\pi} d\vec{\Omega}'\varphi(\vec{r},\vec{\Omega}',E',t), \qquad i = 1....NF, \quad (1.12) \\
C_i(\vec{r},0) = C_i\big|_0, \qquad i = 1....NF, \\
\vec{r}\in V\subseteq R^3,\ \vec{\Omega}\in\left[-\frac{\pi}{2},\frac{\pi}{2}\right]\times[0,2\pi],\ E\in[0,+\infty],\ t\in[0,+\infty]; \\
\varphi(\vec{r},\vec{\Omega},E,t) = \varphi_0(\vec{r},\vec{\Omega},E,t) + A[\varphi](\vec{r},\vec{\Omega},E,t), \\
\vec{r}\in\partial V\subseteq R^2,\ \vec{\Omega}\cdot\hat{n}_+ < 0,\ E\in[0,+\infty]\ \ t\in[0,+\infty].
\end{cases}
$$

In this time dependent equation all of the operators reflecting physical interactions between neutrons and matter are time dependent due to the fact that the composition of the medium could be changing with time.

For the needs of this work the above given forms of the neutron transport equations can be considered as to be sufficiently accurate. It would, nevertheless, be inappropriate not to consider the ad hoc nature of the mathematical entities: F_p, F, β, β_i, χ_i, χ_p and χ. These quantities are averaged and summed over different probabilistic processes thus different isotopes constitute the matter that itself is a statistical medium. It was for this reason that the cross sections in the preceding sections were termed "effective", which, for brevity, will be assumed from this point on.

I.4. The Steady State Second Order Transport Equation

In most reactors, only two boundary conditions are needed for reactor analysis: vacuum and reflected. The vacuum, or void, boundary condition assumes that the incoming flux is zero while the reflected boundary condition assumes the incoming flux is a reflection of the

outgoing flux. With these boundary conditions the steady state transport equation can be written as

$$\begin{cases} \left(\vec{\Omega}\cdot\vec{\nabla}+\Sigma_T\left(\vec{r},\vec{\Omega},E\right)\right)\varphi\left(\vec{r},\vec{\Omega},E\right)=H\left[\varphi\right]\left(\vec{r},\vec{\Omega},E\right)+ \\ F\left[\varphi\right]\left(\vec{r},\vec{\Omega},E\right)+S_{ext}\left(\vec{r},\vec{\Omega},E\right), \\ \vec{r}\in V\subseteq R^3,\ \vec{\Omega}\in\left[-\frac{\pi}{2},\frac{\pi}{2}\right]\times\left[0,2\pi\right],\ E\in\left[0,+\infty\right]; \\ \varphi\left(\vec{r},\vec{\Omega},E\right)=\varphi_0\left(\vec{r},\vec{\Omega}^*,E\right), \quad \vec{r}\in\partial V_{\text{R ef.}}\subseteq R^2,\ \vec{\Omega}\cdot\hat{n}_+<0; \\ \varphi\left(\vec{r},\vec{\Omega},E\right)=0, \quad \vec{r}\in\partial V_{\text{Vac.}}\subseteq R^2,\ \vec{\Omega}\cdot\hat{n}_+<0; \\ \partial V_{\text{R ef.}}\cup\partial V_{\text{Vac.}}\equiv\partial V\subseteq R^2; \end{cases} \tag{1.13}$$

where $\vec{\Omega}^*$ is the conjugate direction of $\vec{\Omega}$.

To obtain the second order form of the transport equation, the angular flux and source is written as a sum of two parts, one symmetric (even) and the other anti-symmetric (odd) with respect to $\vec{\Omega}$

$$\phi\left(\vec{r},\vec{\Omega},E\right)=\frac{1}{2}\left(\varphi\left(\vec{r},\vec{\Omega},E\right)+\varphi\left(\vec{r},-\vec{\Omega},E\right)\right):$$ even neutron angular flux,

$$\psi\left(\vec{r},\vec{\Omega},E\right)=\frac{1}{2}\left(\varphi\left(\vec{r},\vec{\Omega},E\right)-\varphi\left(\vec{r},-\vec{\Omega},E\right)\right):$$ odd neutron angular flux,

$$S^{\pm}\left(\vec{r},\vec{\Omega},E\right)=\frac{1}{2}\left(S\left(\vec{r},\vec{\Omega},E\right)\pm S\left(\vec{r},-\vec{\Omega},E\right)\right):$$ even/odd external group source,

$$H^{\pm}\left[\ \right]\left(\vec{r},\vec{\Omega},E\right)=\int_0^{+\infty}dE'\int_{4\pi}d\vec{\Omega}'\Sigma_s^{\pm}\left(\vec{r},\vec{\Omega}\cdot\vec{\Omega}',E\leftarrow E'\right):$$ even/odd scattering operator,

$$\Sigma_s^{\pm}\left(\vec{\Omega}\cdot\vec{\Omega}',E\leftarrow E'\right)=$$

$$=\frac{1}{2}\left(\Sigma_s\left(\vec{r},\vec{\Omega}\cdot\vec{\Omega}',E\leftarrow E'\right)\pm\Sigma_s\left(\vec{r},-\vec{\Omega}\cdot\vec{\Omega}',E\leftarrow E'\right)\right):$$ even/odd scattering kernel. (1.14)

It is a trivial algebraic task to show that this form of the angular flux has the following properties

$$\begin{cases} \phi\left(\vec{r},\vec{\Omega},E\right)=\phi\left(\vec{r},-\vec{\Omega},E\right), \\ \psi\left(\vec{r},\vec{\Omega},E\right)=-\psi\left(\vec{r},-\vec{\Omega},E\right), \\ S^{\pm}\left(\vec{r},\vec{\Omega},E\right)=\pm S^{\pm}\left(\vec{r},-\vec{\Omega},E\right), \\ \Sigma_s^{\pm}\left(\vec{\Omega}\cdot\vec{\Omega}',E\leftarrow E'\right)=\pm\Sigma_s^{\pm}\left(-\vec{\Omega}\cdot\vec{\Omega}',E\leftarrow E'\right). \end{cases} \tag{1.15}$$

Equation (1.13) can be written in terms of $\vec{\Omega}$ and $-\vec{\Omega}$ (inside the scattering kernel, $\vec{\Omega}'$ and $-\vec{\Omega}'$ are used). The resulting two equations can be added and subtracted from each other leading to the following system where the even and odd parity expressions have been substituted and the spatial, energy and angular dependences are omitted for brevity

$$\begin{cases} \vec{\Omega}\cdot\vec{\nabla}\psi+\Sigma_T\phi=H^{+}\left[\phi\right]+S^{+}+F\left[\phi\right], \\ \vec{\Omega}\cdot\vec{\nabla}\phi+\Sigma_T\psi=H^{-}\left[\psi\right]+S^{-}. \end{cases} \tag{1.16}$$

Note that the fission operator has also been assumed to be isotropic and thus only contains an even component. The scattering operator can be split since the spaces of even and odd functions are orthogonal with respect to the standard scalar product over $L^2\left[-\pi/2,\pi/2\right]\times\left[0,2\pi\right]$ (Lebesgue space). Only symmetric terms characterize the first equation of system (1.16) and only anti-symmetric ones the second one. For this reason they are known as the even and the odd parity equations. The aim of this approach is to reduce the solution space from

$$\varphi\in\left[L^2\left[-\frac{\pi}{2},\frac{\pi}{2}\right]\times\left[0,2\pi\right]\times\left[0,+\infty\right]\right]\times H^1\left(V\subseteq R^3\right) \tag{1.17}$$

to

$$\phi\in\left\{f\in\left[L^2\left[-\frac{\pi}{2},\frac{\pi}{2}\right]\times\left[0,2\pi\right]\times\left[0,+\infty\right]\right]\times H^1\left(V\subseteq R^3\right)\mid f\left(\vec{r},\vec{\Omega}\right)=f\left(\vec{r},-\vec{\Omega}\right)\right\} \tag{1.18}$$

where L^2 and H^1 are the usual Lebesgue and Sobolev spaces.

The main advantage is a strong reduction of the number of degrees of freedom of the solution preserving the most important information for the reactor physics that is the scalar flux (the angular constant part of the neutron flux) In order to reduce the solution space the second

equation of (1.16) must be inverted with respect to ψ. The introduction of the $L^{\pm}$ operators $L^{\pm} = \left(\Sigma_T - H^{\pm}\right)[\ ]$ formally reduces the inversion problem to the inversion of the L^- which only acts in angle. In non-vacuum regions this operator is not singular and thus the inversion is possible [20, 21]. For our interest it will be sufficient to find an expression of its inverse as a Fourier series over L^2 [-1, 1]. In fact the angular part of the scattering kernel could be expressed as a function of the cosine between the incoming and out-going directions ($\vec{\Omega}\cdot\vec{\Omega}' = \mu$, see page 11), thus the angular dependence is mono-dimensional. It is now helpful to introduce the orthogonal Legendre polynomials with respect to the angular dependence

$$L_p(\mu) = \frac{1}{2^n p!}\frac{d^p}{d\mu^p}\left[\left(1-\mu^2\right)^p\right] \qquad \mu \in [-1,1] \quad p = 0,1,2,\ldots,. \tag{1.19}$$

These polynomials obey the following orthogonal relationship

$$\int_{-1}^{1} d\mu L_p(\mu) L_q(\mu) = \delta_{p,q}\frac{2}{2p+1}, \tag{1.20}$$

where $\delta_{p,q}$ is the Kronecker delta. The Legendre polynomials form a complete basis set on the interval [-1, 1], and the Fourier coefficients of the scattering kernel are thus defined by the following projection:

$$\Sigma_{s,p} = \frac{1}{2}\int_{-1}^{1} d\mu \Sigma_s(\mu) L_p(\mu). \tag{1.21}$$

This gives the following Fourier series

$$\Sigma_s(\mu) = \sum_{p=0}^{\infty}(2p+1)\Sigma_{s,p} L_p(\mu). \tag{1.22}$$

The inverse operator is given as [21]

$$\left(L^-\right)^{-1}[\ ] = \frac{1}{\Sigma_T} - \int_{4\pi} d\vec{\Omega}' \sum_{\substack{p=0 \\ p:odd}}^{\infty}(2p+1)\frac{\Sigma_{s,p}}{\Sigma_T}\frac{P_p\left(\vec{\Omega}\cdot\vec{\Omega}'\right)}{\left(\Sigma_T - \Sigma_{s,p}\right)}. \tag{1.23}$$

Now it is possible to invert the odd equation of (1.16) to obtain the strong form of the second order even transport equation

$$\begin{cases} \vec{\Omega}\cdot\vec{\nabla}\left(\left(L^{-}\right)^{-1}\left(-\vec{\Omega}\cdot\vec{\nabla}\phi+S^{-}\right)\right)+\Sigma_{T}\phi=H^{+}\left[\phi\right]+S^{+}+F\left[\phi\right], \\ \vec{r}\in V\subseteq R^{3},\ \vec{\Omega}\in\left[-\frac{\pi}{2},\frac{\pi}{2}\right]\times\left[0,2\pi\right]; \end{cases} \tag{1.24}$$

The boundary conditions for the even flux are provided in [20], which are written as

$$\begin{cases} \left.\begin{array}{ll} \phi=\left(L^{-}\right)^{-1}\left(-\vec{\Omega}\cdot\vec{\nabla}\phi+S^{-}\right) & \vec{\Omega}\cdot\hat{n}_{+}<0, \\ -\phi=\left(L^{-}\right)^{-1}\left(-\vec{\Omega}\cdot\vec{\nabla}\phi+S^{-}\right) & \vec{\Omega}\cdot\hat{n}_{+}<0 \end{array}\right\} & \vec{r}\in\partial V_{\text{Ref.}}\subseteq R^{2},\ \vec{\Omega}\in\left[-\frac{\pi}{2},\frac{\pi}{2}\right]\times\left[0,2\pi\right], \\ \left(L^{-}\right)^{-1}\left(S^{-}\left(\vec{\Omega}\right)-S^{-}\left(\vec{\Omega}*\right)-\vec{\Omega}\cdot\vec{\nabla}\phi\left(\vec{\Omega}\right)+\vec{\Omega}\cdot\vec{\nabla}\phi\left(\vec{\Omega}*\right)\right), & \vec{r}\in\partial V_{\text{Vac.}}\subseteq R^{2},\ \vec{\Omega}\in\left[-\frac{\pi}{2},\frac{\pi}{2}\right]\times\left[0,2\pi\right]. \end{cases}$$

(1.25)

The description of the time dependent second order form of the transport equation will be described in chapter 3 since it is the main subject of this work and needs a more detailed treatment. A final remark about the inversion of the L^{-} operator could be interesting, in fact equation (1.23) shows that not only the inversion of this operator could not be performed in a void region ($\Sigma_{T}=0$) but also it requires that $\left(\Sigma_{T}-\Sigma_{s,p}\right)\neq 0\ \ \forall p=0,.....,\infty$, p odd. The inversion of the L^{-} operator strongly limits the application field of second order type methods.

Chapter II. DISCRETIZATION OF THE NEUTRON TRANSPORT EQUATION

In this chapter the discretization scheme for energy, space, and angle will be discussed along with the numerical treatment of the time variable. For the angular dependence two schemes are considered: the spherical harmonics (P_N) and simplified spherical harmonics (SP_N) methods. The discretization in space and angle is displayed for the steady state second order form of the even transport equation since, later in this chapter, it will be shown that the discretization of the time dependent equation with respect to time leads to a set of equations each of which is formally equivalent to the steady state one.

II.1. The Multi-Group Approximation and Spatial Homogenization

The explicit details of the multi-group approximation and spatial homogenization are beyond the scope of this thesis, thus only the reasons for these approximations and the impact upon the governing equations are discussed. One benefit derived from these approximations is the derivation of average operators which are valid on a coarse space and energy grid. The detailed structure of a nuclear reactor core is generally very complex and contains many different materials. As a consequence, numerous discontinuities exist in the spatial cross sections distribution on a spatial scale of less than 1 mm (e.g. clad of the fuel pin structure). The energy dependence of the cross sections introduces more complexity due to the large number of resonances with narrow energy widths and high peaks. Combined, these characteristics require an extremely complex numerical treatment, which for reactor analysis, results in a numerical description of the spatial and energy dependence well beyond the capabilities of modern

computing technology. It is for this reason that spatial homogenization and energy collapsing are introduced. These approximations lead to average operators that are valid over a coarse space and energy grid, but which maintain approximately the reaction rates of the refined space and energy grid. The typical region over which spatial homogenization is performed is a single reactor fuel assembly split into several axial pieces (each having a length on the order of decimeters). The number of intervals into which the energy domain is split varies. The energy domain itself ranges from 0 eV to the upper energy cutoff of 14 MeV. In thermal reactors where the majority of neutrons in the reactor have energy less than 0.1 eV, 2 to 4 groups are enough to obtain sufficiently accurate results. For fast reactor calculations where a majority of the neutrons have energy >> 100 eV, from 4 to 30 (most time between 10 and 30) groups are generally used.

Several methods have been proposed and used to achieve the coarse group cross sections needed to describe these reactor systems. The main idea behind all of these methods is to split the flux into two components: the macroscopic flux and the microscopic one. The microscopic flux has two main properties: first it is weakly affected by the boundary condition and second the variation in the spatial and energy domain is on a much smaller grid when compared with the macroscopic one [22, 23]. The microscopic flux is typically computed by solving the transport equation only for some regions of interest where reflected boundary conditions are used to simulate the spectrum representative for the reactor. Because of its weak dependence upon the boundary conditions the microscopic flux between two assemblies, having the same spatial composition but different position in the core, can be very similar. Consequently, in modern nuclear reactor analysis, the microscopic flux is only obtained for those fuel assemblies which have significantly different spatial geometry or compositions. In this manner the governing transport equation in the reactor core, for the microscopic flux, can be written in terms of the collection of unique fuel assembly problems that make up the reactor system. The averaged quantities, defining the homogenized operators, resulting from the microscopic flux

calculations are usually termed homogenized parameters. The homogenization process also affects the properties of operators, an example for which is the homogenized velocities which are a function of time, space and direction. Usually this change in the operators structure is neglected due to its low effect in the general solution. Following this tendency in this work operator structure is unchanged from equations(1.11) and (1.12).

From this point forward, we will only consider the system of equations valid for the macroscopic flux and thus the homogenized set of parameters. As a result of this, the remainder of this thesis, unless explicitly stated, implicitly assumes the cross sections refer to a set of homogenized parameters.

NG: number of energy group,

$$[E_{\min}, E_{\max}] = \bigcup_{g=1}^{NG} [E_g, E_{g-1}],$$

$$E_{\max} = E_0 > \ldots > E_{g-1} > E_g > \ldots\ldots > E_{NG} = E_{\min},$$

g = 1,...,NG,

$\theta_g(E)$ characteristic function of sub-domain $E_g = [E_{g-1}, E_g]$,

$$\begin{cases} \theta_g(E) = 1 & E \in E_g, \\ \theta_g(E) = 0 & \mathrm{E} \notin E_g. \end{cases}$$

Nzone: number region with different microscopic flux

$$V = \bigcup_{g=1}^{Nzone} V_j,$$

J = 1,..,Nzone,

$\theta_j(\vec{r})$:= characteristic function of sub-domain V_j,

$$\begin{cases} \theta_j(\vec{r}) = 1 & \vec{r} \in V_j, \\ \theta_j(\vec{r}) = 0 & \vec{r} \notin V_j. \end{cases}$$

$u_g :=$ velocity for energy group g,

$u(E) = \sum_{g=1}^{NG} \theta_g(E) u_g :=$ multi group velocity,

${}^{j}\Sigma_{T,g}(t) :=$ total cross section for group g in zone j,

$\Sigma_{T,g}(\vec{r},t) = \sum_{j=1}^{Nzone} \theta_j(\vec{r})\, {}^{j}\Sigma_{T,g}(t) :=$ total cross section for group g,

$\Sigma_{T,g}(E,\vec{r},t) = \sum_{g=1}^{NG} \theta_g(E) \sum_{j=1}^{Nzone} \theta_j(\vec{r})\, {}^{j}\Sigma_{T,g}(t) :=$ multi group total cross section,

${}^{j}\Sigma_{s,g'\to g}\left(\vec{\Omega}\cdot\vec{\Omega}',t\right) :=$ scattering cross section from group g' to g from direction $\vec{\Omega}'$ to $\vec{\Omega}$,

$H_{g'\to g}[\ ]\left(E,\vec{r},\vec{\Omega},t\right) = \sum_{j=1}^{Nzone} \theta_j(\vec{r}) \int_{4\pi} d\vec{\Omega}'\, {}^{j}\Sigma_{s,g'\to g}\left(\vec{\Omega}\cdot\vec{\Omega}',t\right) :=$

$:=$ scattering operator from group g' to g,

$H[\ ]\left(E,\vec{r},\vec{\Omega},t\right) = \sum_{j=1}^{Nzone} \theta_j(\vec{r}) \sum_{g=1}^{NG} \theta_g(E) \int_{E_{\min}}^{E_{\max}} \sum_{g'=1}^{NG} \theta_{g'}(E') \int_{4\pi} d\vec{\Omega}'\, {}^{j}\Sigma_{s,g'\to g}\left(\vec{\Omega}\cdot\vec{\Omega}',t\right) :=$

$:=$ multi group scattering operator ,

${}^{j}\chi_g(t) :=$ fission spectrum in group g for zone j,

$\chi_g(\vec{r},t) = \sum_{g=1}^{NG} \theta_j(\vec{r})\, {}^{j}\chi_g(t) :=$ fission spectrum for group g,

$\chi(\vec{r},E,t) = \sum_{g=1}^{NG} \theta_g(E) \sum_{j=1}^{Nzone} \theta_j(\vec{r})\, {}^{j}\chi_g(t) :=$ multi-group fission spectrum,

${}^{j}\nu_{g'}(t) :=$ number of secondary neutrons produced by a fission process
induced by a neutron of energy $E_{g'}$ in zone j,

$\nu_{g'}(\vec{r},t) = \sum_{j=1}^{Nzone} \theta_j(\vec{r})\, {}^{j}\nu_{g'}(t) :=$ number of secondary neutrons produced by a
fission process induced by a neutron of energy E,

$\nu(\vec{r},E,t) = \sum_{g'=1}^{NG} \theta_{g'}(E') \sum_{j=1}^{Nzone} \theta_j(\vec{r})\, {}^{j}\nu_{g'}(t) :=$ number of secondary neutrons produced by
a fission process induced by a neutron of energy E,

$\Sigma_{f,g}(\vec{r},t) = \sum_{j=1}^{Nzone} \theta_j(\vec{r})\, {}^{j}\Sigma_{f,g}(t) :=$ total fission cross section for group g,

${}^{j}\Sigma_{f,g}(t) :=$ fission cross section for group g in zone j,

$F_g[\ ]\left(\vec{r},\vec{\Omega},t\right) = \sum_{j=1}^{Nzone} \theta_j(\vec{r})\, {}^{j}\chi_g(t) \int_0^{\infty} dE' \sum_{g'=1}^{NG} \theta_{g'}(E')\, {}^{j}\nu_{g'}(t)\, {}^{j}\Sigma_{f,g'}(t) \int_{4\pi} d\vec{\Omega}' :=$ group fission operator,

$$F[\ ]\left(\vec{r},\vec{\Omega},E,t\right)=\sum_{j=1}^{Nzone}\theta_j\left(\vec{r}\right)\sum_{g=1}^{NG}\theta_g\left(E\right)\,{}^{j}\chi_g\left(t\right)\int_0^{\infty}dE'\sum_{g'=1}^{NG}\theta_{g'}\left(E'\right)\,{}^{j}\nu_{g'}\left(t\right)\,{}^{j}\Sigma_{f,g'}\left(t\right)\int_{4\pi}d\vec{\Omega}':=$$

$:=$ multi group fission operator.

Definitions of the homogenized operators: $\beta\left(\vec{r},E',t\right)$, $F_p[\ ]\left(\vec{r},\vec{\Omega},E,t\right)$, $A[\ ]\left(\vec{r},\vec{\Omega},E,t\right)$, $\chi_i\left(E,t\right)$ and $\beta_i\left(\vec{r},E,t\right)$, are almost similar to ones just provided and therefore not reported here. Starting from these definitions, the transport equation in the homogenized multi-group formalism is equivalent to the previous form in (1.11) and (1.12), but now the unknowns are the macroscopic flux and precursor concentrations. The multi-group equation can be split into a system of equations each of which corresponds to a single energy group by a projection over the characteristic function in energy. The result is (for g=1,…., NG):

$$\begin{cases}\left(u_g^{-1}\partial_t+\vec{\Omega}\cdot\vec{\nabla}+\Sigma_{T,g}\left(\vec{r},t\right)\right)\varphi_g\left(\vec{r},\vec{\Omega},t\right)=H_{g\to g}\left[\varphi_g\right]\left(\vec{r},\vec{\Omega},t\right)+\sum_{\substack{g'=1\\g'\neq g}}^{NG}H_{g'\to g}\left[\varphi_{g'}\right]\left(\vec{r},\vec{\Omega},t\right)\\ \sum_{g'=1}^{NG}F_{p,g'\to g}\left[\varphi\right]\left(\vec{r},\vec{\Omega},t\right)+S_{ext,g}\left(\vec{r},\vec{\Omega},t\right)+\sum_{i=1}^{NF}\chi_{i,g}\left(\vec{r},t\right)\lambda_i C_i\left(\vec{r},t\right),\\ \varphi_g\left(\vec{r},\vec{\Omega},0\right)=\varphi_{T0,g}\left(\vec{r},\vec{\Omega},0\right),\\ \vec{r}\in V\subseteq R^3,\ \vec{\Omega}\in\left[-\frac{\pi}{2},\frac{\pi}{2}\right]\times[0,2\pi],\ \ t\in[0,+\infty];\\ \varphi_g\left(\vec{r},\vec{\Omega},t\right)=\varphi_{0,g}\left(\vec{r},\vec{\Omega},t\right)+\sum_{g'=1}^{NG}A_{g'\to g}\left[\varphi\right]\left(\vec{r},\vec{\Omega},t\right),\\ \vec{r}\in\partial V\subseteq R^2,\ \vec{\Omega}\cdot\hat{n}_+<0,\ \ t\in[0,+\infty],\end{cases}\tag{2.1}$$

Where the multi-group external source has been defined as follow:

$$S_{ext,g}\left(\vec{r},\vec{\Omega},t\right)=\int_{E_{g-1}}^{E_g}dES_{ext}\left(\vec{r},\vec{\Omega},E,t\right).\tag{2.2}$$

The influence of the delayed neutrons is taken in account by the equations describing the precursor concentrations for (i=1,…, NF):

$$\begin{cases} \partial_t C_i(\vec{r},t) = -\lambda_i C_i(\vec{r},t) + \beta_{i,g}(\vec{r},t)\sum_{g'=1}^{NG} \nu(t)\Sigma_{F,g'}(\vec{r},t)\int\limits_{4\pi} d\vec{\Omega}\varphi(\vec{r},\vec{\Omega},t), \\ C_i(\vec{r},0) = C_i\big|_0, \\ \vec{r}\in V\subseteq R^3,\ \vec{\Omega}\in\left[-\frac{\pi}{2},\frac{\pi}{2}\right]\times[0,2\pi],\ \ t\in[0,+\infty]. \end{cases} \tag{2.3}$$

As before, for steady state problems, the normal fission operator (the operator $F_{p,g'\to g}[\ ]$ is replaced by the $F_{g'\to g}[\ ]$ operator) takes into account the fraction of delayed neutrons, with its spectrum, and the equation describing the precursor concentrations is no longer needed:

$$\begin{cases} \left(\vec{\Omega}\cdot\vec{\nabla}+\Sigma_{T,g}(\vec{r})\right)\varphi_g(\vec{r},\vec{\Omega}) = H_{g\to g}\left[\varphi_g\right](\vec{r},\vec{\Omega}) + \sum_{\substack{g'=1\\ g'\neq g}}^{NG} H_{g'\to g}\left[\varphi_{g'}\right](\vec{r},\vec{\Omega}) + \\ +\sum_{g'=1}^{NG} F_{g'\to g}[\varphi](\vec{r},\vec{\Omega}) + S_{ext,g}(\vec{r},\vec{\Omega}), \\ \vec{r}\in V\subseteq R^3,\ \vec{\Omega}\in\left[-\frac{\pi}{2},\frac{\pi}{2}\right]\times[0,2\pi]; \\ \varphi_g(\vec{r},\vec{\Omega}) = \varphi_{0,g}(\vec{r},\vec{\Omega}) + \sum_{g'=1}^{NG} A_{g'\to g}[\varphi](\vec{r},\vec{\Omega}), \\ \vec{r}\in\partial V\subseteq R^2,\ \vec{\Omega}\cdot\hat{n}_+ < 0. \end{cases} \tag{2.4}$$

The reason for splitting the scattering operator in the self-scattering operator $H_{g\to g}$ and group transfer scattering operator $\sum_{\substack{g'=1\\ g'\neq g}}^{NG} H_{g'\to g}$ is to obtain the within group transport equation:

$$\begin{cases} \left(\vec{\Omega}\cdot\vec{\nabla}+\Sigma_{T,g}(\vec{r})\right)\varphi_g(\vec{r},\vec{\Omega}) = H_{g\to g}\left[\varphi_g\right](\vec{r},\vec{\Omega}) + S_g(\vec{r},\vec{\Omega}), \\ \vec{r}\in V\subseteq R^3,\ \vec{\Omega}\in\left[-\frac{\pi}{2},\frac{\pi}{2}\right]\times[0,2\pi]; \\ \varphi_g(\vec{r},\vec{\Omega}) = \varphi_{0,g}(\vec{r},\vec{\Omega}) + \sum_{g'=1}^{NG} A_{g'\to g}[\varphi](\vec{r},\vec{\Omega}), \\ \vec{r}\in\partial V\subseteq R^2,\ \vec{\Omega}\cdot\hat{n}_+ < 0. \end{cases} \tag{2.5}$$

Where $S_g(\vec{r},\vec{\Omega})$ represent the source term for the g-th group which includes neutrons contributed to this group by scattering and fission from all other groups:

$$S_g(\vec{r},\vec{\Omega}) = \sum_{\substack{g'=1\\ g'\neq g}}^{NG} H_{g'\to g}\left[\varphi_{g'}\right](\vec{r},\vec{\Omega}) + \sum_{g'=1}^{NG} F_{g'\to g}[\varphi](\vec{r},\vec{\Omega}) + S_{ext,g}(\vec{r},\vec{\Omega}). \tag{2.6}$$

This formalism is widely used because it reflects the most common strategy for solving the group to group coupling as it is explained in the last paragraph of this chapter. By writing the system (2.5) for $\pm\vec{\Omega}$ with the same procedure illustrated for the transport equation, it is again possible to obtain the second order even parity form of the transport equation. The vacuum and reflected boundary conditions, group by group, are the same as those given in (1.25):

$$\begin{cases} \vec{\Omega}\cdot\vec{\nabla}\psi_g + \Sigma_{T,g}\phi_g = H^{+}_{g\to g}\left[\phi_g\right] + S^{+}_{g}, \\ \vec{\Omega}\cdot\vec{\nabla}\phi_g + \Sigma_{T,g}\psi_g = H^{-}_{g\to g}\left[\psi\right] + S^{-}_{g}, \\ \vec{r}\in V\subseteq R^3,\ \vec{\Omega}\in\left[-\frac{\pi}{2},\frac{\pi}{2}\right]\times[0,2\pi]. \end{cases} \tag{2.7}$$

The second equation can be solved for the odd parity flux and substituted into the first yielding one equation for the even parity component of the flux:

$$\begin{cases} \vec{\Omega}\cdot\vec{\nabla}\left(\left(L^{-}_{g\to g}\right)^{-1}\left(-\vec{\Omega}\cdot\vec{\nabla}\phi_g + S^{-}_{g}\right)\right) + L^{+}_{g\to g}\phi = S^{+}_{g} \\ \vec{r}\in V\subseteq R^3,\ \vec{\Omega}\in\left[-\frac{\pi}{2},\frac{\pi}{2}\right]\times[0,2\pi]. \end{cases} \tag{2.8}$$

The within-group $L^{\pm}_{g\to g}$ operator defined by $L^{\pm}_{g\to g} = \Sigma_{T,g} - H^{\pm}_{g\to g}[\ ]$ was introduced to compact the notation. The inversion of the $L^{-}_{g\to g}$ operator can be performed exactly as done in 1.4 (the homogenization process has no effect in angle under the factorization hypothesis). In the next paragraphs the process of discretizing equation (2.8) with respect to the space and angle variables will be shown. Unless explicitly stated, the derivation continues from here with the within group equation and the group index is dropped for simplicity.

II.2. The Spatial Discretization

The VARIANT code uses a hybrid primal finite element method to discretize the spatial dependence [24-26]. As is typical of the finite element method, the spatial domain (homogenized) is split into non-overlapping regions with constant material proprieties.

V_i open, $V_i \in V$,

$V_i \cap V_l = 0 \leftrightarrow l \neq i$,

$\bar{V} = \bigcup_{i=1}^{I} \bar{V}_i$,

$\Gamma = \bigcup_{i=1}^{I} \partial V_i$.

The hybrid terminology is derived from the means by which the finite elements are coupled together. First, a functional is derived which defines the Euler-Lagrange equation as the second order within group even parity transport equation. Within each finite element a standard Rayleigh-Ritz procedure is applied. In this type of formulation the natural boundary conditions become a relation between two different unknown functions $\vec{\Omega} \cdot \vec{\nabla} \phi = -L^{-}[\chi] + S^{-}$ that is applied on the surface of each element. This type intra-nodal coupling enforces the continuity of the directional derivative ($\vec{\Omega} \cdot \vec{\nabla}$) on the surface. The strong form is maintained along the interface for the odd parity flux (two adjacent elements share the same interface odd parity flux). An additional set of constraints is added to enforce continuity of the even parity flux between adjacent elements in a weak form using a Petrov-Galerkin method. The appropriate test function for this additional set of constraints is the odd parity interface flux (it is the only one having strong continuity at the interface). This result could be obtained by using the Lagrange multipliers method which is why the odd parity flux is often viewed as the Lagrange multiplier of the even parity flux weak continuity constraint. This kind of intra-nodal boundary conditions on the odd parity flux has the characteristic of enforcing the balance in a strong form but with the drawback of inserting a surface unknown that is the odd parity flux over ∂V_i. Starting from this hybrid weak formulation of the problem, it is possible to construct a functional having a unique saddle-point [27] which corresponds to the solution of the Euler-Lagrange equation for equation (2.8) .

The result is the following functional:

$$F\left[\phi,\psi,\phi_{Vac}\right]=$$
$$\sum_{i=1}^{I}\left\{\int_{V_i}dV\int_{4\pi}d\vec{\Omega}\left[\left(L^{-}\right)^{-1}\left(\vec{\Omega}\vec{\nabla}\phi\right)^{2}+L^{+}\phi^{2}-2\phi S^{+}-2\vec{\Omega}\vec{\nabla}\left(\phi\right)\left(L^{-}\right)^{-1}S^{-}\right]+2\int_{\substack{\partial V_i\neq\\ \partial V_{Vacuum}}}dl\int_{4\pi}d\vec{\Omega}\left[\vec{n}\cdot\vec{\Omega}\phi\psi\right]\right\}+$$
$$\int_{\partial V_{Vacuum}}dl\int_{4\pi}d\vec{\Omega}\left[\vec{n}\cdot\vec{\Omega}\phi_{Vac}^{2}-2\vec{n}\cdot\vec{\Omega}\phi_{Vac}\psi\right].$$

(2.9)

Since the functional is imposed separately upon each finite element, detailed inspection of the method only needs to be carried out for the application to a single finite element F_v where the region index is omitted:

$$F_v=\int_{V}dV\int_{4\pi}d\vec{\Omega}\left[\left(L^{-}\right)^{-1}\left(\vec{\Omega}\vec{\nabla}\phi\right)^{2}+L^{+}\phi^{2}-2\phi S^{+}-2\vec{\Omega}\vec{\nabla}\left(\phi\right)\left(L^{-}\right)^{-1}S^{-}\right]+2\int_{\partial V}dl\int_{4\pi}d\vec{\Omega}\left[\vec{n}\cdot\vec{\Omega}\phi\psi\right].$$

(2.10)

The unknown quantities of the functional, the even parity flux over the volume and the odd parity flux along the surface, are approximated using an orthonormal set of polynomials.. These orthornormal polynomial trial functions are constructed along the boundary of and within the hybrid finite element using the Gram-Schmidt procedure [28]. From the literature, this hybrid finite element is typically referred to as a node and consequently, the quantities are defined as intra-nodal.

For the quantities inside of the volume, ϕ, S^{+} and S^{-}, we obtain the following general intra-nodal expansion for each generic unknown $z\left(\vec{r},\vec{\Omega}\right)$, where z is interchangeable with ϕ, S^{+} and S^{-} :

$$z\left(\vec{r},\vec{\Omega}\right)=\sum_{\alpha=0}^{N_\alpha}f_\alpha\left(\vec{r}\right)z_\alpha\left(\vec{\Omega}\right),\tag{2.11}$$

$f_\alpha\left(\vec{r}\right)$ is the set of orthonormal polynomials of order α within the volume and $z_\alpha\left(\vec{\Omega}\right)$ are the associated moments of the $z\left(\vec{r},\vec{\Omega}\right)$ function for $f_\alpha\left(\vec{r}\right)$. N_α is the total number of

polynomials defined in the volumetric set. The odd parity flux for each surface of the node is defined as:

$$\psi\left(\vec{r},\vec{\Omega}\right)=\sum_{\beta=0}^{N_\beta}h_\beta\left(\vec{r}\right)\psi_\beta\left(\vec{\Omega}\right). \tag{2.12}$$

$h_\beta\left(\vec{r}\right)$ is the orthonormal set of polynomials of order β along the surface while $\chi_\beta\left(\vec{\Omega}\right)$ are the associated moments of the odd parity flux for $h_\alpha\left(\vec{r}\right)$. N_β is the total number of polynomials defined along each surface of the node.

As can be inferred, these expansions are used for describing the spatial dependence of the even and odd parity fluxes within each node and along the surfaces of the node. Constraints exist on the intra-nodal expansion order and the surface expansion order due to the LBB (Ladyzhenskaya, Babuska, Brezzi) condition of the discrete form of the problem [32, 33]. This constraint primarily does not allow the intra-nodal expansion order to be less than that of the surface order. The expansion order used to define the intra-nodal unknown quantities leads to the following number of moments where *gr* is the expansion:

intra-nodal expansion 3D: $N_\alpha=\frac{gr+1}{2}\left(gr+2\right)\frac{gr+3}{3}$,

intra-nodal expansion 2D: $N_\alpha=\frac{gr+1}{2}\left(gr+2\right)$,

surface expansion 3D: $N_\beta=\frac{gr+1}{2}\left(gr+2\right)$,

surface expansion 2D: $N_\beta=gr+1$.

A general inspection of the spatial dependence of the operators $L^{\pm}$ shows that they are constant in space and thus constant in the functional (2.10).

II.3. The Angular Discretization by the Method of Spherical Harmonics

One method used to approximate the angular dependence of the unknown quantities is the Spherical Harmonics method (P_N) [36 to 40]. This approximation uses the set of spherical harmonics which form a complete basis on the surface of a unit sphere. The spherical harmonics used in VARIANT are a modified version of the classic cosine and sine series definition given as:

$$\begin{cases} Y_{p,q}\left(\vec{\Omega}\right) = \sqrt{\left(2-\delta_{p,0}\right)\alpha_p^q}\, C_{p,q} P_{p,q}\left(\mu\right)\cos\left(q\omega\right), & q \geq 0, \\ Y_{p,-q}\left(\vec{\Omega}\right) = \sqrt{2\alpha_p^q}\, C_{p,q} P_{p,q}\left(\mu\right)\sin\left(p\omega\right), & q>0, \end{cases} \quad \text{with} \begin{cases} p=0,1,....N, \\ |q|=0,1,...p, \end{cases} \tag{2.13}$$

$P_{p,q}\left(\mu\right)$ are the associate Legendre polynomials defined by:

$$P_{p,q} = \left(1-\mu^2\right)^{q/2} \frac{\partial^q P_p\left(\mu\right)}{\partial \mu^q}, \tag{2.14}$$

$\mu = \cos\left(\phi\right)$ where ϕ is the polar angle and ω is the azimuth angle. The normalization coefficients α_p^q are defined as:

$$\alpha_p^q = \frac{\left(p-q\right)!}{\left(p+q\right)!}, \tag{2.15}$$

while the coefficients $C_{p,q}$ are selected such that:

$$\int_{4\pi} d\vec{\Omega} Y_{p',q'}\left(\vec{\Omega}\right) Y_{p,q}\left(\vec{\Omega}\right) = \delta_{p',p}\delta_{q',q}, \tag{2.16}$$

producing

$$C_{p,q} = \sqrt{\frac{2p+1}{4\pi}}\,. \tag{2.17}$$

For practical purposes, the functions are put into standard vector form where the spherical harmonic functions are ordered as follows:

$$\left\{g^{m+}\right\}=\left[Y_{0,0},Y_{2,-2},Y_{2,-1},Y_{2,0},Y_{2,1},Y_{2,2},Y_{4,4},....\right] \quad \text{even harmonics,}$$
$$\left\{g^{m-}\right\}=\left[Y_{1,-1},Y_{1,0},Y_{1,1},Y_{3,-3},Y_{3,-2},Y_{3,-1},Y_{3,0},Y_{3,1},Y_{3,2},Y_{3,3},Y_{5,-5},....\right] \quad \text{odd harmonics.} \tag{2.18}$$

For the odd parity flux on the finite element surface, the reduced odd parity set of spherical harmonics are used:

$$\left\{K^{\ell}\right\}=\left[Y_{1,0},Y_{3,-2},Y_{3,0},Y_{3,1},Y_{3,2},Y_{5,-4},....\right]. \tag{2.19}$$

For general interface conditions, it has been shown that this odd parity set of functions (without taking in account eventually surface sources) must obey the Rumyantsev [33, 35, 38] interface conditions. These conditions are generally simple when applied for a plane perpendicular to the polar direction, but for the azimuthal and general rotated systems, the solution is very complex. Given that all of the nodes used to define the problem domain have the same surface orientation, the odd parity functions are rotated such that the polar angle is always aligned with the outward normal from each surface. This allows the Rumyantsev conditions to be directly applied to the generic set of odd parity functions of a given order. The selected odd parity spherical harmonics shown in (2.18) have been found to be compliant with the Rumyantsev interface conditions for the second order even-parity transport equation, although they are not strictly those imposed by the Rumyantsev interface condition [38].

The order of the P_N approximation is given by the value of *p* at which the expansion set is cut. For q, it is always complete within the volume such that $-p <= q <= +p$ while along the surface, $-p+1 <= q <= q +p-1$. It has been shown [36, 38] that the set of functions shown requires an odd order value of *p* leading to a full even parity set of spherical harmonics used internally to the node of order $p-1$ and a truncated set (Rumyantsev) of odd parity functions of order *p* used along the surfaces of the node.

Combining the spatial and angular expansions yields the following expansions for the nodal unknowns:

$$\begin{aligned}
\phi\left(\vec{r},\vec{\Omega}\right) &= \sum_{\alpha} f_{\alpha}\left(\vec{r}\right) \sum_{m+} \mathrm{g}^{\mathrm{m+}}\left(\vec{\Omega}\right) \phi_{\alpha,m+}, \\
S^{+}\left(\vec{r},\vec{\Omega}\right) &= \sum_{\alpha} f_{\alpha}\left(\vec{r}\right) \sum_{m+} \mathrm{g}^{\mathrm{m+}}\left(\vec{\Omega}\right) S^{+}_{\alpha,m+}, \\
S^{-}\left(\vec{r},\vec{\Omega}\right) &= \sum_{\alpha} f_{\alpha}\left(\vec{r}\right) \sum_{m+} \mathrm{g}^{\mathrm{m-}}\left(\vec{\Omega}\right) S^{-}_{\alpha,m-}, \\
\psi\left(\vec{r},\vec{\Omega}\right) &= \sum_{\beta} h_{\beta}\left(\vec{r}\right) \sum_{\ell} K^{\ell}\left(\vec{\Omega}\right) \psi_{\beta,\ell}.
\end{aligned} \tag{2.20}$$

For a *N*th order expansion, the total number of unknowns derived from the angular approximation are given as:

even parity functions intra-nodal 3D: $N\left(N+1\right)/2$,

odd parity functions intra-nodal 3D: $\left(N/2+1\right)\left(N+1\right)$,

even parity functions intra-nodal 2D: $\left(\frac{N+1}{2}\right)^{2}$,

odd parity functions intra-nodal 2D: $\left(\frac{N+1}{2}\right)\left(\frac{N+3}{2}\right)$,

odd parity functions interface 3D: $N\left(N+1\right)/2$,

odd parity functions interface 2D: $\left(\frac{N+1}{2}\right)^{2}$,

Not only do the unknowns need to be expanded using the preceding trial functions but the $L^{\pm}$ operators [26] must also be expanded with respect to angle. By means of the addition theorem for Legendre polynomials:

$$P_{p}\left(\vec{\Omega}\cdot\vec{\Omega}'\right) = \sum_{|q|=0}^{p} Y_{p,q}\left(\vec{\Omega}\right) Y_{p,q}\left(\vec{\Omega}'\right). \tag{2.21}$$

Inserting this expansion into (1.22) and (1.23) produces:

$$\Sigma_s(\mu)=\sum_{p=0}^{\infty}(2p+1)\Sigma_{s,p}\sum_{|q|=0}^{p}Y_{p,q}(\vec{\Omega})Y_{p,q}(\vec{\Omega}'),$$

$$L^{-}[\ ]=\Sigma_T-\sum_{\substack{p=0\\ p:odd}}^{\infty}(2p+1)\Sigma_{s,p}\sum_{|q|=0}^{p}Y_{p,q}(\vec{\Omega})\int_{4\pi}d\vec{\Omega}'Y_{p,q}(\vec{\Omega}')[\ ], \tag{2.22}$$

$$(L^{-})^{-1}[\ ]=\frac{1}{\Sigma_T}-\sum_{\substack{p=0\\ p:odd}}^{\infty}(2p+1)\frac{\Sigma_{s,p}}{\Sigma_T}\frac{1}{(\Sigma_T-\Sigma_{s,p})}\sum_{|q|=0}^{p}Y_{p,q}(\vec{\Omega})\int_{4\pi}d\vec{\Omega}'Y_{p,q}(\vec{\Omega}')[\ ],$$

and for the L^{+}:

$$(L^{+})[\ ]=\Sigma_T-\sum_{\substack{p=0\\ p:even}}^{\infty}(2p+1)\Sigma_{s,p}\sum_{|q|=0}^{p}Y_{p,q}(\vec{\Omega})\int_{4\pi}d\vec{\Omega}'Y_{p,q}(\vec{\Omega}')[\ ]. \tag{2.23}$$

After the expansions (2.8) defined by (2.20), (2.22) and (2.23) are inserted into the functional (2.9) it is possible to investigate variations of the unknowns which will force the functional to be stationary. This process provides the algebraic system needed for the solution of the unknown moments. The solution algorithm of the algebraic system is beyond the scope of this thesis, but it is easy to imagine that a direct method for such a large system of equation is impractical [40 to 43]. For 3D reactor analysis, a typical rectangular mesh implementing a 4th order intra-nodal spatial expansion, a 2nd order spatial surface expansion and P_3 angular approximation leads to 99 moments per node. When combined with the number of nodes needed to model a typical reactor (hundreds) and the number of energy groups (tens), this yields a system of equations with almost 100000 unknowns.

II.4. The Angular Discretization by the Method of Simplified Spherical Harmonics

The simplified spherical harmonics method (SP_N) was developed in the early 1960s [44, 45]. It has been widely used in reactor calculations [46, 47] and radiation transport problems [48 to 50]. The mathematical derivation of this method is not rigorous, although it has been proven that the SP_N methodology is able to produce an asymptotic solution of the rigorous solution of the neutron transport equation [51]. An alternative approach to deriving the simplified spherical

harmonics equations [52] has been achieved by using a truncated Neumann series of a rescaled $\vec{\Omega}\cdot\vec{\nabla}$ operator. Although this last approach does seem to be the best one for providing a solid mathematical basis of the SP_N method, as pointed out in [53], the convergence of the Neumann series is not assured since the operator is unbounded. Even if the SP_N method is somewhat based upon the P_N method (the original derivation starts from the one-dimensional P_N equations) there is a substantial difference in the mathematical approach. In fact the P_N method is based upon an approximation of the neutron angular flux while the SP_N is based on an approximation of the operator acting upon the neutron angular flux. This methodology has shown, nevertheless, a great capability to reduce the computational time without resulting in a significant loss of accuracy for the problems dealing with homogenized material distribution which are typical of reactor analysis.

The derivation shown here, is an extension of the original one which can be found in [44] and extended to higher SP_N order for the VARIANT code [54].

To begin, the one-dimensional transport equation is considered in one dimension $\vec{r} = x$. The angular dependence $(\omega,\ \theta)$ is reduced to a one-dimensional space since the solution contains symmetry with respect to the azimuth angle ω. Note that in this case polar axis is assumed to be aligned with the primary spatial axis. These considerations reduce the dependences as follows: $\left(\vec{r},\vec{\Omega}\right)\rightarrow\left(x,\theta\right)$. The corresponding within group equation for (1.16) in the one-dimensional system is given by:

$$\begin{cases}\cos\left(\theta\right)\cdot\partial_x\psi\left(x,\theta\right)+L^{+}\left[\phi\right]\left(x,\theta\right)=S^{+}\left(x,\theta\right),\\ \cos\left(\theta\right)\cdot\partial_x\phi\left(x,\theta\right)+L^{-}\left[\psi\right]\left(x,\theta\right)=S^{-}\left(x,\theta\right).\end{cases} \tag{2.24}$$

For practical purpose a change of variable is made where $\theta\rightarrow\mu=\cos\left(\theta\right)$:

$$\begin{cases}\mu\partial_x\psi\left(x,\mu\right)+L^{+}\left[\phi\right]\left(x,\mu\right)=S^{+}\left(x,\mu\right),\\ \mu\partial_x\phi\left(x,\mu\right)+L^{-}\left[\psi\right]\left(x,\mu\right)=S^{-}\left(x,\mu\right).\end{cases} \tag{2.25}$$

For the SP_N method, it is at this point that a formal transformation is applied to construct a three-dimensional structure.

This transformation makes the following assumptions:

$$\begin{aligned}
&\phi(x,\mu)\to\phi(\vec{r},\mu),\\
&\psi(x,\mu)\to\psi(\vec{r},\mu),\\
&L^{+}[\ ](x,\mu)\to L^{+}[\ ](\vec{r},\mu),\\
&L^{-}[\ ](x,\mu)\to L^{-}[\ ](\vec{r},\mu),\\
&S^{+}(x,\mu)\to S^{+}(\vec{r},\mu),\\
&S^{-}(x,\mu)\to S^{-}(\vec{r},\mu).
\end{aligned} \tag{2.26}$$

The odd parity quantities become three-dimensional vectors, except for the $L^{-}[\ ]$ operator which is physically invariant under rotation:

$$\begin{aligned}
&\psi(\vec{r},\mu)\to\vec{\psi}(\vec{r},\mu),\\
&S^{-}(\vec{r},\mu)\to\vec{S}^{-}(\vec{r},\mu).
\end{aligned} \tag{2.27}$$

The derivative with respect to x is replaced by $\vec{\nabla}$, the gradient operator, when acting upon even parity quantities and by $\vec{\nabla}\cdot$, the divergence operator, when acting upon odd parity quantities. This produces the final system of equations:

$$\begin{cases}
\mu\vec{\nabla}\cdot\vec{\psi}(\vec{r},\mu)+L^{+}[\phi](\vec{r},\mu)=S^{+}(\vec{r},\mu),\\
\mu\vec{\nabla}\phi(\vec{r},\mu)+L^{-}[\vec{\psi}](\vec{r},\mu)=\vec{S}^{-}(\vec{r},\mu).
\end{cases} \tag{2.28}$$

This equation combined with the two equations of (2.24) yields the second order even parity SP_N transport equation:

$$\begin{aligned}
\mu\vec{\nabla}\left(\left(L^{-}\right)^{-1}\left[-\mu\vec{\nabla}\cdot\phi+\vec{S}^{-}\right](\vec{r},\mu)\right)+\Sigma_T(\vec{r},\mu)\phi(\vec{r},\mu)=\\
=H^{+}[\phi](\vec{r},\mu)+S^{+}(\vec{r},\mu).
\end{aligned} \tag{2.29}$$

It is important to note that the inversion of the L^{-} operator which makes use of the addition theorem for the Legendre polynomial must be reformulated to account for the reduced angular dependence.

$$P_p(\mu\cdot\mu')=Y_{p,0}(\mu)Y_{p,0}(\mu'). \tag{2.30}$$

The Legendre polynomials and the spherical harmonics of order p,0 are the same functions used previously, except the normalization coefficients are changed to $\sqrt{\frac{2p+1}{4\pi}}$ (refer to equation (2.13)):

$$P_p(\mu\cdot\mu') = \frac{2p+1}{4\pi} P_p(\mu) P_p(\mu'). \tag{2.31}$$

This simplifies the expression of $L^{\pm}$:

$$\begin{aligned} L^-[\ ] &= \Sigma_T - \sum_{\substack{p-=0 \\ p-:\,odd}}^{\infty} \frac{(2p_-+1)^2}{2} \Sigma_{s,p-} P_{p-}(\mu) \int_{-1}^{1} d\mu' P_{p-}(\mu')[\ ], \\ L^+[\ ] &= \Sigma_T - \sum_{\substack{p+=0 \\ p+:\,even}}^{\infty} \frac{(2p_++1)^2}{2} \Sigma_{s,p+} P_{p+}(\mu) \int_{-1}^{1} d\mu' P_{p+}(\mu')[\ ], \end{aligned} \tag{2.32}$$

and the inverted L^-:

$$\left(L^-\right)^{-1}[\ ] = \frac{1}{\Sigma_T} - \sum_{\substack{p-=0 \\ p-:\,odd}}^{\infty} \frac{(2p_-+1)^2}{2} \frac{\Sigma_{s,p-}}{\Sigma_T} \frac{1}{\left(\Sigma_T - \Sigma_{s,p-}\right)} P_{p-}(\mu) \int_{-1}^{-1} d\mu' P_{p-}(\mu')[\ ], \tag{2.33}$$

given in (2.21). The even parity quantities (neutron flux and source) can be expanded as follows:

$$\begin{aligned} \varphi(x,\mu) &= \sum_{\substack{p+=0 \\ p+\ even}}^{\infty} (2p_++1) P_{p+}(\mu) \varphi_{p+}(\vec{r}), \\ S^+(x,\mu) &= \sum_{\substack{p+=0 \\ p+\ even}}^{\infty} (2p_++1) P_{p+}(\mu) q_{p+}(\vec{r}). \end{aligned} \tag{2.34}$$

The odd parity quantities, now being vector quantities, are expanded as follows:

$$\begin{aligned} \vec{\chi}(\vec{r},\mu) &= \sum_{\substack{p-=0 \\ p-\ \mathrm{odd}}}^{\infty} (2p_-+1) P_{p-}(\mu) \left(\chi^x_{p-}(\vec{r}), \chi^y_{p-}(\vec{r}), \chi^z_{p-}(\vec{r})\right), \\ \vec{S}^-(\vec{r},\mu) &= \sum_{\substack{p-=0 \\ p-\ \mathrm{odd}}}^{\infty} (2p_-+1) P_{p-}(\mu) \left(S^{-,x}_{p-}(\vec{r}), S^{-'y}_{p-}(\vec{r}), S^{-,z}_{p-}(\vec{r})\right). \end{aligned} \tag{2.35}$$

The equation (2.29) is formally equivalent to equation (2.8) thereby leading to the same functional as (2.10) where the angular projection over $\vec{\Omega}$ is replaced by $\frac{1}{2}\int_{-1}^{-1} d\mu$ with the following changes to the boundary integral:

$$\begin{aligned} &\vec{\Omega} \to \mu, \\ &\psi\left(\vec{r},\vec{\Omega}\right) \to \vec{\psi}\left(\vec{r},\mu\right). \end{aligned} \tag{2.36}$$

As in the P_N method the expansion provided by (2.35), (2.34) in conjunction with the spatial expansion are inserted into the SP_N functional. Forcing variations in the even and odd parity fluxes to be stationary yields a well posed algebraic system of equations for the moments of the approximating functions. Compared with the P_N method, the number of angular unknowns in the SP_N method is substantially reduced. For an expansion of order N, where N is again odd, the angular approximations yield:

even functions intra-nodal 3D: $(N+1)/2$,

odd functions intra-nodal 3D: $3(N+1)/2$,

even functions intra-nodal 2D: $(N+1)/2$,

odd functions intra-nodal 2D: $(N+1)$,

odd functions interface 3D: $(N+1)/2$,

odd functions interface 2D: $(N+1)/2$,

II.5. The Multi-Group Strategy

As already mentioned the coupling between the within-group equations is done by the source terms that contain contribution from down- and up-scattering and fission happening in other energy groups plus of course a possibly present external source.

Therefore it possible to write the following expression for the within odd and even group sources (for group g):

$$\begin{aligned} S_g^+\left(\vec{r},\vec{\Omega}\right) &= \sum_{\substack{g'=1 \\ g'\neq g}}^{NG} H_{g'\to g}^+\left[\phi_{g'}\right]\left(\vec{r},\vec{\Omega}\right) + \sum_{g'=1}^{NG} F_{g'\to g}\left[\phi_{g'}\right]\left(\vec{r},\vec{\Omega}\right) + S_{ext,g}^+\left(\vec{r},\vec{\Omega}\right) \\ S_g^-\left(\vec{r},\vec{\Omega}\right) &= \sum_{\substack{g'=1 \\ g'\neq g}}^{NG} H_{g'\to g}^-\left[\psi_{g'}\right]\left(\vec{r},\vec{\Omega}\right) \end{aligned} \tag{2.37}$$

As can be noticed, there is no odd external source in (2.37) because up to now such an option has not been available among the VARIANT capabilities. It turns out that this kind of coupling in conjunction with the solution scheme based on the second order even equation shows a clear problem: the intra-nodal odd source is related to the intra-nodal odd flux which is a quantity not taken in account by the within-group second order form of transport equation. To overcome this difficulty, the intra-nodal odd flux is expressed by means of the inversion of the second equation of the system (2.7) leading to a new expression for the within-group source:

$$\begin{aligned} S_g^+\left(\vec{r},\vec{\Omega}\right) &= \sum_{\substack{g'=1 \\ g'\neq g}}^{NG} H_{g'\to g}^+\left[\phi_{g'}\right]\left(\vec{r},\vec{\Omega}\right) + \sum_{g'=1}^{NG} F_{g'\to g}\left[\phi_{g'}\right]\left(\vec{r},\vec{\Omega}\right) + S_{ext,g}^+\left(\vec{r},\vec{\Omega}\right), \\ S_g^-\left(\vec{r},\vec{\Omega}\right) &= \sum_{\substack{g'=1 \\ g'\neq g}}^{NG} H_{g'\to g}^-\left[\left(L_{g'\to g'}^-\right)^{-1}\left(-\vec{\Omega}\cdot\vec{\nabla}\phi_{g'} + S_{g'}^-\right)\right]\left(\vec{r},\vec{\Omega}\right). \end{aligned} \tag{2.38}$$

Both these source components represent an energy coupling between groups. In fact in order to compute the source for the g-th group it is necessary to know the even flux moments and odd source (both up to the scattering order) for all the groups for which, respectively, the $H_{g'\to g}^+$ and $H_{g'\to g}^-$ are not zero. In order to better understand the type of coupling arising from the scattering source is generally preferable to refer to the matrix representation of the scattering operator (discretized in energy): $\underline{\underline{H}}_{g'\to g}^{\pm} = \left\{H_{g',g}^{\pm}\right\}$ (double underlining stands for a matrix entity). In a fast reactor usually this matrix is of lower triangular type (with a very low bandwidth if no light elements are present). In reactor types with essentially thermal neutron spectrum it is possible to have a non-zero area also in the lower right side of the matrix. The reason for such

structure is that as long as the neutron kinetic energy is higher than the average thermodynamic energy of the surrounding media, neutron moderation will happen, i.e. in a collision the neutron will either remain in the same energy group or will be scattered down to a lower energy group. On the other hand, when the neutron kinetic energy is almost the same as the average thermodynamic energy of the collision target, the neutron could gain energy during a scattering process. The physical interpretation of the scattering matrix suggests that the lower triangular component will be, in any case of interest for the physics of reactors, dominant. This last consideration suggests that an optimal numerical inversion of this matrix could be achieved by a Gauss-Seidel algorithm that in case of a pure lower triangular matrix is reduced to a direct inversion. Another group coupling arises from the presence of the fission operator. The neutron production operator, F, i.e. the fission spectrum and the fission cross section are such that they tend to strongly couple the last energy groups with the uppermost ones. This fact unfortunately tends to decrease slightly the efficiency of the Gauss-Seidel scheme. The general scheme could be summarized as follows: the within-group equation for the highest energy group is solved first using a guess for the source (usually it is coupled with the other groups just by the fission source), then the process goes down in energy using the flux in the already solved energy group to update the down scattering source. Once the last group is reached a new fission source is available and the process is repeated until convergence.

II.6. Time Discretization by the Direct Method

In this section the time dependent scheme used by KIN3D [55] before this thesis is displayed with some minor modification. The first step is to create a time dependent system formally equivalent to the steady state one (1.16) that can be solved by means of the VARIANT code. To achieve this, it is necessary to start from the first equation of the system (1.12). As done before, in the steady state case, the equations of system (1.12) are written for plus and minus $\vec{\Omega}$. The two resulting equations are once subtracted and once added to each other and even and odd parity quantities are introduced.

Observing that the delayed neutron source is isotropic, after these manipulations the final equations could be written as the following system:

$$\begin{cases} \dfrac{1}{u}\partial_t\phi + \vec{\Omega}\cdot\vec{\nabla}\psi + \Sigma_T\phi = H^+[\phi] + S^+ + F_p[\phi] + \sum_{i=1}^{NF}\chi_{i,g}\lambda_i C_i, \\ \dfrac{1}{u}\partial_t\psi + \vec{\Omega}\cdot\vec{\nabla}\phi + \Sigma_T\psi = H^-[\psi], \\ \partial_t C_i = -\lambda_i C_i + \beta_i\int_0^\infty dE'\nu\Sigma_f\int_{4\pi} d\vec{\Omega}'\phi \qquad i = 1,.....,N.family, \end{cases} \tag{2.39}$$

where the boundary conditions and domain definitions are omitted and the dependences and the quantities are the same as those of (1.12).

In the system (2.39) the odd component of the external source has been neglected in the original version of KIN3D since it could not be treated by the VARIANT flux solver existing at that time. To compact the notation, a production operator is introduced, defined by:

$$P[\ ](\vec{r},\vec{\Omega},E,t) = \int_0^\infty dE'\nu(\vec{r},E',t)\Sigma_f(\vec{r},E',t)\int_{4\pi} d\vec{\Omega}'[\ ]. \tag{2.40}$$

Inserting this inside the prompt fission operator we obtain the following relation:

$$\begin{aligned} &F_p[\ ](\vec{r},\vec{\Omega},E,t) = \\ &= \chi_p(\vec{r},E,t)\left[P[\ ](\vec{r},\vec{\Omega},E,t) - \int_0^\infty dE'\nu(\vec{r},E',t)\beta(\vec{r},E',t)\Sigma_f(\vec{r},E',t)\int_{4\pi} d\vec{\Omega}'[\ ]\right], \end{aligned} \tag{2.41}$$

under the assumption that $\beta(\vec{r},E',t) \approx \beta(\vec{r},t)$ (this simplifying assumption is sometimes disregarded in a more general treatment):

$$F_p[\ ](\vec{r},\vec{\Omega},E,t) = \chi_p(\vec{r},E,t)(1-\beta(\vec{r},t))P[\ ](\vec{r},\vec{\Omega},E,t). \tag{2.42}$$

Using these new operators, the system (2.39) becomes:

$$\begin{cases} \dfrac{1}{u}\partial_t\phi + \vec{\Omega}\cdot\vec{\nabla}\psi + \Sigma_T\phi = H^+[\phi] + S^+ + \chi_p(1-\beta)P[\phi] + \sum_{i=1}^{NF}\chi_i\lambda_i C_i, \\ \dfrac{1}{u}\partial_t\psi + \vec{\Omega}\cdot\vec{\nabla}\phi + \Sigma_T\psi = H^-[\psi], \\ \partial_t C_i = -\lambda_i C_i + \beta_i P[\phi]. \end{cases} \tag{2.43}$$

The original direct time discretization scheme was based on the assumption that the time derivative of the odd component of the flux is negligible. The physical interpretation of this approximation will be clarified later, by comparison with the new time discretization scheme which is introduced in this thesis work. The time integration scheme is based on a first order backward Euler scheme of the first equation of system (2.39), a mixed Crank-Nicholson (with respect to the fission source) and exact (with respect to the precursor concentration) integration scheme in the 3rd equation. The scheme could be described with the following approximations (right superscript indicates the time interval):

$$\begin{aligned} &\frac{1}{u}\partial_t\phi\big|_{i+1} \approx \frac{{}^{i+1}\phi - {}^{i}\phi}{u\Delta t_{i+1}}, \\ &\frac{1}{u}\partial_t\psi\big|_{i+1} \approx 0, \\ &\beta_i P[\phi](t_i \le t \le t_{i+1}) \approx {}^{i}\beta_i\,{}^{i}P\left[{}^{i}\phi\right] + \frac{{}^{i+1}\beta_i\,{}^{i+1}P\left[{}^{i+1}\phi\right] - {}^{i}\beta_i\,{}^{i}P\left[{}^{i}\phi\right]}{\Delta t_{i+1}}(t_{i+1}-t). \end{aligned} \tag{2.44}$$

This scheme leads to:

$$\begin{cases} \dfrac{1}{u}\dfrac{{}^{i+1}\phi - {}^{i}\phi}{\Delta t_{i+1}} + \vec{\Omega}\cdot\vec{\nabla}\,{}^{i+1}\psi + {}^{i+1}\Sigma_T\,{}^{i+1}\phi = {}^{i+1}H^+\left[{}^{i+1}\phi\right] + {}^{i+1}S^+ + \\ + {}^{i+1}\chi_p\left(1-{}^{i+1}\beta\right){}^{i+1}P\left[{}^{i+1}\phi\right] + \sum_{i=1}^{NF}{}^{i+1}\chi_i\,{}^{i+1}\lambda_i\,{}^{i+1}C_i, \\ \vec{\Omega}\cdot\vec{\nabla}\,{}^{i+1}\phi + {}^{i+1}\Sigma_T\,{}^{i+1}\psi = {}^{i+1}H^-\left[{}^{i+1}\psi\right], \\ {}^{i+1}C_i e^{\lambda_i t_{i+1}} - e^{\lambda_i t_i}\,{}^{i}C_i = \int_{t_i}^{t_{i+1}} dt e^{\lambda_i t}\left({}^{i}\beta_i\,{}^{i}P\left[{}^{i}\phi\right] + \dfrac{{}^{i+1}\beta_{i+1}\,{}^{i+1}P\left[{}^{i+1}\phi\right] - {}^{i}\beta_i\,{}^{i}P\left[{}^{i}\phi\right]}{\Delta t_{i+1}}(t_{i+1}-t)\right), \end{cases} \tag{2.45}$$

where $\Delta t_{i+1} = t_{i+1} - t_i$. Now the exact integration of the equation for precursor concentration [55] leads to an expression for ${}^{i+1}C_i$ as a linear functional of ${}^{i+1}\phi$ of the form: ${}^{i+1}C_i = {}^{i+1}a_i + {}^{i+1}c_i\left[{}^{i+1}\phi\right]$. By insertion of this expression in the first equation of the system one obtains:

$$\begin{aligned}&\frac{1}{u}\frac{{}^{i+1}\phi - {}^{i}\phi}{\Delta t_{i+1}} + \vec{\Omega}\cdot\vec{\nabla}\,{}^{i+1}\psi + {}^{i+1}\Sigma_T\,{}^{i+1}\phi = {}^{i+1}H^+\left[{}^{i+1}\phi\right] + {}^{i+1}S^+ + \\ &+ {}^{i+1}\chi_p\left(1 - {}^{i+1}\beta\right){}^{i+1}P\left[{}^{i+1}\phi\right] + \sum_{i=1}^{NF}{}^{i+1}\chi_i\lambda_i\left({}^{i+1}a_i + {}^{i+1}c_i\,{}^{i+1}[\phi_i]\right).\end{aligned} \tag{2.46}$$

At this point it is usual to define modified operators to recast equation (2.46) in a form formally equivalent to the first equation of the system (1.13).

$$\begin{aligned}&{}^{i+1}\tilde{\Sigma}_T = {}^{i+1}\Sigma_T + \frac{1}{u\Delta t_{i+1}},\\ &{}^{i+1}\tilde{S}^+ = {}^{i+1}S^+ + \frac{1}{u}\frac{{}^{i}\phi}{\Delta t_{i+1}} + \sum_{i=1}^{NF}{}^{i+1}\chi_i\lambda_i\,{}^{i+1}a_i,\\ &{}^{i+1}\tilde{\chi}_p = {}^{i+1}\chi_p\left(1 - {}^{i+1}\beta\right),\\ &{}^{i+1}P[\ ] = P\left(t_{i+1}\right),\\ &{}^{i+1}\tilde{F}[\ ] = \left({}^{i+1}\tilde{\chi}_p\,{}^{i+1}P + \sum_{i=1}^{NF}{}^{i+1}\chi_i\lambda_i\,{}^{i+1}c_i\,{}^{i+1}\right)[\ ]\left(\vec{r},\vec{\Omega},E\right).\end{aligned} \tag{2.47}$$

In the remainder of this section, $\frac{1}{u\Delta t_{i+1}}$ will be referred as the time absorption term and $\frac{1}{u}\frac{{}^{i}\phi}{\Delta t_{i+1}}$ as the time source term.

Using these definitions, the system (2.45) can be reformulated in the following way:

$$\begin{cases}\vec{\Omega}\cdot\vec{\nabla}\,{}^{i+1}\psi + {}^{i+1}\tilde{\Sigma}_T\,{}^{i+1}\phi = {}^{i+1}H^+\left[{}^{i+1}\phi\right] + {}^{i+1}\tilde{S}^+ + {}^{i+1}\tilde{F}\left[{}^{i+1}\phi\right],\\ \vec{\Omega}\cdot\vec{\nabla}\,{}^{i+1}\phi + {}^{i+1}\Sigma_T\,{}^{i+1}\psi = {}^{i+1}H^-\left[{}^{i+1}\psi\right].\end{cases} \tag{2.48}$$

This is formally equivalent to (1.13). By means of the new definitions:

$$\begin{aligned}&{}^{i+1}L^{\pm}[\ ] = \left({}^{i+1}\Sigma_T + {}^{i+1}H^{\pm}\right)[\ ],\\ &{}^{i+1}\tilde{L}^{+}[\ ] = \left({}^{i+1}\tilde{\Sigma}_T + {}^{i+1}H^{+}\right)[\ ],\end{aligned} \tag{2.49}$$

it is possible to obtain a system in the same form of (1.24):

$$\begin{cases} \vec{\Omega}\cdot\vec{\nabla}\left(\left({}^{i+1}L^{-}\right)^{-1}\left(-\vec{\Omega}\cdot\vec{\nabla}\,{}^{i+1}\phi\right)\right)+{}^{i+1}\tilde{L}^{+}\,{}^{i+1}\phi={}^{i+1}\tilde{S}^{+}+{}^{i+1}\tilde{F}\left[{}^{i+1}\phi\right], \\ \vec{r}\in V\subseteq R^{3},\ \vec{\Omega}\in\left[-\frac{\pi}{2},\frac{\pi}{2}\right]\times[0,2\pi]; \end{cases} \tag{2.50}$$

where the boundary conditions are the same as those in (1.25) (it is assumed that the boundary conditions are constant in time). Another fundamental hypothesis is that the reactor being studied by the transient analysis is initially in a steady state mode (including its energy production and heat removal) where the initial conditions are provided by the solution of the system:

$$\begin{cases} \vec{\Omega}\cdot\vec{\nabla}\left(\left({}^{0}L^{-}\right)^{-1}\left(-\vec{\Omega}\cdot\vec{\nabla}\,{}^{0}\phi\right)\right)+{}^{0}L^{+}\,{}^{0}\phi={}^{0}S^{+}+{}^{0}F\left[{}^{0}\phi\right], \\ \lambda_i\,{}^{0}C_i={}^{0}\beta_i\,{}^{0}P\left[{}^{0}\phi\right]. \end{cases} \tag{2.51}$$

The first problem that should be solved when trying to apply a time discretization, is how to modify L^{+} without any modification of L^{-}. From the first equation of (2.48) a modified total cross section is present which is absent in the second one. If one wants to use VARIANT as a black box for the solution of a pseudo steady state problem (given by (2.50)), it is not reasonable to introduce a modification in the format of the cross section file (distinguishing between the total cross section present in the $L^{\pm}$ operators). As a consequence, the ${}^{i+1}H^{+}$ operator is modified in the following manner:

$$\begin{aligned} &\left({}^{i+1}\tilde{H}^{+}\right)[\ ]=\sum_{\substack{p=0\\ p:even}}^{\infty}(2p+1)\,{}^{i+1}\tilde{\Sigma}_{s,p}\sum_{|q|=0}^{p}Y_{p,q}\left(\vec{\Omega}\right)\int_{4\pi}d\vec{\Omega}'\,Y_{p,q}\left(\vec{\Omega}'\right)[\ ], \\ &{}^{i+1}\tilde{\Sigma}_{s,0}={}^{i+1}\Sigma_{s,0}+\frac{1}{u\Delta t_{i+1}}, \\ &{}^{i+1}\tilde{\Sigma}_{\substack{s,p\\ p\neq 0}}={}^{i+1}\Sigma_{s,p}. \end{aligned} \tag{2.52}$$

This leads to the new definition of ${}^{i+1}\tilde{L}^{+}$:

$$\left({}^{i+1}\tilde{\tilde{L}}^{+}\right)[\ ] = {}^{i+1}\Sigma_T + \left({}^{i+1}\tilde{H}^{+}\right)[\ ]. \tag{2.53}$$

In this way it was possible to modify only the zeroth order moments of the scattering kernel, when using VARIANT as a black box steady state flux solver. This approach has the advantage of acting on a component of the scattering that exists in every physical model of interest (no change between cross section file structure of the steady state analysis) and it only affects the even-parity part of the scattering kernel. Unfortunately, as was discovered in the first part of this thesis, this scheme is unbalanced with respect to the time source and time absorption. In fact making a comparison between ${}^{i+1}\tilde{L}^{+}$ and ${}^{i+1}\tilde{\tilde{L}}^{+}$, defined, respectively, by (2.49) and (2.53), one can find:

$$\left({}^{i+1}\tilde{L}^{+}\right)[\ ] - \left({}^{i+1}\tilde{\tilde{L}}^{+}\right)[\ ] = \frac{1}{u\Delta t_{i+1}}[\ ] - \frac{1}{u\Delta t_{i+1}}\int_{4\pi} d\vec{\Omega}'[\ ]. \tag{2.54}$$

This difference arises from the fact that the time absorption defined by (2.52) acts only on the zeroth moment of the flux while the one defined by (2.47) acts on all the angular components of the even-parity flux. In order to obviate this difficulty, two approaches are feasible. The first one is based on correcting the moments of the scattering kernel up to the order (of the main index p) used in the angular flux expansion:

$${}^{i+1}\tilde{\Sigma}_{s,l} = {}^{i+1}\Sigma_{s,l} + \frac{1}{u\Delta t_{i+1}} \qquad \forall l \le p. \tag{2.55}$$

This approach is undesirable since it artificially increases the size of the scattering kernel. Such an introduction of additional components in the scattering kernel first requires a modification of the cross section file and secondly requires an increase of the computational time due to enlargement of the scattering matrix size. Nonetheless, this approach could be wiser to use in the future because the second approach involves additional approximations. Moreover, the exact approach shown in the next chapter can became too expensive to use, especially in situations when the computational cost of the spatial and energy solution becomes comparable

to the time interpolation process. The second option, which is used for the new implementation in the code, is based on the assumption that the time inertia in the higher angular flux moments (i.e. p>0) is negligible. To explain this concept, it would be better to refer to the system of equations arising by projection over the spherical harmonics basis of the transport equation. This system has one equation for each angular moment which is coupled by the $\vec{\Omega}\cdot\vec{\nabla}$ operator. When the time derivative inside one of these equations is neglected, the corresponding moment is not assumed to be constant in time, but instead, the moment is assumed to respond so fast to the excitation arising from the external source and coupling terms that it has no memory of the past. In other words, it immediately reaches the asymptotic solution without memory of the past (i.e. no inertia). Using this scheme we have to change the first approximation described in (2.44) as follows:

$$\left.\frac{1}{u}\partial_t\phi\right|_{i+1} \approx \frac{1}{u}\frac{\frac{1}{4\pi}\int_{4\pi} d\vec{\Omega}\left({}^{i+1}\phi - {}^{i}\phi\right)}{\Delta t}. \tag{2.56}$$

Of course the time source associated to this scheme must be redefined:

$${}^{i+1}\tilde{S}^{+} = {}^{i+1}S^{+} + \frac{1}{u}\frac{\frac{1}{4\pi}\int_{4\pi} d\vec{\Omega}\,{}^{i}\phi}{\Delta t_{i+1}} + \sum_{i=1}^{NF} {}^{i+1}\chi_i\lambda_i\,{}^{i+1}a_i\,. \tag{2.57}$$

This new definition of the time source is now in balance with the definition of the modified even-parity scattering kernel defined by (2.52). The time discretization process up to this point can be easily repeated starting from the multi-group equation (2.1) and (2.3) leading to an equation formally equivalent to that shown in paragraphs II.2 II.3 and II.4. In this case the within group time source will be:

$${}^{i+1}\tilde{S}_g^{+} = {}^{i+1}S_g^{+} + \frac{1}{u}\frac{\frac{1}{4\pi}\int_{4\pi} d\vec{\Omega}\,{}^{i}\phi_g}{\Delta t_{i+1}} + \sum_{i=1}^{NF} {}^{i+1}\chi_{i,g}\lambda_i\,{}^{i+1}a_i\,, \tag{2.58}$$

and the time absorption:

$$\frac{1}{u\Delta t_{i+1}}. \tag{2.59}$$

One final comment about this scheme is that even if the coupling terms between the precursor concentration and flux equations are treated by a partially explicitly time integration scheme, due to the low value of the norms of the coupling operators, instability can only arise for values of the time step for which the error in the flux evaluation is already intolerable.

The method described by equations. (2.56), (2.57), (2.52) and the second and third of (2.44), in the following chapters, will be referred as the old (time direct) scheme.

Chapter III. EXTENSIONS OF THE DIRECT METHOD FOR THE TIME DISCRETIZATION

The aim of this chapter is to describe a new direct discretization scheme for the time dependence which accounts for the time derivatives of the angular moments of the flux (both the even and odd components). The purpose of introducing this additional feature was to accommodate the scheme to very short time scale phenomena where the time inertia of higher angular moments may not be negligible. In this chapter, the differences in the mathematical structure of the problem that arise from the two different schemes are displayed. This work, from a practical perspective, has also extended the capability of this new scheme by a higher order time discretization approximation in conjunction with an automatic time step control. This allows the simulation of a realistic transient with a reasonable computational cost. The introduction of the adaptive time control has been carried out by an analysis of the overall order of precision of the time integration scheme such that with reasonable assumptions, the stability and precision of the algorithm is maintained.

III.1. The New Direct Scheme Equations (P_N Case)

The starting point is a first order backward Euler scheme in time for all the even and odd parity flux moments. The same discretization scheme used in the previous scheme for the precursor concentration equation is also used.

This scheme can be described by the following set of approximations:

$$\begin{aligned}
&\frac{1}{u}\partial_t\phi\big|_{i+1} \approx \frac{{}^{i+1}\phi - {}^{i}\phi}{u\Delta t_{i+1}},\\
&\frac{1}{u}\partial_t\psi\big|_{i+1} \approx \frac{{}^{i+1}\psi - {}^{i}\psi}{u\Delta t_{i+1}},\\
&\beta_i P[\phi]\left(t_i \le t \le t_{i+1}\right) \approx \beta_i\, {}^{i}P\left[{}^{i}\phi\right] + \frac{\beta_{i+1}\, {}^{i+1}P\left[{}^{i+1}\phi\right] - \beta_i\, {}^{i}P\left[{}^{i}\phi\right]}{\Delta t_{i+1}}\left(t_{i+1} - t\right).
\end{aligned} \tag{3.1}$$

Since the treatment for delayed neutrons is the same as that used in the old scheme, its description will be omitted here. Later, it will be revisited during the analysis of the order of precision of the general scheme. Using the approximations given by (3.1) in the first two equations of system (2.43) (without delayed neutrons contribution) the following is obtained:

$$\begin{cases}
\dfrac{1}{u}\dfrac{{}^{i+1}\phi - {}^{i}\phi}{\Delta t_{i+1}} + \vec{\Omega}\cdot\vec{\nabla}\,{}^{i+1}\psi + {}^{i+1}\Sigma_T\,{}^{i+1}\phi = {}^{i+1}H^{+}\left[{}^{i+1}\phi\right] + {}^{i+1}S^{+} + {}^{i+1}F_p\left[{}^{i+1}\phi\right],\\
\dfrac{1}{u}\dfrac{{}^{i+1}\psi - {}^{i}\psi}{\Delta t_{i+1}} + \vec{\Omega}\cdot\vec{\nabla}\,{}^{i+1}\phi + {}^{i+1}\Sigma_T\,{}^{i+1}\psi = {}^{i+1}H^{-}\left[{}^{i+1}\psi\right].
\end{cases} \tag{3.2}$$

In accordance with the limited capability of VARIANT the odd parity source term, S^{-}, has been omitted in the last equation of (3.2). With the introduction of the time absorption $(u\Delta t_{i+1})^{-1}$, the equation is balanced by the presence of the even and odd parity time-dependent sources ${}^{i}\phi/\left(u\Delta t_{i+1}\right)$ and ${}^{i}\psi/\left(u\Delta t_{i+1}\right)$. With this, it is possible to define the following modified quantities:

$$\begin{aligned}
&{}^{i+1}\tilde{\Sigma}_T = {}^{i+1}\Sigma_T + \frac{1}{u\Delta t_{i+1}},\\
&{}^{i+1}\tilde{L}^{\pm}[\ ] = \left({}^{i+1}\tilde{\Sigma}_T - {}^{i+1}H^{\pm}\right)[\ ],\\
&{}^{i+1}\tilde{S}^{+} = {}^{i+1}S^{+} + \frac{1}{u}\frac{{}^{i}\phi}{\Delta t_{i+1}},\\
&{}^{i+1}\tilde{S}^{-} = \frac{1}{u}\frac{{}^{i}\psi}{\Delta t_{i+1}}.
\end{aligned} \tag{3.3}$$

Inserting (3.3) in (3.2):

$$\begin{cases} \vec{\Omega}\cdot\vec{\nabla}\,{}^{i+1}\psi + {}^{i+1}\tilde{L}^{+}\left[{}^{i+1}\phi\right] = {}^{i+1}\tilde{S}^{+} + {}^{i+1}F_{p}\left[{}^{i+1}\phi\right], \\ \vec{\Omega}\cdot\vec{\nabla}\,{}^{i+1}\phi + {}^{i+1}\tilde{L}^{-}\left[{}^{i+1}\psi\right] = {}^{i+1}\tilde{S}^{-}. \end{cases} \tag{3.4}$$

Since the angular structure of the $\tilde{L}^{-}$ operator is identical to the L^{-} operator, the inversion can be done in the same way as that done in 1.4. Consequently, the second equation of the system can be eliminated:

$$\vec{\Omega}\cdot\vec{\nabla}\left(\left({}^{i+1}\tilde{L}^{-}\right)^{-1}\left(-\vec{\Omega}\cdot\vec{\nabla}\,{}^{i+1}\phi + {}^{i+1}\tilde{S}^{-}\right)\right) + {}^{i+1}\tilde{L}^{+}\left[{}^{i+1}\phi\right] = {}^{i+1}\tilde{S}^{+} + {}^{i+1}F_{p}\left[{}^{i+1}\phi\right]. \tag{3.5}$$

The resulting time integration scheme is a backward Euler form for all of the angular components of the flux (not taking in account delayed neutrons contribution) and it requires only the change of the total cross section since one has a coherent time source for all of the flux components. The main drawback of this scheme is the introduction of an odd parity component of the time source that is difficult to create and implement. VARIANT, as it turns out, does not provide any information about the odd parity spatial and angular moments of the flux and is not able to treat external odd parity sources. Unfortunately, due the group coupling that arises during the treatment of the odd parity source, it is not possible to transfer directly the time discretization from the continuous energy treatment to the multi-group formalism as done in the previous scheme. It is therefore better to put system (3.4) and equation (3.5) directly in the multi-group form:

$$\begin{cases} \vec{\Omega}\cdot\vec{\nabla}\,{}^{i+1}\psi_{g} + {}^{i+1}\tilde{L}_{g}^{+}\left[{}^{i+1}\phi_{g}\right] = {}^{i+1}\tilde{S}_{g}^{+} + {}^{i+1}F_{p,g}\left[{}^{i+1}\phi\right], \\ \vec{\Omega}\cdot\vec{\nabla}\,{}^{i+1}\phi_{g} + {}^{i+1}\tilde{L}_{g}^{-}\left[{}^{i+1}\psi_{g}\right] = {}^{i+1}\tilde{S}_{g}^{-}, \end{cases} \tag{3.6}$$

$$\vec{\Omega}\cdot\vec{\nabla}\left(\left({}^{i+1}\tilde{L}_{g}^{-}\right)^{-1}\left(-\vec{\Omega}\cdot\vec{\nabla}\,{}^{i+1}\phi_{g} + {}^{i+1}\tilde{S}_{g}^{-}\right)\right) + {}^{i+1}\tilde{L}^{+}\left[{}^{i+1}\phi_{g}\right] = {}^{i+1}\tilde{S}_{g}^{+} + {}^{i+1}F_{p,g}\left[{}^{i+1}\phi\right]. \tag{3.7}$$

The multi-group quantities corresponding to the ones defined in (3.3) are defined as:

$${}^{i+1}\tilde{\Sigma}_{T,g} = {}^{i+1}\Sigma_{T,g} + \frac{1}{u_{g}\Delta t_{i+1}},$$

$${}^{i+1}\tilde{L}_{g}^{\pm}[\ ] = \left({}^{i+1}\tilde{\Sigma}_{T,g} - {}^{i+1}H_{g\to g}^{\pm}\right)[\ ],$$

$$
\begin{aligned}
{}^{i+1}\tilde{S}_g^{+} &= {}^{i+1}S_g^{+} + \frac{1}{u_g}\frac{{}^{i}\phi_g}{\Delta t_{i+1}} + \sum_{\substack{g' \\ g'\neq g}}^{NG} {}^{i+1}H_{g'\to g}^{+}[{}^{i+1}\phi_{g'}], \\
{}^{i+1}\tilde{S}_g^{-} &= \frac{1}{u_g}\frac{{}^{i}\psi_g}{\Delta t_{i+1}} + \sum_{\substack{g' \\ g'\neq g}}^{NG} {}^{i+1}H_{g'\to g}^{-}[{}^{i+1}\psi_{g'}].
\end{aligned}
\tag{3.8}
$$

The first problem that has to be solved is how to reconstruct the odd parity flux at the previous time step (i) such that the odd parity component of the time source ($\frac{1}{u_g}\frac{{}^{i}\psi_g}{\Delta t_{i+1}}$) is obtained. The starting point is the second equation of system (3.6) evaluated at time step i. Writing equations (3.6) and (3.7) for each volume of the spatial discretization and using the expansion for the intra-nodal spatial dependence as done in Section I.2:

$$
\vec{\Omega}\cdot\vec{\nabla}\sum_{\alpha=0}^{N_\alpha} f_\alpha(\vec{r})\,{}^{i}\phi_g^{\alpha} + {}^{i}\tilde{L}_{g\to g}^{-}\left[\sum_{\alpha=0}^{N_\alpha} f_\alpha(\vec{r})\,{}^{i}\psi_g^{\alpha}\right] = \frac{1}{u_g}\frac{\sum_{\alpha=0}^{N_\alpha} f_\alpha(\vec{r})\,{}^{i-1}\psi_g^{\alpha}}{\Delta t_i} + \sum_{\substack{g' \\ g'\neq g}}^{NG} {}^{i+1}H_{g'\to g}^{-}\left[\sum_{\alpha=0}^{N_\alpha} f_\alpha(\vec{r})\,{}^{i}\psi_{g'}^{\alpha}\right].
\tag{3.9}
$$

Recalling the fact that inside of each volume the homogenized operators ${}^{i}\tilde{L}_{g\to g}^{-}$, and ${}^{i}H_{g'\to g}^{-}$ are constant and that the spatial trial functions are orthogonal, a projection over $f_{\alpha'}(\vec{r})$ leads to:

$$
{}^{i}\tilde{L}_{g\to g}^{-}\left[{}^{i}\psi_g^{\alpha'}\right] = \frac{1}{u_g}\frac{{}^{i-1}\psi_g^{\alpha'}}{\Delta t_{i+1}} + \sum_{\substack{g' \\ g'\neq g}}^{NG} {}^{i}H_{g'\to g}^{-}\left[{}^{i}\psi_{g'}^{\alpha'}\right] - \int_{Vol} dV f_{\alpha'}(\vec{r})\,\vec{\Omega}\cdot\vec{\nabla}\sum_{\alpha=0}^{N_\alpha} f_\alpha(\vec{r})\,{}^{i}\phi_g^{\alpha}. \tag{3.10}
$$

In order to facilitate the algebraic manipulation, it is better to introduce the single indexing in the angular expansion of the odd parity scattering operator with the following convention:

$$
\begin{aligned}
&(2p_{m-}+1)\Sigma_{s,m-} = (2\cdot 1+1)\Sigma_{s,1} && m\text{-} = 1,2,3, \\
&(2p_{m-}+1)\Sigma_{s,m-} = (2\cdot 3+1)\Sigma_{s,3} && m\text{-} = 4,.....,10, \\
&(2p_{m-}+1)\Sigma_{s,m-} = (2\cdot 5+1)\Sigma_{s,5} && m\text{-} = 11,.....,21. \\
&..... &&
\end{aligned}
\tag{3.11}
$$

This scheme accounts for the fact that a change in the secondary index q has no effect on the scattering kernel and thus it should be modified for the 2D or 1D case in which the number of

expansions on the secondary index is reduced for the symmetry conditions. Now the expression in (3.8) for ${}^{i+1}\tilde{L}_g^-[\ ]$ can be reformulated as follows:

$$ {}^{i}\tilde{L}^{-}_{g\to g}[\ ] = {}^{i}\tilde{\Sigma}_{\underset{g}{T}} - \sum_{m-}(2p_{m-}+1)\,{}^{i}\Sigma_{\underset{g\to g}{s,m-}}\, g_{m-}(\vec{\Omega})\int_{4\pi} d\vec{\Omega}'\, g_{m-}(\vec{\Omega}')[\ ]. \tag{3.12} $$

The same formalism for the down/up scattering operator $H^-_{g'\to g}$ gives:

$$ {}^{i}H^{-}_{g'\to g}[\ ] = \sum_{m-}(2p_{m-}+1)\,{}^{i}\Sigma_{\underset{g'\to g}{s,m-}}\, g_{m-}(\vec{\Omega})\int_{4\pi} d\vec{\Omega}'\, g_{m-}(\vec{\Omega}')[\ ]. \tag{3.13} $$

Equation (3.10) can be reformulated as follows by using the intra-nodal angular expansions for even and odd parity functions:

$$ \begin{aligned} &{}^{i}\tilde{\Sigma}_{\underset{g}{T}}\sum_{m-}\mathrm{g}^{\mathrm{m}\text{-}}(\vec{\Omega})\,{}^{i}\psi_g^{\alpha',m-} - \\ &-\sum_{m-}(2p_{m-}+1)\,{}^{i}\Sigma_{\underset{g\to g}{s,m-}}\, g_{m-}(\vec{\Omega})\int_{4\pi} d\vec{\Omega}'\, g_{m-}(\vec{\Omega}')[\sum_{(m-)'}\mathrm{g}^{(m-)'}(\vec{\Omega}')\,{}^{i}\psi_g^{\alpha',(m-)'}\ ] = \\ &=\frac{1}{u_g}\frac{\sum_{m-}\mathrm{g}^{m-}(\vec{\Omega}')\,{}^{i-1}\psi_g^{\alpha',m-}}{\Delta t_i} + \\ &+\sum_{\substack{g'\\ g'\neq g}}^{NG}\sum_{m-}(2p_{m-}+1)\,{}^{i}\Sigma_{\underset{g'\to g}{s,m-}}\, g_{m-}(\vec{\Omega})\int_{4\pi} d\vec{\Omega}'\, g_{m-}(\vec{\Omega}')[\sum_{(m-)'}\mathrm{g}^{(m-)'}(\vec{\Omega}')\,{}^{i}\psi_{g'}^{\alpha',(m-)'}\ ] - \\ &-\int_{Vol} dVf_{\alpha'}(\vec{r})\,\vec{\Omega}\cdot\vec{\nabla}\sum_{\alpha=0}^{N_\alpha} f_\alpha(\vec{r})\sum_{m+}\mathrm{g}^{m+}(\vec{\Omega})\,{}^{i}\phi_g^{\alpha,m+}. \end{aligned} \tag{3.14} $$

Using the orthogonal relation of the spherical harmonics the last equation is reduced to:

$$ \begin{aligned} &\sum_{m-}\mathrm{g}^{\mathrm{m}\text{-}}(\vec{\Omega})\left({}^{i}\tilde{\Sigma}_{\underset{g}{T}} - (2p_{m-}+1)\,{}^{i}\Sigma_{\underset{g\to g}{s,m-}}\right){}^{i}\psi_g^{\alpha',m-} = \\ &=\frac{1}{u_g}\frac{\sum_{m-}\mathrm{g}^{m-}(\vec{\Omega}')\,{}^{i-1}\psi_g^{\alpha',m-}}{\Delta t_i} + \sum_{\substack{g'\\ g'\neq g}}^{NG}\sum_{m-}(2p_{m-}+1)\,{}^{i}\Sigma_{\underset{g'\to g}{s,m-}}\, g_{m-}(\vec{\Omega})\,{}^{i}\psi_{g'}^{\alpha',m-} - \\ &-\int_{Vol} dVf_{\alpha'}(\vec{r})\,\vec{\Omega}\cdot\vec{\nabla}\sum_{\alpha=0}^{N_\alpha} f_\alpha(\vec{r})\sum_{m+}\mathrm{g}^{m+}(\vec{\Omega})\,{}^{i}\phi_g^{\alpha,m+}. \end{aligned} \tag{3.15} $$

Projecting the last equation over g_{m-} one obtains:

$$\begin{aligned}
&\left({}^{i}\tilde{\Sigma}_{\underset{g}{T}} - \left(2p_{m-}+1\right) {}^{i}\Sigma_{\underset{g\to g}{s,m-}} \right) {}^{i}\psi_{g}^{\alpha',m-} = \\
&= \frac{1}{u_g}\frac{{}^{i-1}\psi_{g}^{\alpha',m-}}{\Delta t_i} + \sum_{\substack{g' \\ g'\neq g}}^{NG} \left(2p_{m-}+1\right) {}^{i}\Sigma_{\underset{g'\to g}{s,m-}} {}^{i}\psi_{g'}^{\alpha',m-} - \\
&- \sum_{\alpha=0}^{N_\alpha} \sum_{m+} {}^{i}\phi_{g}^{\alpha,m+} \int_{4\pi} d\vec{\Omega} \int_{Vol} dV f_{\alpha'}\left(\vec{r}\right) \mathrm{g}^{m-}\left(\vec{\Omega}\right) \mathrm{g}^{m+}\left(\vec{\Omega}\right) \vec{\Omega}\cdot\vec{\nabla} f_{\alpha}\left(\vec{r}\right).
\end{aligned} \tag{3.16}$$

The values of the integrals in (3.16) are currently pre-computed for all the possible combinations of the basis functions (α, m+, m-) for a standard element, and thus, by means of the Jacobian, can be adapted to the volume element under consideration.

$$\begin{aligned}
&M_{\alpha',m-}\left[{}^{i}\phi_{g}^{\alpha,m+} \right] = \sum_{\alpha=0}^{N_\alpha} \sum_{m+} {}^{i}\phi_{g}^{\alpha,m+} \int_{4\pi} d\vec{\Omega} \int_{Vol} dV f_{\alpha'}\left(\vec{r}\right) \mathrm{g}^{m-}\left(\vec{\Omega}\right) \mathrm{g}^{m+}\left(\vec{\Omega}\right) \vec{\Omega}\cdot\vec{\nabla} f_{\alpha}\left(\vec{r}\right), \\
&{}^{i}\tilde{L}_{\underset{g\to g}{m-}} = \left({}^{i}\tilde{\Sigma}_{\underset{g}{T}} - \left(2p_{m-}+1\right) {}^{i}\Sigma_{\underset{g\to g}{s,m-}} \right).
\end{aligned} \tag{3.17}$$

After the substitutions:

$$\begin{aligned}
&{}^{i}\psi_{g}^{\alpha',m-} = \left({}^{i}\tilde{L}_{m-,g} \right)^{-1} \frac{1}{u_g}\frac{{}^{i-1}\psi_{g}^{\alpha',m-}}{\Delta t_i} + \left({}^{i}\tilde{L}_{m-,g} \right)^{-1} \sum_{\substack{g' \\ g'\neq g}}^{NG} \left(2p_{m-}+1\right) {}^{i}\Sigma_{\underset{g'\to g}{s,m-}} {}^{i}\psi_{g'}^{\alpha',m-} - \\
&- \left({}^{i}\tilde{L}_{m-,g} \right)^{-1} M_{\alpha',m-}\left[{}^{i}\phi_{g}^{\alpha,m+} \right].
\end{aligned} \tag{3.18}$$

Unfortunately the system is not yet in an explicit form since the terms $\sum_{\substack{g' \\ g'\neq g}}^{NG} \left(2p_{m-}+1\right) {}^{i}\Sigma_{\underset{g'\to g}{s,m-}} {}^{i}\psi_{g'}^{\alpha',m-}$ induce a coupling between the odd flux moments in different energy groups. The direct inversion of this part of the operator is almost prohibitive, but on the other hand, the discrete form of the operator is generally lower triangular. This is due primarily to the fact that in fast reactors, the up scattering is almost negligible. In this case, the use of an iterative Gauss-Seidel scheme is very fast.

With this, the following iteration scheme is proposed (upper right *r* and *r+1* are the iteration indices for the Gauss-Seidel algorithm):

$$\begin{aligned}\left({}^{i}\psi_{g}^{\alpha',m-}\right)^{r+1} &= \left({}^{i}\tilde{L}_{m-,g}\right)^{-1}\frac{1}{u_g}\frac{{}^{i-1}\psi_{g}^{\alpha',m-}}{\Delta t_i}-\left({}^{i}\tilde{L}_{\substack{m-\\ g\to g}}\right)^{-1}M_{\alpha',m-}\left[{}^{i}\phi_{g}^{\alpha,m+}\right]\\ &+\left({}^{i}\tilde{L}_{m-,g}\right)^{-1}\sum_{\substack{g'\\ g'<g}}^{NG}\left(2p_{m-}+1\right){}^{i}\Sigma_{\substack{s,m-\\ g'\to g}}\left({}^{i}\psi_{g'}^{\alpha',m-}\right)^{r+1}+\\ &\left({}^{i}\tilde{L}_{m-,g}\right)^{-1}\sum_{\substack{g'\\ g'>g}}^{NG}\left(2p_{m-}+1\right){}^{i}\Sigma_{\substack{s,m-\\ g'\to g}}\left({}^{i}\psi_{g'}^{\alpha',m-}\right)^{r}.\end{aligned} \tag{3.19}$$

Once that the odd parity moments of the flux at the previous time (*i*) step are known, the odd parity time source for the next time step (*i+1*) can be constructed:

$${}^{i+1}\tilde{S}_{g}^{-}=\frac{1}{u_g}\frac{{}^{i}\psi}{\Delta t_{i+1}}=\sum_{g}^{NG}\theta_g\left(E\right)\sum_{j=1}^{Nreg}\theta_j\left(\vec{r}\right)\sum_{m-}g^{m-}\left(\vec{\Omega}\right)\sum_{\alpha}^{N\alpha}f_{\alpha}\left(\vec{r}\right)\frac{{}^{i}\psi_{g}^{\alpha',m-}}{u_g\Delta t_{i+1}}. \tag{3.20}$$

Unfortunately, as already mentioned, the VARIANT code is not able to treat external odd parity sources. To overcome this problem, its contribution to the functional for the second order even form is computed externally. The procedure for this starts with the functional for each node in the multi-group formalism which can be obtained by the modified problem of equation (3.7):

$$\begin{aligned}{}^{i+1}F_{\substack{v\\ g}} &= \int_{V}dV\int_{4\pi}d\vec{\Omega}\left[\left({}^{i+1}\tilde{L}_{g}^{-}\right)^{-1}\left(\vec{\Omega}\vec{\nabla}\,{}^{i+1}\phi_g\right)^2+{}^{i+1}\tilde{L}_{g}^{-}\,{}^{i+1}\phi_{g}^{\,2}-2\,{}^{i+1}\phi_g\,{}^{i+1}\tilde{S}_{g}^{+}-2\vec{\Omega}\vec{\nabla}\left({}^{i+1}\phi_g\right)\left({}^{i+1}\tilde{L}_{g}^{-}\right)^{-1}\,{}^{i+1}\tilde{S}_{g}^{-}\right]\\ &+2\int_{\partial V}dl\int_{4\pi}d\vec{\Omega}\left[\vec{n}\cdot\vec{\Omega}\,{}^{i+1}\phi_g\,{}^{i+1}\psi_g\right].\end{aligned} \tag{3.21}$$

Focusing on the term:

$$\int_{V}dV\int_{4\pi}d\vec{\Omega}\left[{}^{i+1}\phi_g\,{}^{i+1}\tilde{S}_{g}^{+}+\vec{\Omega}\vec{\nabla}\left(\left({}^{i+1}\phi_g\right)\left({}^{i+1}\tilde{L}_{g}^{-}\right)^{-1}\,{}^{i+1}\tilde{S}_{g}^{-}\right)\right]. \tag{3.22}$$

It is helpful to recall the expression of the two sources (even and odd):

$$
\begin{aligned}
{}^{i+1}\tilde{S}_g^{+} &= \frac{1}{u_g}\frac{{}^{i}\phi_g}{\Delta t_{i+1}} + \sum_{\substack{g'=1\\ g'\neq g}}^{NG} {}^{i+1}H^{+}_{g'\to g}\left[{}^{i+1}\phi_{g'}\right] + \sum_{g'=1}^{NG} {}^{i+1}F_{g'\to g}\left[{}^{i+1}\phi_{g'}\right] + {}^{i+1}S^{+}_{ext,g}, \\
{}^{i+1}\tilde{S}_g^{-} &= \frac{1}{u_g}\frac{{}^{i}\psi_g}{\Delta t_{i+1}} + \sum_{\substack{g'=1\\ g'\neq g}}^{NG} {}^{i+1}H^{-}_{g'\to g}\left[{}^{i+1}\psi_{g'}\right] = \frac{1}{u_g}\frac{{}^{i}\psi_g}{\Delta t_{i+1}} + \sum_{\substack{g'=1\\ g'\neq g}}^{NG} {}^{i+1}H^{-}_{g'\to g}\left[\left({}^{i+1}L^{-}_{g'}\right)^{-1}\left(-\vec{\Omega}\cdot\vec{\nabla}\,{}^{i+1}\phi_{g'} + {}^{i+1}\tilde{S}^{-}_{g'}\right)\right],
\end{aligned}
\tag{3.23}
$$

The treatment of the even parity source is straightforward since the time source can be included in the external even parity source. For the odd parity source treatment, the odd parity component of flux is decomposed in two parts:

$$
{}^{i+1}\psi_{g'} = {}^{i+1}\xi_{g'} + {}^{i+1}\zeta_{g'}, \tag{3.24}
$$

which are solutions of the two equations:

$$
\begin{aligned}
{}^{i+1}\xi_{g'} &= \left({}^{i+1}L^{-}_{g'\to g'}\right)^{-1}\left(-\vec{\Omega}\cdot\vec{\nabla}\,{}^{i+1}\phi_{g'} + \sum_{\substack{g''=1\\ g''\neq g'}}^{NG} {}^{i+1}H^{-}_{g''\to g'}\left[{}^{i+1}\xi_{g''}\right]\right), \\
{}^{i+1}\zeta_{g'} &= \left({}^{i+1}L^{-}_{g'\to g'}\right)^{-1}\left(\frac{1}{u_{g'}}\frac{{}^{i}\psi_{g'}}{\Delta t_{i+1}} + \sum_{\substack{g''=1\\ g''\neq g'}}^{NG} {}^{i+1}H^{-}_{g''\to g'}\left[{}^{i+1}\zeta_{g''}\right]\right).
\end{aligned}
\tag{3.25}
$$

The sum of these equations yields the exact equation for the odd parity flux component:

$$
\left({}^{i+1}\xi_{g'} + {}^{i+1}\zeta_{g'}\right) = \left({}^{i+1}L^{-}_{g'\to g'}\right)^{-1}\left(\frac{1}{u_{g'}}\frac{{}^{i}\psi_{g'}}{\Delta t_{i+1}} - \vec{\Omega}\cdot\vec{\nabla}\,{}^{i+1}\phi_{g'} + \sum_{\substack{g''=1\\ g''\neq g'}}^{NG} {}^{i+1}H^{-}_{g''\to g'}\left[{}^{i+1}\xi_{g''} + {}^{i+1}\zeta_{g''}\right]\right). \tag{3.26}
$$

Removing the external odd parity source $\frac{1}{u_g}\frac{{}^{i}\psi_g}{\Delta t_{i+1}}$ in VARIANT results in the computation of the within-group odd parity source based only upon the first of the two equations (3.25).

Inserting (3.25) into the second equation of (3.23):

$$
\begin{aligned}
&{}^{i+1}\tilde{S}_g^- = \frac{1}{u_g}\frac{{}^{i}\psi_g}{\Delta t_{i+1}} + \sum_{\substack{g'=1\\ g'\neq g}}^{NG} {}^{i+1}H^-_{g'\to g}\left[{}^{i+1}\xi_{g'} + {}^{i+1}\zeta_{g'}\right] = \\
&\underbrace{\frac{1}{u_g}\frac{{}^{i}\psi_g}{\Delta t_{i+1}} + \sum_{\substack{g'=1\\ g'\neq g}}^{NG} {}^{i+1}H^-_{g'\to g}\left[\left({}^{i+1}L^-_{g'}\right)^{-1}\left(\frac{1}{u_{g'}}\frac{{}^{i}\psi_{g'}}{\Delta t_{i+1}} + \sum_{\substack{g''=1\\ g''\neq g}}^{NG} {}^{i+1}H^-_{g''\to g'}\left[{}^{i+1}\zeta_{g''}\right]\right)\right]}_{\text{Arising from the odd time source}} + \\
&\underbrace{\sum_{\substack{g''=1\\ g''\neq g'}}^{NG} {}^{i+1}H^-_{g''\to g'}\left[\left({}^{i+1}L^-_{g''}\right)^{-1}\left(-\vec{\Omega}\cdot\vec{\nabla}\,{}^{i+1}\phi_{g''} + \sum_{\substack{g''=1\\ g''\neq g'}}^{NG} {}^{i+1}H^-_{g''\to g'}\left[{}^{i+1}\xi_{g''}\right]\right)\right]}_{\text{Computed correctly by VARIANT}}.
\end{aligned}
\tag{3.27}
$$

Splitting the odd parity source into two parts:

$$
\begin{aligned}
&{}^{i+1}\tilde{S}_g^- = {}^{i+1}S_g^{V-} + {}^{i+1}\tilde{S}_g^{T-} \\
&{}^{i+1}\tilde{S}_g^{T-} = \frac{1}{u_g}\frac{{}^{i}\psi_g}{\Delta t_{i+1}} + \sum_{\substack{g'=1\\ g'\neq g}}^{NG} {}^{i+1}H^-_{g'\to g}\left[\left({}^{i+1}L^-_{g'}\right)^{-1}\left(\frac{1}{u_{g'}}\frac{{}^{i}\psi_{g'}}{\Delta t_{i+1}} + \sum_{\substack{g''=1\\ g''\neq g'}}^{NG} {}^{i+1}H^-_{g''\to g'}\left[{}^{i+1}\zeta_{g''}\right]\right)\right] \\
&{}^{i+1}S_g^{V-} = \sum_{\substack{g'=1\\ g'\neq g}}^{NG} {}^{i+1}H^-_{g'\to g}\left[\left({}^{i+1}L^-_{g'}\right)^{-1}\left(-\vec{\Omega}\cdot\vec{\nabla}\,{}^{i+1}\phi_{g'} + \sum_{\substack{g''=1\\ g''\neq g'}}^{NG} {}^{i+1}H^-_{g''\to g'}\left[{}^{i+1}\xi_{g''}\right]\right)\right].
\end{aligned}
\tag{3.28}
$$

The equation for ${}^{i+1}\tilde{S}_g^{T-}$ can be reformulated as follows:

$$
{}^{i+1}\tilde{S}_g^{T-} = \frac{1}{u_g}\frac{{}^{i}\psi_g}{\Delta t_{i+1}} + \sum_{\substack{g'=1\\ g'\neq g}}^{NG} {}^{i+1}H^-_{g'\to g}\left[\left({}^{i+1}L^-_{g'}\right)^{-1}\,{}^{i+1}\tilde{S}_{g'}^{T-}\right]. \tag{3.29}
$$

This source can be expanded over the Legendre polynomial basis in space, and spherical harmonics in angle:

$$
{}^{i+1}\tilde{S}_g^{T-} = \sum_{m-} g^{m-}\left(\vec{\Omega}\right)\sum_{\alpha}^{N\alpha} f_\alpha\left(\vec{r}\right)\,{}^{i+1}\tilde{S}_g^{\alpha,m-}. \tag{3.30}
$$

Since the operator $\left(1/\left(u_g\Delta t_{i+1}\right) + {}^{i+1}H^-_{g'\to g}\cdot\left({}^{i+1}L^-_{g'}\right)^{-1}\right)[\ ]$ is diagonal in space and angle over the basis, the Fourier coefficients of the last series are:

$$ {}^{i+1}\tilde{S}_g^{T-,\alpha,m-} = \frac{1}{u_g}\frac{{}^{i}\psi_g^{\alpha',m-}}{\Delta t_{i+1}} + \sum_{\substack{g'=1 \\ g'\neq g}}^{NG} {}^{i+1}\Sigma_{\substack{s,m- \\ g'\to g}} \left[\left({}^{i+1}\tilde{L}_{m-,g'} \right)^{-1} {}^{i+1}\tilde{S}_{g'}^{T-,\alpha,m-} \right]. \tag{3.31} $$

This is not yet an explicit formulation of ${}^{i+1}\tilde{S}_g^{T-,\alpha,m-}$ due the group coupling, but nevertheless, it suggests an iterative strategy for solving it as done for (3.19). This yields the following scheme:

$$ \left({}^{i+1}\tilde{S}_g^{T-,\alpha,m-} \right)^{r+1} = \frac{1}{u_g}\frac{{}^{i}\psi_g^{\alpha',m-}}{\Delta t_{i+1}} + \sum_{\substack{g'=1 \\ g'\neq g}}^{NG} {}^{i+1}\Sigma_{\substack{s,m- \\ g'\to g}} \left[\left({}^{i+1}\tilde{L}_{m-,g'} \right)^{-1} \left({}^{i+1}\tilde{S}_{g'}^{T-,\alpha,m-} \right)^{r} \right]. \tag{3.32} $$

Recasting the functional term (3.22) in the following way:

$$ \int_V dV \int_{4\pi} d\vec{\Omega} \left[\underbrace{{}^{i+1}\phi_g \, {}^{i+1}\tilde{S}_g^{+}}_{1} + \underbrace{\vec{\Omega}\vec{\nabla}\left({}^{i+1}\phi_g \right)\left({}^{i+1}\tilde{L}_g^{-} \right)^{-1} {}^{i+1}\tilde{S}_g^{T-}}_{2} + \underbrace{\vec{\Omega}\vec{\nabla}\left({}^{i+1}\phi_g \right)\left(\left({}^{i+1}\tilde{L}_g^{-} \right)^{-1} {}^{i+1}S_g^{V-} \right)}_{3} \right]. \tag{3.33} $$

Once the ${}^{i+1}\tilde{L}^{-}$ is correctly changed, by adding the time absorption to the total cross section, the third term is correctly treated by VARIANT. The next step is the evaluation of the first two terms by finding a discrete operator O that will satisfy:

$$ \int_V dV \int_{4\pi} d\vec{\Omega}\vec{\Omega}\vec{\nabla}\left({}^{i+1}\phi_g \right)\left(\left({}^{i+1}\tilde{L}_g^{-} \right)^{-1} {}^{i+1}\tilde{S}_g^{T-} \right) = \int_V dV \int_{4\pi} d\vec{\Omega} \, {}^{i+1}\phi_g \, {}^{i+1}O_g \left[{}^{i+1}\tilde{S}_g^{T-} \right]. \tag{3.34} $$

First the expansions of ${}^{i+1}\phi_g$ and ${}^{i+1}\tilde{S}_g^{T-}$ are introduced (the last is given by (3.30)) and then the $\left({}^{i+1}\tilde{L}_g^{-} \right)^{-1}$ operator is applied:

$$ \begin{aligned} &\int_V dV \int_{4\pi} d\vec{\Omega}\vec{\Omega}\vec{\nabla}\left(\left({}^{i+1}\phi_g \right)\left({}^{i+1}\tilde{L}_g^{-} \right)^{-1} {}^{i+1}\tilde{S}_g^{T-} \right) = \\ &= \sum_{m-}\sum_{\alpha}^{N\alpha} \left\{ {}^{i+1}\phi_g^{\alpha,m+} \left[\sum_{m-}\sum_{\alpha'}^{N\alpha'} \left(\int_V dV f_\alpha(\vec{r})\vec{\nabla} f_{\alpha'}(\vec{r}) \int_{4\pi} d\vec{\Omega}\vec{\Omega} g^{m+}\left(\vec{\Omega}\right) g^{m-}\left(\vec{\Omega}\right) \left({}^{i+1}\tilde{L}_{\substack{m- \\ g\to g}} \right)^{-1} \right) {}^{i+1}\tilde{S}_g^{T-,\alpha',m-} \right] \right\}. \end{aligned} \tag{3.35} $$

From the last expression, it is possible to define the form of the discrete O operator:

$$
\begin{aligned}
&{}^{i+1}O_g = \left\{ {}^{i+1}O_g^{(m+,\alpha),(m-,\alpha')} \right\}, \\
&{}^{i+1}O_g^{(m+,\alpha),(m-,\alpha')} = \int_V dV f_\alpha(\vec{r}) \vec{\nabla} f_{\alpha'}(\vec{r}) \int_{4\pi} d\vec{\Omega}\vec{\Omega} g^{m+}(\vec{\Omega}) g^{m-}(\vec{\Omega}) \left({}^{i+1}\tilde{L}_{\substack{m- \\ g\to g}} \right)^{-1}.
\end{aligned}
\tag{3.36}
$$

This gives a form of the contribution arising from the odd parity time source that can be added to the external even parity source. Defining:

$$
{}^{i+1}\tilde{S}_g^{Tot+} = {}^{i+1}\tilde{S}_g^{+} + {}^{i+1}O_g \left[{}^{i+1}\tilde{S}_g^{T-} \right] = \frac{1}{u_g} \frac{{}^{i}\phi_g}{\Delta t_{i+1}} + {}^{i+1}S_g^{+} + {}^{i+1}O_g \left[{}^{i+1}\tilde{S}_g^{T-} \right]. \tag{3.37}
$$

leads to the following form of the intra-nodal functional:

$$
\begin{aligned}
{}^{i+1}F_{\substack{v \\ g}} &= \int_V dV \int_{4\pi} d\vec{\Omega} \left[\left({}^{i+1}\tilde{L}_g^{-} \right)^{-1} \left(\vec{\Omega}\vec{\nabla}\, {}^{i+1}\phi_g \right)^2 + {}^{i+1}\tilde{L}_g^{-}\, {}^{i+1}\phi_g{}^2 - 2\, {}^{i+1}\phi_g\, {}^{i+1}\tilde{S}_g^{Tot+} - 2\vec{\Omega}\vec{\nabla}\left({}^{i+1}\phi_g \right) \left({}^{i+1}\tilde{L}_g^{-} \right)^{-1} {}^{i+1}S_g^{V-} \right] \\
&+ 2 \int_{\partial V} dl \int_{4\pi} d\vec{\Omega} \left[\vec{n}\cdot\vec{\Omega}\, {}^{i+1}\phi_g\, {}^{i+1}\psi_g \right].
\end{aligned}
\tag{3.38}
$$

Now it is possible to describe the implementation of the algorithm:

- At the end of time step *i*, the following information is available ${}^{i}\phi$ (computed by VARIANT), the cross section at time step i (${}^{i}L^{\pm}$), and ${}^{i-1}\psi$ (stored from previous calculation).
- Using the loop described by equation (3.19) ${}^{i}\psi_g^{\alpha',m-}$ is computed and stored.
- Now it is possible to perform the transition between time steps ($\Delta t_i \to \Delta t_{i+1}$, ${}^{i}L^{\pm} \to {}^{i+1}L^{\pm}$). By (3.20), (3.32), and (3.37) it is possible to compute subsequently ${}^{i+1}\tilde{S}^{-}$ (only discretization of time derivative), ${}^{i+1}\tilde{S}_g^{-}$ (taking in account down scattering), and ${}^{i+1}\tilde{S}_g^{Tot+}$ (transformation from odd to even by means of O operator).
- The new cross sections and ${}^{i+1}\tilde{S}_g^{Tot+}$ are provided to VARIANT and it solves the pseudo steady state problem for time step *i+1* providing ${}^{i+1}\phi$ for the next time step (restart from point 1).

The last point of the derivation is the definition of the initial condition. As in (2.51) the basic hypothesis is that the reactor is in a steady state before the beginning of the transient analysis therefore the initial condition for the even and odd parity fluxes are given by:

$$\begin{aligned}
&\vec{\Omega}\cdot\vec{\nabla}\left(\left({}^{0}L^{-}\right)^{-1}\left(-\vec{\Omega}\cdot\vec{\nabla}\,{}^{0}\phi\right)\right)+{}^{0}L^{+}\,{}^{0}\phi={}^{0}S^{+}+{}^{0}F\left[{}^{0}\phi\right], && \text{by VARIANT,}\\
&{}^{0}\psi=\left({}^{0}L^{-}\right)^{-1}\left(-\vec{\Omega}\cdot\vec{\nabla}\,{}^{0}\phi\right), && \text{by KIN3D,}\\
&\lambda_i\,{}^{0}C_i={}^{0}\beta_i\,{}^{0}P\left[{}^{0}\phi\right], && \text{by KIN3D.}
\end{aligned} \tag{3.39}$$

The solution of the second equation is performed by means of :

$$\begin{aligned}
{}^{i}\psi_g^{\alpha',m-}&=\left({}^{i}L_{m-,g}\right)^{-1}\sum_{\substack{g'\\ g'\neq g}}^{NG}\left(2p_{m-}+1\right){}^{i}\Sigma_{\substack{s,m-\\ g'\to g}}\,{}^{i}\psi_{g'}^{\alpha',m-}-\\
&-\left({}^{i}L_{m-,g}\right)^{-1}M_{\alpha',m-}\left[{}^{i}\phi_g^{\alpha,m+}\right],
\end{aligned} \tag{3.40}$$

that is the limit by $\dfrac{1}{u_g\Delta t_{i+1}}\to 0$ of equation (3.18).

III.2. The New Direct Scheme Equations (SP_N Case)

The time discretization scheme in the framework of the SP_N angular approximation is, of course, similar to the one just illustrated for the P_N method. The starting point is a time dependent form of equation (2.28) given by (within group equation, no delayed neutrons):

$$\begin{cases}
\partial_t\phi_g\left(\vec{r},\mu\right)+\mu\vec{\nabla}\cdot\vec{\psi}_g\left(\vec{r},\mu\right)+L_g^{+}\left[\phi_g\right]\left(\vec{r},\mu\right)=S_g^{+}\left(\vec{r},\mu\right)+F_p\left[\phi_g\right]\left(\vec{r},\mu\right),\\
\partial_t\vec{\psi}_g\left(\vec{r},\mu\right)+\mu\vec{\nabla}\phi_g\left(\vec{r},\mu\right)+L_g^{-}\left[\vec{\psi}_g\right]\left(\vec{r},\mu\right)=\vec{S}_g^{-}\left(\vec{r},\mu\right).
\end{cases} \tag{3.41}$$

The treatment of the delayed neutron contribution can be dropped here since it only affects the zero order moment of the even parity flux and no changes to the treatment carried out in the old scheme with the P_N angular discretization are needed. The time discretization employed in this scheme, is defined as:

$$\frac{1}{u_g}\partial_t\phi_g\Big|_{i+1}\approx\frac{{}^{i+1}\phi_g-{}^{i}\phi_g}{u_g\Delta t_{i+1}},$$

$$\frac{1}{u_g}\partial_t \vec{\psi}_g\Big|_{i+1} \approx \frac{{}^{i+1}\vec{\psi}_g - {}^{i}\vec{\psi}_g}{u_g \Delta t_{i+1}}. \tag{3.42}$$

Starting from the last approximation it is possible to introduce the modified operator and quantities:

$$\begin{aligned} {}^{i+1}\tilde{\Sigma}_{T,g} &= {}^{i+1}\Sigma_{T,g} + \frac{1}{u_g \Delta t_{i+1}}, \\ {}^{i+1}\tilde{L}_g^{\pm}[\ ] &= \left({}^{i+1}\tilde{\Sigma}_{T,g} + {}^{i+1}H^{\pm}_{g\to g}\right)[\ ], \end{aligned} \tag{3.43}$$

$$\begin{aligned} {}^{i+1}\tilde{S}_g^{+} &= {}^{i+1}S_g^{+} + \frac{1}{u_g}\frac{{}^{i}\phi_g}{\Delta t_{i+1}} + \sum_{\substack{g' \\ g'\neq g}}^{NG} {}^{i+1}H^{+}_{g'\to g}[\,{}^{i+1}\phi_{g'}\,], \\ {}^{i+1}\vec{\tilde{S}}_g^{-} &= \frac{1}{u_g}\frac{{}^{i}\vec{\psi}_g}{\Delta t_{i+1}} + \sum_{\substack{g' \\ g'\neq g}}^{NG} {}^{i+1}H^{-}_{g'\to g}[\,{}^{i+1}\vec{\psi}_{g'}\,]. \end{aligned} \tag{3.44}$$

Where, of course the ${}^{i+1}\tilde{L}_g^{\pm}[\ ]$ and ${}^{i+1}H^{+}_{g'\to g}$ are in agreement with the SP_N representation given in (2.32). The resulting discretized system is:

$$\begin{cases} \vec{\Omega}\cdot\vec{\nabla}\,{}^{i+1}\vec{\psi}_g + {}^{i+1}\tilde{L}_g^{+}\left[{}^{i+1}\phi_g\right] = {}^{i+1}\tilde{S}_g^{+} + {}^{i+1}F_{p,g}\left[{}^{i+1}\phi\right], \\ \vec{\Omega}\cdot\vec{\nabla}\,{}^{i+1}\phi_g + {}^{i+1}\tilde{L}_g^{-}\left[{}^{i+1}\vec{\psi}_g\right] = {}^{i+1}\vec{\tilde{S}}_g^{-}. \end{cases} \tag{3.45}$$

The determination of the angular and spatial moments of ${}^{i}\vec{\psi}_g$ needed for ${}^{i+1}\vec{\tilde{S}}_g^{-}$ is done similarly to that in the P_N method via a projection of each vector component of the second equation of system (3.45) over the set of angular (in this case the Legendre Polynomials), and spatial functions:

$$\begin{aligned} {}^{i}\vec{\psi}_g^{\alpha',p-} &= \left({}^{i}\tilde{L}^{-}_{p-,g}\right)^{-1}\left(\frac{1}{u_g}\frac{{}^{i-1}\vec{\psi}_g^{\alpha'}}{\Delta t_{i+1}}\right) + \\ &+\left({}^{i}\tilde{L}^{-}_{p-,g}\right)^{-1}\sum_{\substack{g' \\ g'\neq g}}^{NG}\left(2p_- +1\right){}^{i}\Sigma_{s,\substack{p- \\ g'\to g}}\,{}^{i}\vec{\psi}_{g'}^{\alpha',p-} - \left({}^{i}\tilde{L}^{-}_{p-,g}\right)^{-1}\vec{M}_{\alpha',p-}\left[{}^{i}\phi_g^{\alpha,p+'}\right]. \end{aligned} \tag{3.46}$$

Where:

$$
\begin{aligned}
{}^{i}\tilde{L}^{-}_{\substack{p-\\ g\to g}} &= \left({}^{i}\tilde{\Sigma}_{T,g} - (2p_{-}+1)\, {}^{i}\Sigma_{\substack{s,p-\\ g\to g}} \right) \\
\vec{M}_{\alpha',p-}\left[{}^{i}\phi_{g}^{\alpha,p'} \right] &= \sum_{\alpha=0}^{N_\alpha} \sum_{\substack{p+=0 \\ p+:\ even}}^{SNP} {}^{i}\phi_{g}^{\alpha,p+} \frac{1}{2} \int_{-1}^{1} d\mu \int_{Vol} dV\, (2p_{-}+1) P_{p-}(\mu)\, \mu P_{p+}(\mu)\, f_{\alpha'}(\vec{r})\, \vec{\nabla} f_{\alpha}(\vec{r}).
\end{aligned}
\tag{3.47}
$$

The solution of the multi-group coupling, arising between components of the odd parity flux, is done in the SP_N scheme the as that in the P_N scheme (equation (3.19)). The next step is the definition of the equivalent of ${}^{i+1}\tilde{S}_{g}^{T-}$ for the SP_N case:

$$
{}^{i+1}\vec{\tilde{S}}_{g}^{T-} = \frac{1}{u_g} \frac{{}^{i}\vec{\psi}_{g}}{\Delta t_{i+1}} + \sum_{\substack{g'=1 \\ g'\neq g}}^{NG} {}^{i+1}H^{-}_{g'\to g} \left[\left({}^{i+1}L^{-}_{g'} \right)^{-1} {}^{i+1}\vec{S}_{g}^{T-} \right]. \tag{3.48}
$$

The moments are:

$$
{}^{i+1}\vec{\tilde{S}}_{g}^{\alpha,p-} = \frac{1}{u_g} \frac{{}^{i}\vec{\psi}_{g}^{\alpha',p-}}{\Delta t_{i+1}} + \sum_{\substack{g'=1 \\ g'\neq g}}^{NG} (2p_{-}+1)\, {}^{i+1}\Sigma_{\substack{s,p-\\ g'\to g}} \left[\left({}^{i+1}\tilde{L}^{-}_{p-,g'} \right)^{-1} {}^{i+1}\vec{\tilde{S}}_{g'}^{\alpha,p-} \right]. \tag{3.49}
$$

The multi-group coupling should be solved in the usual way.

The $O[\ ]$ operator in this case becomes a matrix of vectors the components of which are:

$$
{}^{i+1}\vec{O}_{g}^{(p+,\alpha),(p-,\alpha')} = \int_{V} dV f_{\alpha}(\vec{r})\, \vec{\nabla} f_{\alpha'}(\vec{r}) \frac{1}{2} \int_{-1}^{1} d\mu\, \mu (2p_{-}+1) P_{p+}(\mu) P_{p-}(\mu) \left({}^{i+1}\tilde{L}^{-}_{p-,g} \right)^{-1}. \tag{3.50}
$$

Once defined the $O[\ ]$ operator, the time procedure can be performed as done in the P_N case.

III.3. Comparison of the Two Schemes

In this section, an analytic comparison between the old scheme and the new one is shown under some simplifying hypothesis. This analytic comparison between models focuses on the time derivative of the odd parity component of the flux under the following assumptions:

- Operators are constant in time and space.
- One energy group.
- The flux has a linear behavior in angle:
  $\varphi(\vec{r},\vec{\Omega},E,t) = \sum_{p=0}^{1} \sum_{|q|=0}^{p} Y_{p,q}(\vec{\Omega})\, \varphi_{q}^{p}(\vec{r},E,t)$ (P_1 approximation).

- No fission source; i.e. only external isotropic source, S_0.
- No delayed neutrons.

The following definitions are also introduced (the definitions that follow are classical in reactor theory, here only their mono-group expressions are provided, the multi-group expression are more complex and the explanation of their evaluation, although basically equivalent, is outside of the scope of this dissertation):

- Scalar flux: $\Phi = \int_{4\pi} \mathrm{d}\vec{\Omega}\varphi\left(\vec{r},\vec{\Omega},E\right)$.
- Neutron current: $\vec{J} = \int_{4\pi} \mathrm{d}\vec{\Omega}\vec{\Omega}\varphi\left(\vec{r},\vec{\Omega},E\right)$.
- Removal cross section: $\Sigma_R = \Sigma_T - \Sigma_{s,0}$.
- Transport cross section: $\Sigma_{Tr} = \Sigma_T - \Sigma_{s,1}$.
- Scalar source: $S_0 = \int_{4\pi} \mathrm{d}\vec{\Omega}S\left(\vec{r},\vec{\Omega},E,t\right)$.

Under the above hypotheses, the system (2.39) is equivalent to:

$$\begin{cases} \frac{1}{v}\partial_t\Phi + \vec{\nabla}\vec{J} + \Sigma_R\Phi = S_0, \\ \frac{1}{v}\partial_t\vec{J} + \frac{1}{3}\vec{\nabla}\Phi + \Sigma_{Tr}\vec{J} = 0, \end{cases} \tag{3.51}$$

and the second equation of the system can be eliminated to obtain:

$$\frac{1}{v^2\Sigma_{tr}}\partial_t^2\Phi + \left(\frac{1}{v} + \frac{\Sigma_R}{v\Sigma_{Tr}}\right)\partial_t\Phi + \Sigma_R\Phi - \frac{1}{3\Sigma_{Tr}}\nabla^2\Phi = S_0 + \frac{1}{v\Sigma_{tr}}\frac{\partial S_0}{\partial t}. \tag{3.52}$$

This last equation is formally equivalent to the well known telegrapher's equation. This equation has been well studied in the electromagnetic field which is a characteristic of a perturbation propagating at finite velocity equal to $v/\sqrt{3}$. In case the time derivative of the current is neglected, it ends with the more simple equation:

$$\frac{1}{v}\partial_t \Phi - \frac{1}{3\Sigma_{Tr}}\nabla^2 \Phi + \Sigma_R \Phi = S_0. \tag{3.53}$$

This is clearly the time dependent neutron diffusion equation. The hypothesis, under which the diffusion approximation of the telegraph's equation is good, are also well known from a physical point of view. In the time dependent diffusion equation, the basic assumption is that the regime is collision dominated and therefore $\left\|\partial_t \vec{J}\right\| / \left\|\vec{J}\right\| \ll v\Sigma_{Tr}$ (the relative time variation of the current is much less than the collision frequency). Statistically, it means that the particles should never remain un-collided for a reasonably long time interval (changes in the source should not be appreciable during this time interval). A consequence of this assumption is that the neutrons theoretically move at infinity velocity, but the high number of collisions determine the characteristic diffusion time. Nevertheless, even if a characteristic diffusion velocity and time could be defined from a statistical point of view, at an infinite distance from an initial perturbation it is possible to notice some effect starting at the same time when the perturbations take place. As a conclusion the two different solutions for the telegrapher's (3.52) equation and the diffusion equations (3.53) are reported for a 1d (infinite media), 1 energy group model [56, 57] with a source of type $S_0 = Q\delta(t)\delta(x)$.

- Telegrapher's equation:

$$\phi(x,t) = \frac{e^{-at}}{2} Q \left\{ \delta\left(ct - |x|\right) + \beta h\left(ct - |x|\right) \left[\frac{ct}{\sqrt{(ct)^2 - x^2}} I_1(\theta) + I_0(\theta) \right] \right\}; \tag{3.54}$$

$$a = u\left(\Sigma_{tot} - \frac{1}{2}\Sigma_s\right), \qquad b = \frac{u}{2}\Sigma_s, \qquad c = \frac{u}{\sqrt{3}}, \qquad \beta = \frac{b}{c}, \qquad \theta = \beta\sqrt{(ct)^2 - x^2},$$

$\delta(z)$: Dirac's delta-function,

$h(z)$: Heaviside's step-function,

$I_0(\theta)$: 1st kind modified Bessel function of order 0,

$I_1(\theta) = \frac{dI_0(\theta)}{d\theta}$: modified Bessel function of the 1st order.

- Diffusion equation:

$$\phi(x,t) = Qve^{-\Sigma_a ut} e^{-x^2 3\Sigma_{tr}/4ut} \Big/ \left(\frac{4\pi ut}{3\Sigma_{tr}}\right)^{1/2}; \tag{3.55}$$

Of course, in the limit of the validity of the diffusion approximation, it can be shown that (3.54) is equivalent to (3.55). These observations are confirmed later in the numerical tests comparing the two different models. In general the diffusion model can be rather accurate for describing the behavior of nuclear reactors and thus the differences between the two approximations should be limited and vanish over large time scales. The stronger differences should be limited to the transient part for which the hypothesis on the source (negligible source changes in collision time scale) fails. At the end of this section, a last remark should call attention to the fact that the "numerical diffusion" of the time discretization schemes has a tendency to decrease the difference in the results between the two models.

III.4. Estimations of the Error

This section is dedicated to the analysis of the truncation error in the new time discretization scheme. This analysis has been provided to better understand the behavior of the scheme and sets the basis for the adaptive time step control strategy shown in the next section. Up to this point, the scheme proposed is based on a first order discretization in time. The fact that, both the even and odd parity fluxes, computed at the previous time step, are used to provide the time source, leads to the hope that the global error could be higher than of first order. In fact the odd parity flux is connected to the time derivative of the even parity flux via the second equation of the system (2.39), suggesting a reduction scheme has been used. Beginning with the systems (2.39) (without delayed neutrons and using the definitions of the $L^{\pm}$ operators):

$$\begin{cases} \frac{1}{u}\partial_t \phi + \vec{\Omega}\cdot\vec{\nabla}\psi + L^+[\phi] = S^+ + F_p[\phi], \\ \frac{1}{u}\partial_t \psi + \vec{\Omega}\cdot\vec{\nabla}\phi + L^-[\psi] = 0; \end{cases} \tag{3.56}$$

where the absence of an external odd parity source is in agreement with the capability of the VARIANT code, although its presence would not affect the results given in the following. Next, the second equation of the system is eliminated by means of the following manipulation:

$$\begin{cases} \vec{\Omega}\cdot\vec{\nabla}\psi = S^{+} + F_{p}\left[\phi\right] - L^{+}\left[\phi\right] - \dfrac{1}{u}\partial_{t}\phi, \\ \dfrac{1}{u}\partial_{t}\left(\vec{\Omega}\cdot\vec{\nabla}\psi\right) + \vec{\Omega}\cdot\vec{\nabla}\left[\left(L^{-}\right)^{-1}\left[\vec{\Omega}\cdot\vec{\nabla}\phi\right]\right] + \vec{\Omega}\cdot\vec{\nabla}\psi = 0. \end{cases} \tag{3.57}$$

The final result is:

$$\begin{aligned} &\frac{1}{u^{2}}\left(L^{-}\right)^{-1}\left[\partial_{t}^{2}\phi\right] + \frac{1}{u}\left(L^{-}\right)^{-1}\left[\partial_{t}\left(L^{+}\left[\phi\right]\right)\right] + \frac{1}{u}\partial_{t}\phi + L^{+}\left[\phi\right] - \vec{\Omega}\cdot\vec{\nabla}\left[\left(L^{-}\right)^{-1}\left[\vec{\Omega}\cdot\vec{\nabla}\phi\right]\right] = \\ &F\left[\phi\right] + \frac{1}{u}\left(L^{-}\right)^{-1}\left[\partial_{t}\left(F\left[\phi\right]\right)\right] + S^{+} + \frac{1}{u}\left(L^{-}\right)^{-1}\left[\partial_{t}S^{+}\right]. \end{aligned} \tag{3.58}$$

Now the idea is to compare a well known time discretization scheme applied to this equation to the result of the scheme developed in the previous chapter. Since the scheme is expected to be (without taking in account the delayed neutrons) a fully implicit one, and it is at maximum of second order in precision, the more reasonable scheme for the comparison seems to be a backward Euler scheme of second order. The approximations for the comparison scheme to be used in the approximating equation (3.58) are:

$$\partial_{t}^{2}\phi\Big|_{i+1} = 2\frac{\phi_{i+1}\dfrac{r}{1+r} - \phi_{i} + \phi_{i-1}\dfrac{1}{1+r}}{r\Delta t_{i+1}^{2}} + \mathrm{O}\left(\Delta t_{i+1}\right),$$

$$\partial_{t}\phi\Big|_{i+1} = \frac{\phi_{i+1} - \phi_{i}}{\Delta t_{i+1}} + \mathrm{O}\left(\Delta t_{i+1}\right),$$

$$\partial_{t}F\left[\phi\right]\Big|_{i+1} = \frac{F_{i+1}\left[\phi_{i+1}\right] - F_{i}\left[\phi_{i}\right]}{\Delta t_{i+1}} + \mathrm{O}\left(\Delta t_{i+1}\right),$$

$$\partial_{t}L^{+}\left[\phi\right]\Big|_{i+1} = \frac{L_{i+1}^{+}\left[\phi_{i+1}\right] - L_{i}^{+}\left[\phi_{i}\right]}{\Delta t_{i+1}} + \mathrm{O}\left(\Delta t_{i+1}\right), \tag{3.59}$$

where $r = \Delta t_i / \Delta t_{i+1}$. With the preceding and the introduction of $\overline{\Delta t} = \left(\Delta t_{i+1} + \Delta t_i\right)/2$, equation (3.58) is reduced to:

$$\begin{aligned}&\frac{1}{u^2 L^-_{i+1}}\frac{1}{\overline{\Delta t}}\left(\frac{\left[\phi_{i+1}-\phi_i\right]}{\Delta t_{i+1}}-\frac{\left[\phi_i-\phi_{i-1}\right]}{\Delta t_i}\right)+\frac{1}{L^-_{i+1}u}\frac{L^+_{i+1}\left[\phi_{i+1}\right]-L^+_i\left[\phi_i\right]}{\Delta t_{i+1}}-\vec{\Omega}\cdot\vec{\nabla}\left[\left(\frac{1}{L^-_{i+1}}\vec{\Omega}\cdot\vec{\nabla}\right)\phi_{i+1}\right]+\\&+\frac{1}{u}\frac{\phi_{i+1}-\phi_i}{\Delta t_{i+1}}+L^+_{i+1}\left[\phi_{i+1}\right]=S^+_{i+1}+\frac{1}{uL^-_{i+1}}\frac{\left[S^+_{i+1}-S^+_i\right]}{\Delta t_{i+1}}+\frac{1}{L^-_{i+1}v}\frac{F_{i+1}\left[\phi_{i+1}\right]-F_i\left[\phi_i\right]}{\Delta t_{i+1}}+\mathrm{O}\left(\Delta t_{i+1}\right).\end{aligned} \tag{3.60}$$

The solution for ϕ_{i+1} of this equation ($\mathrm{O}(\Delta t_{i+1}) \approx 0$) gives the second order backward reference estimation. Next, the first order approximation given by (3.1) is used to write the following system:

$$\begin{cases}\dfrac{1}{u}\dfrac{\tilde{\phi}_{n+1}-\phi_n}{\Delta t_{n+1}}+\vec{\Omega}\cdot\vec{\nabla}\left[\widetilde{\psi}_{n+1}\right]+L^+_{n+1}\left[\tilde{\phi}_{n+1}\right]=F_{n+1}\left[\phi_{n+1}\right]+S^+_{n+1},\\ \dfrac{1}{u}\dfrac{\phi_n-\phi_{n-1}}{\Delta t_n}+\vec{\Omega}\cdot\vec{\nabla}\left[\psi_n\right]+L^+_n\left[\phi_n\right]=F_n\left[\phi_n\right]+S^+_n,\\ \dfrac{1}{u}\dfrac{\widetilde{\psi}_{n+1}-\psi_n}{\Delta t_{n+1}}+\vec{\Omega}\cdot\vec{\nabla}\left[\tilde{\phi}_{n+1}\right]+L^-_{n+1}\left[\widetilde{\psi}_{n+1}\right]=0;\end{cases} \tag{3.61}$$

where the upper symbol $\tilde{}$ is used for the approximate solution given by the implemented scheme that is to be compared with the even parity flux estimation of (3.60). The application of the $\vec{\Omega}\cdot\vec{\nabla}\left[\left(L^-_{n+1}\right)[\ ]\right]$ operator allows the elimination of $\widetilde{\psi}_{n+1}$ and ψ_n, and results in the equation:

$$\begin{aligned}&\frac{1}{u^2 L^-_{n+1}\Delta t_{n+1}}\left(\frac{\left[\tilde{\phi}_{n+1}-\phi_n\right]}{\Delta t_{n+1}}-\frac{\left[\phi_n-\phi_{n-1}\right]}{\Delta t_n}\right)+\frac{1}{uL^-_{n+1}}\frac{L^+_{n+1}\left[\tilde{\phi}_{n+1}\right]-L^+_n\left[\phi_n\right]}{\Delta t_{n+1}}-\vec{\Omega}\cdot\vec{\nabla}\frac{1}{L^-_{n+1}}\vec{\Omega}\cdot\vec{\nabla}\left[\tilde{\phi}_{n+1}\right]+\\&+\frac{1}{u}\frac{\tilde{\phi}_{n+1}-\phi_n}{\Delta t_{n+1}}+L^+_{n+1}\left[\tilde{\phi}_{n+1}\right]=F_{n+1}\left[\phi_{n+1}\right]+\frac{1}{L^-_n u}\frac{F_{n+1}\left[\tilde{\phi}_{n+1}\right]-F_n\left[\phi_n\right]}{\Delta t_{n+1}}+S^+_{n+1}+\left(\frac{\left[S^+_{n+1}-S^+_n\right]}{uL^-_n\Delta t_{n+1}}\right).\end{aligned} \tag{3.62}$$

Introducing the difference between the two solutions $e = \phi_{n+1} - \tilde{\phi}_{n+1}$ and subtracting equation (3.62) from equation (3.60) it is possible to obtain:

$$e = \frac{(r-1)\Delta t^2_{n+1}}{2}\frac{\partial^2\phi}{\partial t^2}+O\left(\Delta t^3\right). \tag{3.63}$$

This final result shows that the discretization scheme proposed in III.1 is equivalent to the second order backward Euler scheme directly applied to the equation (3.58) only when the time step is constant ($r = 1 \rightarrow \Delta t_i = \Delta t_{i+1}$) or, of course, when the second order time derivative is zero. It is therefore clear that an adoption of a variable time step will decrease the order of precision below the one required to fully maintain the mathematical structure of the equation (3.58) that is second order with respect to time. The mathematical analysis carried on is of course formally correct on the asymptotic limit $\Delta t \rightarrow 0$, but in practical applications, the very low value of the coefficient of the second order time derivative in (3.58) ($\left(L^{-}\right)^{-1} / u^2 \ll 1$) makes the first order approximation on the first order derivative (3.59) in many cases dominant with respect to the mathematical second order precision. This behavior has also been detected in numerical tests which have shown a full second order decreasing of the error only in conjunction with very small time steps ($u\Delta t \ll 1$)).

The treatment of the delayed neutrons, as already mentioned, is not done in a fully implicit manner but, on the other hand, it is a phenomenon characterized by very large time scales. Therefore an accurate time step on the solution of the other part of the time structure of the equations will be a conservative criterion for the stability of this contribution. In fact, numerical instability due to the presence of delayed neutrons will arise only in cases of perturbations to the system (external source and composition changes) and a time step size on the time scales of delayed neutrons. These conditions are unrealistic given the transients under consideration.

For this work (to prove that the scheme can be of second order), it is sufficient to show that the precision in the delayed neutron terms ($\sum_{i=1}^{NF} \chi_{i,g} \lambda_i C_i$) treatment in equation (2.43) is at least of first order as was the case for the first order time derivative ($\frac{1}{u} \partial_t \phi$).

It is sufficient to prove it for the family *I*, thus the start is taken to be:

$$\begin{cases} \partial_t C = -\lambda C + \beta P[\phi], \\ \beta P[\phi](t_i \le t \le t_{i+1}) = {}^{i}\beta^{i} P\left[{}^{i}\phi\right] + \dfrac{{}^{i+1}\beta^{i+1} P\left[{}^{i+1}\phi\right] - {}^{i}\beta^{i} P\left[{}^{i}\phi\right]}{\Delta t_{i+1}}\left(t_{i+1} - t\right) + O\left(t_{i+1} - t\right)^2. \end{cases} \quad (3.64)$$

Introducing the integrating factor $e^{\lambda t}$ in the first equation yields:

$$\partial_t \left(e^{\lambda t} C\right) = e^{\lambda t}\left({}^{i}\beta^{i} P\left[{}^{i}\phi\right] + \frac{{}^{i+1}\beta^{i+1} P\left[{}^{i+1}\phi\right] - {}^{i}\beta^{i} P\left[{}^{i}\phi\right]}{\Delta t_{i+1}}\left(t_{i+1} - t\right) + O\left(t_{i+1} - t\right)^2 \right). \quad (3.65)$$

The solution of this equation is:

$${}^{i+1}C = e^{-\lambda \Delta t_{i+1}}\, {}^{i}C + \int_0^{\Delta t_{i+1}} d\tau e^{-\lambda\tau}\left({}^{i}\beta^{i} P\left[{}^{i}\phi\right] + \frac{{}^{i+1}\beta^{i+1} P\left[{}^{i+1}\phi\right] - {}^{i}\beta^{i} P\left[{}^{i}\phi\right]}{\Delta t_{i+1}}\tau \right) + \int_0^{\Delta t_{i+1}} d\tau e^{-\lambda\tau} O\left(\tau\right)^2 . \quad (3.66)$$

It is now clear (using for example the Taylor expansion of the exponential in the last integral) that the evaluation of ${}^{i+1}C$ is done with second order precision and thus the above condition is satisfied. The final conclusion is that the scheme proposed is at least of second order (for constant time step) and in the application field of interest, it is unconditionally stable since it is based upon a fully implicit scheme (delayed neutron instability is out of the application range)

III.5. Higher Time Discretization Scheme

The natural consequence derived from III.4 is that the introduction of a variable time step size requires a higher order time discretization scheme that will guarantee at least second order precision and stability regardless of the changes in the time step size. The option which is able to satisfy this requirement is a second order backward evaluation of the time derivative inside the first two equations of system (2.43).

Consequently, the following set of approximations is applied for the system (2.43):

$$\begin{aligned}
&\partial_t \phi_{i+1}^{(ex)} = \frac{\phi_{i+1}^{(ex)} r\left(r+2\right) - \phi_i \left(1+r\right)^2 + \phi_{i-1}}{\Delta t_{i+1} r\left(1+r\right)} + \mathrm{O}\left(\Delta t_{i+1}\right)^2, \\
&\partial_t \psi_{i+1}^{(ex)} = \frac{\psi_{i+1}^{(ex)} r\left(r+2\right) - \psi_i \left(1+r\right)^2 + \psi_{i-1}}{\Delta t_{i+1} r\left(1+r\right)} + \mathrm{O}\left(\Delta t_{i+1}\right)^2, \\
&\beta_i P\left[\phi\right]\left(t_i \le t \le t_{i+1}\right) = {}^{i}\beta_i \, {}^{i}P\left[{}^{i}\phi\right] + \frac{{}^{i+1}\beta_i \, {}^{i+1}P\left[{}^{i+1}\phi\right] - {}^{i}\beta_i \, {}^{i}P\left[{}^{i}\phi\right]}{\Delta t_{i+1}}\left(t_{i+1} - t\right) + \mathrm{O}\left(\Delta t_{i+1}\right)^2.
\end{aligned} \tag{3.67}$$

Since the treatment of delayed neutrons is unchanged and it is already done with second order precision, its contribution is neglected in the following discussion. The insertion of the above approximations into system (2.43) (without delayed neutrons contribution) leads to:

$$\begin{cases}
\dfrac{\phi_{i+1}\left(r+2\right)}{u\Delta t_{i+1}\left(1+r\right)} + \vec{\Omega}\cdot\vec{\nabla}\psi_{i+1} + L_{i+1}^{+}\left[\phi_{i+1}\right] = S_{i+1}^{+} + F_{i+1}\left[\phi_{i+1}\right] + \dfrac{\phi_i\left(1+r\right)^2 - \phi_{i-1}}{u\Delta t_{i+1} r\left(1+r\right)}, \\
\dfrac{\psi_{i+1}\left(r+2\right)}{u\Delta t_{i+1}\left(1+r\right)} + \vec{\Omega}\cdot\vec{\nabla}\phi_{i+1} + L_{i+1}^{-}\left[\psi_{i+1}\right] = \dfrac{\psi_i\left(1+r\right)^2 - \psi_{i-1}}{u\Delta t_{i+1} r\left(1+r\right)}.
\end{cases} \tag{3.68}$$

The system could be reformulated as done in (3.4) where the only differences are associated with the definition of the time sources reported in (3.3). Applying this produces:

$$\begin{aligned}
{}^{i+1}\tilde{S}^{+} &= {}^{i+1}S^{+} + \frac{\phi_i\left(1+r\right)^2 - \phi_{i-1}}{u\Delta t_{i+1} r\left(1+r\right)}, \\
{}^{i+1}\tilde{S}^{-} &= \frac{\psi_n\left(1+r\right)^2 - \psi_{i-1}}{u\Delta t_{i+1} r\left(1+r\right)}.
\end{aligned} \tag{3.69}$$

Starting from this new definition of the time source, the procedure shown in III.1 could be repeated without changes in the formalism. Thus, it is not displayed again. The initial conditions are also nearly the same since, under the hypothesis that the reactor is in a steady state mode before the transient analysis, ${}^{0}\phi$, ${}^{0}\psi$, and ${}^{0}C_i$ can be computed via (3.39) with ${}^{-1}\phi = {}^{0}\phi$, ${}^{-1}\psi = {}^{0}\psi$, and ${}^{-1}C_i = {}^{0}C_i$. The only difference is that it is necessary to define Δt_0 for the computation of r at the first time step. This value affects the numerical stiffness of the

system (the larger Δt_0 is, the stiffer the system). The usual choice is $\Delta t_0 = \Delta t_1$. This scheme is based on the second order backward scheme applied to the system of odd and even parity equations and will ensure at least the second order precision regardless of the changes in the time step size (the treatment of delayed neutrons is second order precision). The stability characteristics of the general scheme are also maintained.

III.6. Time Step Control Options

The next step is to take advantage of the possibility of having a variable time step size. The key issue is how to determine an appropriate time step size for the next time iteration. Under a conservative hypothesis the error at the next time step (i+2) can be estimated as:

$$err_{i+2}^{rel} = \left(\partial_t^3 \phi \Big|_{i+2} \frac{\Delta t_{i+2}^3}{6} \right) / \phi_{i+2} + O\left(\Delta t\right)^4 . \tag{3.70}$$

This hypothesis is conservative since it is based on the truncation error in the first order time derivative evaluation inside the even-odd system. However, as shown in III.4, the global error in solving the system could decrease depending on the ratio (*r*) between the time step sizes for succesive time iterations. Writing the above expression using a forward zero order Taylor expansion:

$$err_{i+2}^{rel} = \frac{\left(\partial_t^3 \phi \Big|_{i+1} + O\left(\Delta t\right) \right)}{\phi_{i+1} + O\left(\Delta t\right)} \frac{\Delta t_{i+2}^3}{6} + O\left(\Delta t\right)^4 = \left(\partial_t^3 \phi \Big|_{i+1} \frac{\Delta t_{i+2}^3}{6} \right) / \phi_{i+1} + O\left(\Delta t\right)^4 . \tag{3.71}$$

In this way, the error at the next time step is a function of Δt_{i+2}, a cubic time derivative, and the even-parity flux at the current time step (*i+1*). Restriction of the error below a fixed value (*tol*) leads to the following inequality:

$$\Delta t_{i+2}^3 \le 6 \left| \frac{\phi_{i+1}}{\partial_t^3 \phi \Big|_{i+1}} \right| tol . \tag{3.72}$$

Therefore the problem is now reduced to the estimation of the cubic derivative. It should be pointed out that, for the moment, $\left| \ \right|$ is the standard norm over R, thus Δt_{i+2} actually depends

upon all the variables $\left(\vec{r},\vec{\Omega},E\right)$ (the domain of $\vec{\Omega}$ could be reduced by half if only the even-parity flux is considered). Writing the expression for the first order derivative using the third order backward Euler scheme with only two points and leaving the third order derivative unresolved leads to:

$$\partial_t\phi\Big|_{i+1}^{(ex)}=\frac{\phi_{i+1}^{(ex)}r\left(r+2\right)-\phi_i\left(1+r\right)^2+\phi_{i-1}}{\Delta t_{i+1}r\left(1+r\right)}-\partial_t^3\phi\Big|_{i+1}^{(ex)}\frac{\Delta t_{i+1}^2\left(1+r\right)}{6}+\mathrm{O}\left(\Delta t_{i+1}\right)^3. \tag{3.73}$$

Implementing the second order backward scheme approximation produces:

$$\partial_t\phi\Big|_{i+1}^{(2b)}\approx\frac{\phi_{i+1}^{(2b)}r\left(r+2\right)-\phi_i\left(1+r\right)^2+\phi_{i-1}}{\Delta t_{i+1}r\left(1+r\right)}. \tag{3.74}$$

The indices (*ex*) and (*2b*) stand, respectively, for exact and second order approximate (backward Euler) solutions at time step i+1. Now the first equation of (3.56) is compared with the expression of the first derivative given by equation (3.73) and its approximation using the expression of the first derivative given by equation (3.74):

$$\begin{cases}\dfrac{1}{u}\dfrac{\phi_{i+1}^{(ex)}\left(r+2\right)-\phi_i\dfrac{\left(1+r\right)^2}{r}+\phi_{i-1}\dfrac{1}{r}}{\Delta t_{i+1}\left(1+r\right)}-\partial_t^3\phi_{i+1}^{(ex)}\dfrac{\Delta t_{i+1}^2\left(1+r\right)}{u6}+\vec{\Omega}\cdot\vec{\nabla}\psi_{i+1}^{(ex)}+L^+\left[\phi_{i+1}^{(ex)}\right]= \\ =F\left[\phi_{i+1}^{(ex)}\right]+S_{i+1}^+ +\mathrm{O}\left(\Delta t_{i+1}\right)^3, \\ \dfrac{1}{u}\dfrac{\phi_{i+1}^{(2b)}\left(r+2\right)-\phi_i\dfrac{\left(1+r\right)^2}{r}+\phi_{i-1}\dfrac{1}{r}}{\Delta t_{i+1}\left(1+r\right)}+\vec{\Omega}\cdot\vec{\nabla}\psi_{i+1}^{(2b)}+L^+\left[\phi_{i+1}^{(2b)}\right]=F\left[\phi_{i+1}^{(2b)}\right]+S_{i+1}^+.\end{cases} \tag{3.75}$$

It is helpful to mention that the first equation of the above system represents the property of the exact solution and the second one is the definition of the function $\phi_{i+1}^{(2b)}$. It is also helpful to note that:

$$\begin{cases}L^+\left[\phi_{i+1}^{(ex)}\right]=L^+\left[\phi_{i+1}^{(2b)}\right]+L^+\left[\mathrm{O}\left(\Delta t_{i+1}\right)^3\right]=L^+\left[\phi_{i+1}^{(2b)}\right]+\mathrm{O}\left(\Delta t_{i+1}\right)^3, \\ \vec{\Omega}\cdot\vec{\nabla}\chi_{i+1}^{(ex)}=\vec{\Omega}\cdot\vec{\nabla}\psi_{i+1}^{(2b)}+\vec{\Omega}\cdot\vec{\nabla}\mathrm{O}\left(\Delta t_{i+1}\right)^3=\vec{\Omega}\cdot\vec{\nabla}\psi_{i+1}^{(2b)}+\mathrm{O}\left(\Delta t_{i+1}\right)^3, \\ F\left[\phi_{i+1}^{(ex)}\right]=F\left[\phi_{i+1}^{(2b)}\right]+F\left[\mathrm{O}\left(\Delta t_{i+1}\right)^3\right]=F\left[\phi_{i+1}^{(2b)}\right]+\mathrm{O}\left(\Delta t_{i+1}\right)^3.\end{cases} \tag{3.76}$$

After substituting the last relations in equation (3.75) the following results:

$$\phi_{i+1}^{(ex)} - \partial_t^3 \phi_{i+1}^{(ex)} \frac{\Delta t_{i+1}^3 (1+r)^2}{6(r+2)} = \phi_{i+1}^{(2b)} + \mathrm{O}(\Delta t_{i+1})^4 . \tag{3.77}$$

The centered Euler scheme (*2c*) is used to obtain (equations (3.73) to (3.76) are implicitly repeated):

$$\begin{cases} \dfrac{r^2 \phi_{i+1}^{(ex)} - \phi_{i-1} + \phi_i (1-r^2)}{u(r+1) r \Delta t_{i+1}} - \partial_t^3 \phi_i \dfrac{r \Delta t_{i+1}^2}{u6} + \vec{\Omega} \cdot \vec{\nabla} \psi_i + L^+ [\phi_i] = S_i^+ + \mathrm{O}(\Delta t_{i+1})^3 , \\ \dfrac{r^2 \phi_{i+1}^{(2c)} - \phi_{i-1} + \phi_i (1-r^2)}{u(r+1) r \Delta t_{i+1}} + \vec{\Omega} \cdot \vec{\nabla} \psi_i + L^+ [\phi_i] = S_i^+ , \end{cases} \tag{3.78}$$

from which it is possible to get another expression for the third order time derivative as a function of the exact solution and the second order centered scheme solution:

$$\phi_{i+1}^{(ex)} - \partial_t^3 \phi_i^{(ex)} \frac{\Delta t_{i+1}^3 (1+r)}{6} = \phi_{i+1}^{(2c)} + \mathrm{O}(\Delta t_{i+1})^4 . \tag{3.79}$$

By observing that:

$$\partial_t^3 \phi_i^{(ex)} \frac{\Delta t_{i+1}^3 (1+r)}{6} = \partial_t^3 \phi_{i+1}^{(ex)} \frac{\Delta t_{i+1}^3 (1+r)}{6} + \mathrm{O}(\Delta t_{i+1})^4 , \tag{3.80}$$

the following system of equations can be obtained:

$$\begin{cases} \phi_{i+1}^{(ex)} - \partial_t^3 \phi_{i+1} \dfrac{\Delta t_{i+1}^3 (1+r)^2}{6(r+2)} = \phi_{i+1}^{(2b)} + \mathrm{O}(\Delta t_{i+1})^4 , \\ \phi_{i+1}^{(ex)} - \partial_t^3 \phi_{i+1} \dfrac{\Delta t_{i+1}^3 (1+r)}{6} = \phi_{i+1}^{(2c)} + \mathrm{O}(\Delta t_{i+1})^4 . \end{cases} \tag{3.81}$$

It is now easy to see that:

$$\partial_t^3 \phi_{i+1} = \frac{6(r+2)}{(1+r)} \frac{\phi_{i+1}^{(2b)} - \phi_{i+1}^{(2c)}}{\Delta t_{i+1}^3} + \mathrm{O}(\Delta t_{i+1}) . \tag{3.82}$$

The last task is to define the error in an appropriate norm since the actual intention is to use a common time step for all energy groups, regions, and angular moments. First of all, the average

scalar flux is used within each region (upper left index *n*) and energy group (lower left index *j*) defined by:

$$ {}^{n}_{j}\bar{\phi}_i = \frac{1}{4\pi}\int_{4\pi} d\vec{\Omega}\frac{1}{\Delta E_j}\int_{\Delta E_j} dE\frac{1}{V_n}\int_{Vol} dV\,\phi_i\left(\vec{r},\vec{\Omega},E\right). \tag{3.83} $$

Now a maximum norm can be introduced over all energy groups and regions:

$$ \left\|\bullet\right\|_e = \max_{1\le n\le nreg}\ \max_{1\le j\le ngroup}\left|\bullet\right|. \tag{3.84} $$

In this norm the relative error over the average scalar flux within each region and energy group becomes:

$$ {}^{n}_{j}err^{rel}_{i+2} = \left\| \frac{\partial^3_t\, {}^{n}_{j}\bar{\phi}\big|_{i+1}}{{}^{n}_{j}\bar{\phi}_{i+1}} \right\|_e \frac{\Delta t^3_{i+2}}{6}. \tag{3.85} $$

By introducing equation (3.82) for the third order derivative in equation (3.84) and adhering to the inequality $err^{rel}_{n+2} \le tol$, the following expression is obtained for Δt_{n+2}:

$$ \Delta t_{i+2} \le \Delta t_{i+1}\sqrt[3]{\frac{tol\left(1+r\right)}{\left(r+2\right)}\left\|\frac{{}^{n}_{j}\bar{\phi}^{(2b)}_{i+1}}{{}^{n}_{j}\bar{\phi}^{(2b)}_{i+1}-{}^{n}_{j}\bar{\phi}^{(2c)}_{i+1}}\right\|_e} = \Delta t_{i+1}\sqrt[3]{\frac{tol\left(1+r\right)}{\left(r+2\right)}\max_{1\le n\le nreg}\ \max_{1\le j\le ngroup}\left|\frac{{}^{n}_{j}\bar{\phi}^{(2b)}_{i+1}}{{}^{n}_{j}\bar{\phi}^{(2b)}_{i+1}-{}^{n}_{j}\bar{\phi}^{(2c)}_{i+1}}\right|}. \tag{3.86} $$

The use of the semi-norm (the evaluation is done in a sub-space of the spawn of the basis function used by the VARIANT code in space and angle) instead of the full norm means ignoring some of the information about the error behavior. However, this choice is nevertheless physically reasonable since the spatial average value of the scalar flux within each region and energy group is 'monitored'. This is of course the primary quantity of interest in reaction rate calculations. There can be, of course, some limiting cases in which this error definition can be weak. However, by decreasing the tolerance, it should be possible to treat every realistic case successfully. It should also be pointed out that such a choice for the error definition greatly simplifies the effort required for the solution of the centered second order scheme, since only the average scalar fluxes are needed.

They can be calculated from the following balance equation:

$$\left(\frac{r}{v\left(r+1\right)\Delta t_{i+1}}\right){}_{j}^{n}\overline{\phi}_{i+1}^{(2c)}=\left(\frac{{}_{j}^{n}\overline{\phi}_{i-1}-{}_{j}^{n}\overline{\phi}_{i}\left(1-r^{2}\right)}{v\left(r+1\right)\Delta t_{i+1}}-{}_{j}^{n}\Sigma_{R}\,{}_{j}^{n}\overline{\phi}_{i}+{}_{j}^{n}S_{i}^{+}\right)-\frac{1}{V_{n}}\sum_{\alpha}^{Nsurf_{n}}\int_{S_{\alpha}}ds\,{}_{j}^{n}\vec{J}_{i}\cdot\vec{n}\,. \quad (3.87)$$

Here, ${}_{j}^{n}\vec{J}$ is the net current on the surface $S_{\alpha}\subset\partial V_{n}$ and ${}_{j}^{n}\Sigma_{\mathrm{R}}$ is the removal cross section for region *n* and group *j*. Before the analysis of the results for the time step control scheme, some preliminary considerations are instructive. First of all, although the estimation of the third order derivative is not used to improve the flux approximation, the scheme cannot be considered to be a linear partial implicit one, since the estimation of Δt_{i+2} is done using centered and forward schemes. For this reason, the estimation of this quantity could be affected by instability and, therefore, by inaccuracy. Especially in cases where very fast changes of the time scale (i.e. an order of magnitude) can lead to oscillations or fluctuations in the estimated time step. The influence of this phenomenon can usually be damped by using some average or limits for the range of time step variations, like an arithmetic or geometrical averaging between the next estimated time step and the actual one. This kind of instability is also enhanced by a low convergence criterion while computing the pseudo static flux. Of course this kind of error prediction based upon the forward scheme can lead to some inaccuracy, thus only an imperfect matching should be expected between the imposed tolerance and the relative error with respect to any reference solution.

Chapter IV. NUMERICAL SIMULATION RESULTS AND CONCLUSIONS

The order in which results will be presented reflects the development path of the code and thus they will be presented starting from a 1D test for the new first order scheme with a constant time step to a full 3D simulation of a source transient in an ADS using the adaptive high order scheme. Some very simple tests are also presented which are not representative of any real physical situation for two reasons. First, in such tests, the behavior of the differences between the old and new scheme are qualitatively foreseeable by means of the physical interpretation of the different mathematical approximations. This feature allows one to check the correctness of the method and get a feeling of the differences that can arise in a realistic case. Second, such simple tests are needed in order to understand the optimal value of parameters like the time step, convergence criteria, order of the spatial approximation, spatial mesh size, etc…

IV.1. One-Dimensional Analytic Benchmark

This test is the simplest one performed, but it plays a key role in this work. The problem considered is a 1-dimensional slab without fissile material. As will be explained later on, the boundary condition in the time interval considered plays no role for the new time integration scheme while are chosen of vacuum type for the old one. A one energy group approximation is used combined with an isotropic scattering cross section and source. The cross section data are given as follows:

$u = 10^8 cm/s,$
$\Sigma_{tot} = 0.8 cm^{-1},$
$\Sigma_s = 0.4 cm^{-1}.$

The half length of the slab is 0.9 cm and the spatial mesh size is 0.001 cm. Two different spatial distributions of the source: $S_1(x)$ and $S_2(x)$ have been considered in conjunction with the same triangular variation in time:

$$S_1(x,t) = S_1(x)S(t) = 1/2\left(h(0.001-x) - h(x-0.001)\right)S(t),$$
$$S_2(x,t) = S_2(x)S(t) = 1/2\left(h(0.1-x) - h(x-0.1)\right)S(t),$$
$$S(t) = \begin{cases} 2\cdot 10^{12}t & 0 < t < 0{,}5\cdot 10^{-9}, \\ -2\cdot 10^{12}t + 2\cdot 10^{3} & 0{,}5\cdot 10^{-9} < t < 1\cdot 10^{-9}, \\ 0 & t > 1\cdot 10^{-9}. \end{cases}$$

$h(x)$ is the Heaviside's step-function. It is clear that the time dependent part of the source is close to being a Dirac delta-function like the spatial part of S_1. Such a choice for the source transients explains the very fine spatial discretization step ($\Delta x = 0.001\ cm$). In fact, even if the scheme is always stable, it is necessary to control the numerical diffusion that can arise from a coarse choice of time and spatial step size. This transient has been analyzed with the new time dependent P_1 model and with the old diffusion model. Before analyzing the numerical results some preliminary considerations are possible. First, the last term of equation (3.52), which is absent in the diffusion model (3.53), reaches very high values during the source variation:

$$\frac{1}{u\Sigma_{tr}}\left|\frac{\partial S(x,t)}{\partial t}\right| = \frac{1}{10^8\cdot 0{,}4} S_{1\,or\,2}(x)\,2\cdot 10^{12} = 5\cdot 10^4 S_{1\,or\,2}(x). \tag{4.1}$$

Moreover the time derivative of the source is also discontinuous in fact:

$$\begin{aligned} &\frac{1}{u\Sigma_{tr}}\frac{\partial S(x,t)}{\partial t}\bigg|_{t\to\left(0{,}5\cdot 10^{-9}\right)_{left}} - \frac{1}{u\Sigma_{tr}}\frac{\partial S(x,t)}{\partial t}\bigg|_{t\to\left(0{,}5\cdot 10^{-9}\right)_{rigth}} = 1\cdot 10^5 S_{1\,or\,2}(x). \\ &\frac{1}{u\Sigma_{tr}}\frac{\partial S(x,t)}{\partial t}\bigg|_{t\to\left(1\cdot 10^{-9}\right)_{left}} - \frac{1}{u\Sigma_{tr}}\frac{\partial S(x,t)}{\partial t}\bigg|_{t\to\left(1\cdot 10^{-9}\right)_{rigth}} = 5\cdot 10^4 S_{1\,or\,2}(x) \end{aligned} \tag{4.2}$$

Consequently, strong differences are expected in the results provided by means of the two models. In the 1D P_1 model the perturbation moves at a fixed velocity that is $u/\sqrt{3}$ thus if the analysis is limited to a *t* that satisfies:

$$t_{\max} < \left(0.9 - x_{\max\ source}\right)\sqrt{3}/10^{-8} \cong 1{,}385 \cdot 10^{-8} s\,, \tag{4.3}$$

it is possible to neglect the boundary condition effect (the argument of the Heaviside's step-function in (3.54) will be less than zero). In the diffusion approximation, boundary conditions affect the solution starting from $t = 0$, and vacuum boundary conditions were used.

Of course the direct comparison between the analytic solution to the P_1 equations provided by (3.54) for a Dirac delta-function in time and space source and the numerical evaluation provided by the code could not be more than qualitative since the sources $S_{1\ or\ 2}$ are not analytic delta-functions. In order to overcome this situation, a small code has been written to numerically evaluate the convolution of the solution $\phi_{\delta\left(\substack{x=0\\t=0}\right)}(x,t)$ provided by (3.54). Therefore for this simple test it is possible to have a reference solution provided by the numerical evaluation of:

$$\phi(x,t) = \int_{-x}^{x} dx' \int_{0}^{t} dt'\, S_1(x',t')\, \phi_{\delta\left(\substack{x=0\\t=0}\right)}(x-x',t-t')\,. \tag{4.4}$$

Figure 4 and 5 show, for the $S_1(x,t)$ source, the comparison between the pseudo analytical solution (numerical evaluation of (4.4)), the solution obtained with the new version of the code using different time steps (i.e. 10^{-12}, 10^{-11}, 10^{-10} s), and the solution by the diffusion model (multiplied by a factor of 10) obtained using the old version of the code with a time step of 10^{-11} s. It is clear how this severe test causes the diffusion approximation to be far from the P_1. This fact was somehow expected since the vacuum boundary condition in the diffusion model immediately starts to absorb neutrons from the system. The results provided by the new version of the code are observed to converge to the pseudo analytic solution with respect to a decreasing time step. This demonstrates very good performance by the method. Similar types of tests have been performed with other numerical methods [58] achieving performance similar

to the ones shown here. A good indication of the robustness and stability of the scheme comes from the evaluation of the position of the flux peak that, despite the numerical diffusion phenomenon, is in the correct position predicted by $ct-|x|=0$. This fact shows that the mathematical structure of the equations is maintained. The test performed with the source $S_2(x,t)$ is more easily handled by the numerical scheme. In fact, Figures 6 and 7 show acceptable results even with a time step of 10^{-10}s. The explanation of this phenomenon is related to the behavior of the numerical diffusion. Without going into details, numerical diffusion analysis relates the smaller spatial resolution of the solution to the time step size. In the $S_1(x,t)$ test with a time step of 10^{-10}s the front and backward side of the wave are smeared by the numerical diffusion in overlapping areas, leading to a mutual influence of approximation errors. This phenomena is absent when considering the $S_2(x,t)$ source due to the larger distance between the front and backward side of the wave.

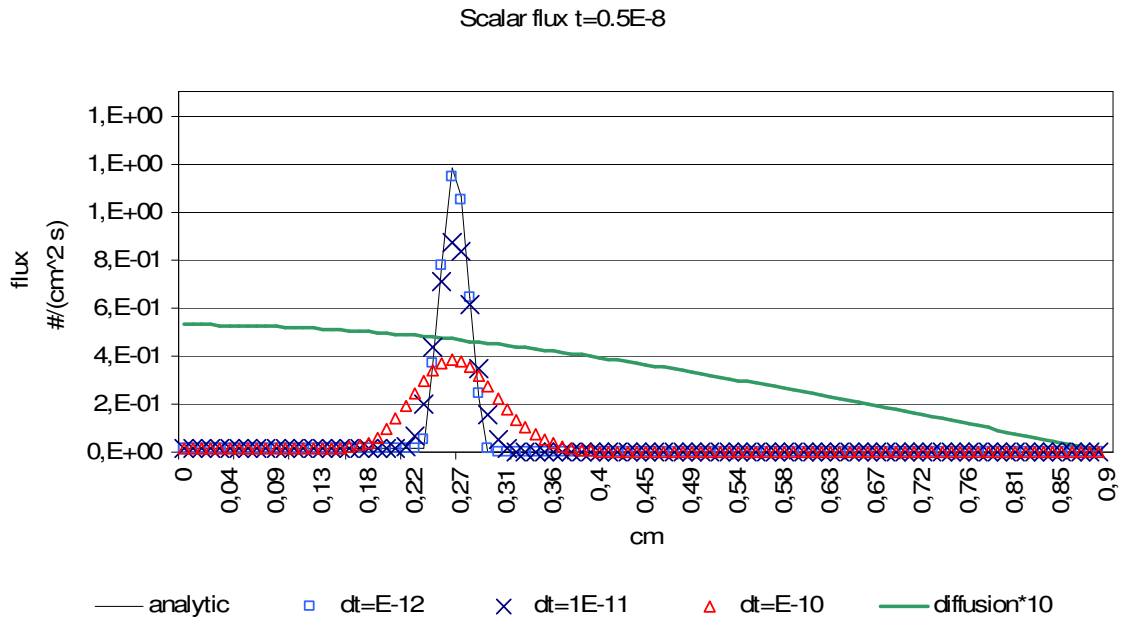

Figure 4: Scalar flux comparison, numerical P_1, analytical and diffusion, t= 0.5 10^{-8} s, S= S_1.

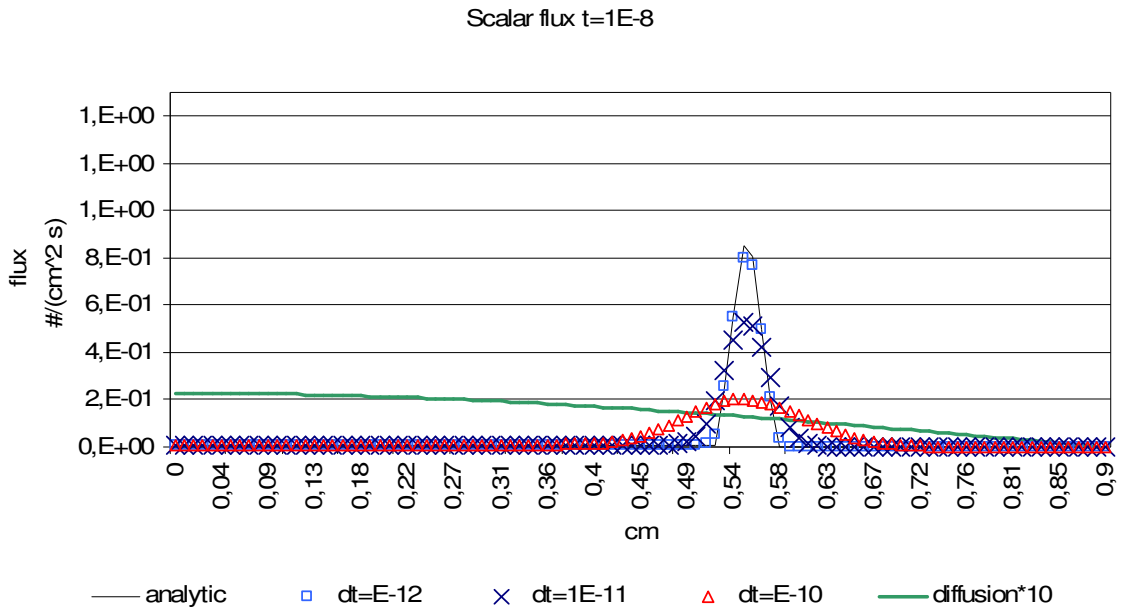

Figure 5: Scalar flux comparison, numerical P_1, analytical and diffusion, t=10^{-8} s, S= S_1 .

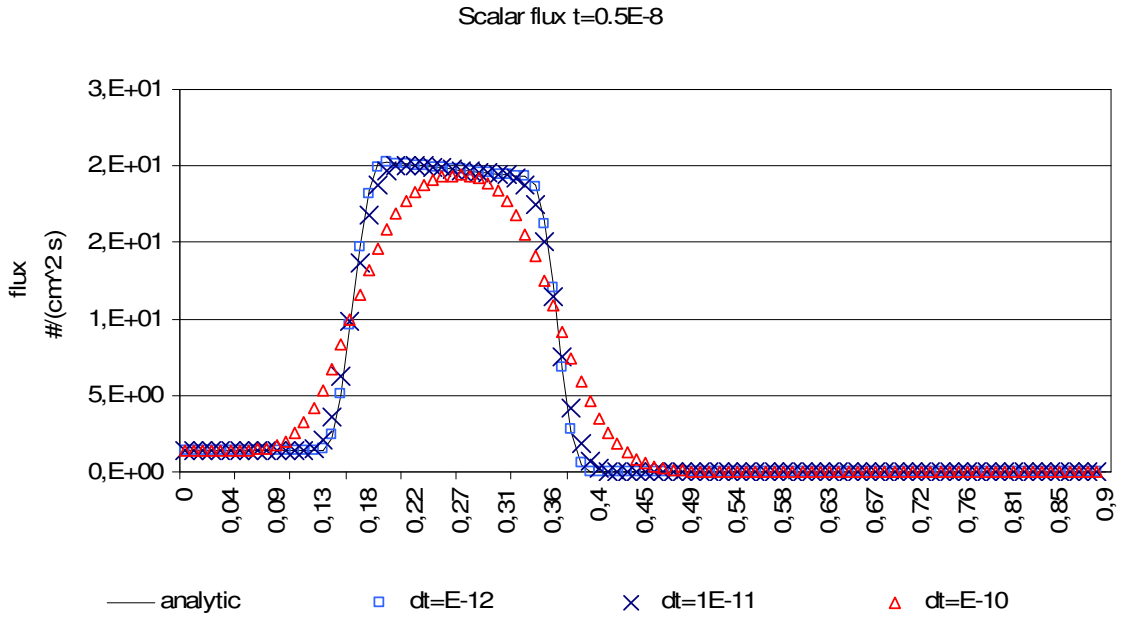

Figure 6: Scalar flux comparison, numerical P_1, analytical and diffusion, t= 0.5 10^{-8} s, S= S_2.

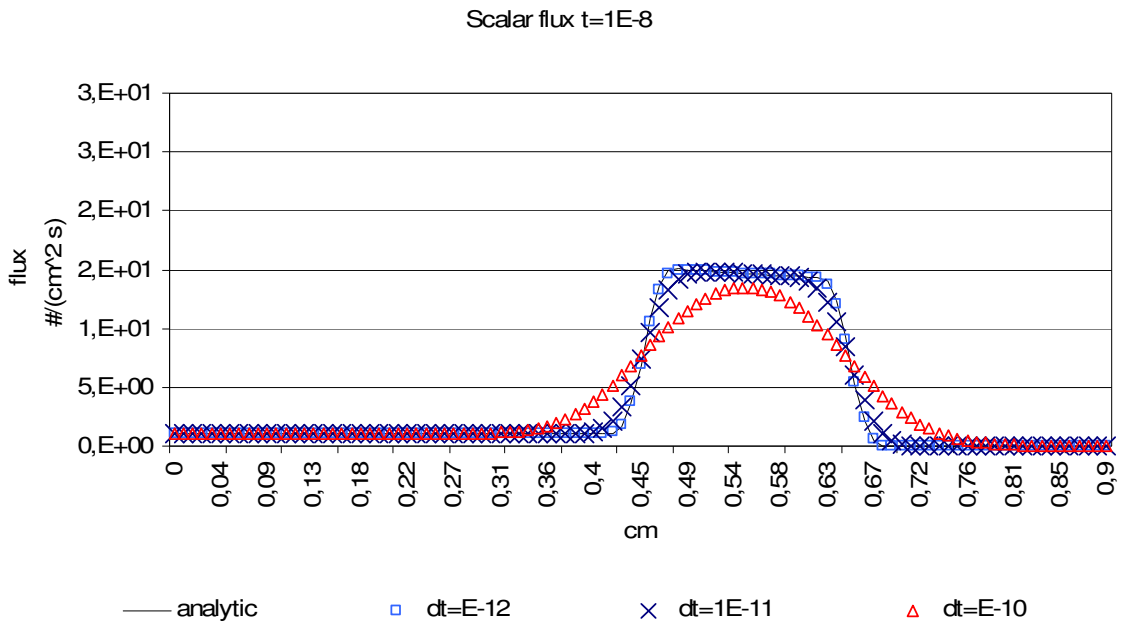

Figure 7: Scalar flux comparison, numerical P_1, analytical and diffusion, t=10^{-8} s, S= S_2.

IV.2. Two Dimensional Muse Transient Analysis

The main aim of this test is to compare how the non-adaptive second order scheme described in III.1 and III.2 and the old one differ in simulating the flux variations in a realistic case using P_1, SP_3 and P_3 angular approximations. The test has been performed on a simplified 2D representation of the MUSE experiment (described briefly in I.2) by means of a 33 energy group structure (typical for fast reactor analysis), and a simplified source present only in the first energy group. As already mentioned, in sub-critical experiments, the objective is to compute the flux inside of the reactor during the transient. Of course the flux is not directly measurable, thus, some correlated quantities are used such as reaction rates measured by fission chambers. One of the commonly used reaction rates is derived from ^{235}U which has a very well known fission cross section. For these reasons, comparison of the predicted detector response is used instead of the numerical values of the flux.

The response of a detector placed in spatial region *i,* can be computed using:

$$D_i(t) = \int_{E_{\min}}^{E_{\max}} dE \int_{4\pi} d\vec{\Omega} \int_{V_i} d\vec{r}\, \varphi\left(\vec{r}, \vec{\Omega}, E, t\right) \Sigma_f^{235} = 4\pi \sum_{g=1}^{NG} \Sigma_{f,g}^{235} \phi_{0,0}^{i,g}(t), \tag{4.5}$$

where $\phi_{0,0}^{i,g}$ is the zero order spatial and angular moment of the even parity flux for the region *i* and group *g*. Figure 8 shows the position of 3 detectors (^{235}U fission chambers) the source region and the computational spatial mesh (i.e. each rectangle is a mesh used by the VARIANT code in order to describe the spatial geometry) considered in this test.

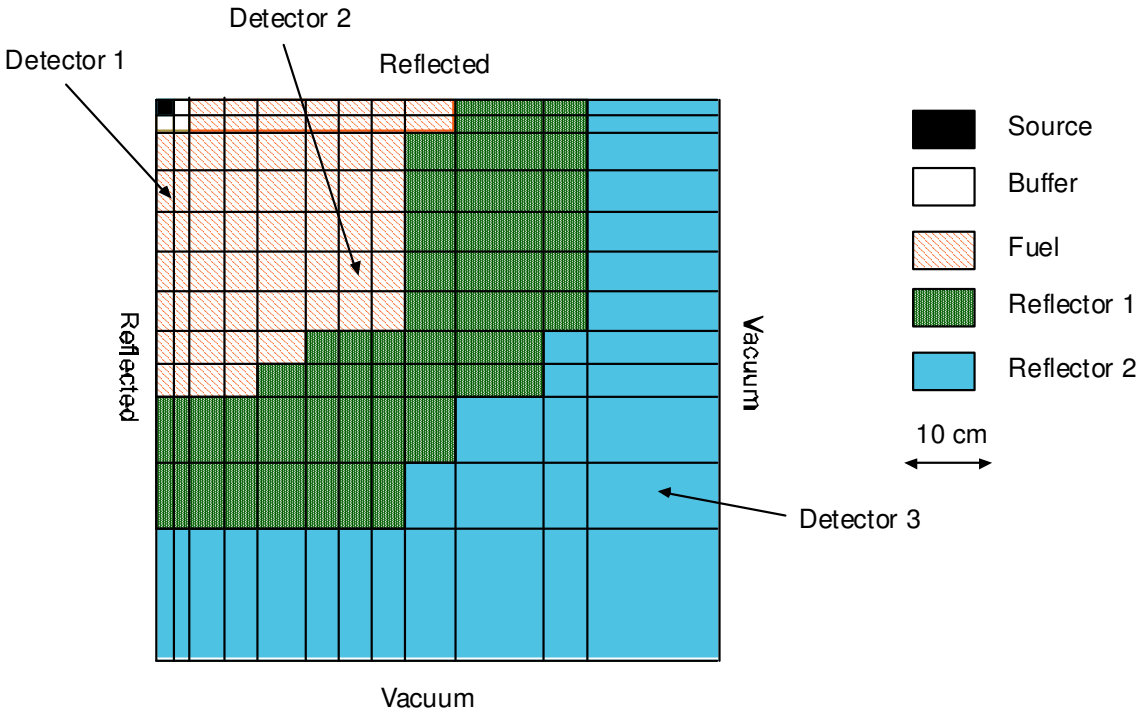

Figure 8: 2D MUSE geometry.

In the past, when high order angular approximations were not available or too expensive to be used in transient simulations, simple procedures have been developed to approximately account for the angular effect. One of these procedures involves the comparison of k_{eff} with a high angular approximation with the one used for the transient simulation. This procedure

renormalizes or adjust the average number of neutrons released by each fissions, $\bar{\nu}$, in order to achieve the same k_{eff} with a lower angular discretization in the transient analysis. The general idea is that the neutron balance for the fundamental mode is forced to be the same for all of the angular discretizations during the transient. If the neutron flux during the transient can be fully described by the fundamental mode, this process allows one to obtain the same ratio between the steady state and the time dependent flux regardless of the angular discretization that is used during the transient simulation. Unfortunately, although the fundamental mode is important for the neutron flux distribution, it is not necessarily the only mode important for transients in sub-critical systems. In order to show the improvements achievable with this new time dependent scheme with respect to the available methodologies, the P_1 and SP_3 angular schemes are modified, by the renormalization procedure just described, such that they have the same k_{eff} given by the P_3 scheme (taken to be the reference). Table 1 shows the k_{eff} of the lower angular approximations and the reference value. Moreover, instead of directly comparing the detector rate multiplication factors, $f_i(t) = D_i(t)/D_i(t=0)$ are compared. The steady state detector errors are also reported in Table 1. Figure 9 shows the time behavior of the source multiplication factor $(S_f(t) = S\left(\vec{r},\vec{\Omega},E,t\right)/S\left(\vec{r},\vec{\Omega},E,t=0\right))$ and the detector rate multiplication factors (det. stands for detector) obtained by the reference scheme (P_3). As seen in Figure 9 the peaks in the detector response are delayed and smoothed in time according to their respective distance from the source region. This is in agreement with an increasing dominance of the diffusion model with time and spatial distance from the source transient. Figures 10 to 14 show the relative error of the multiplicative detector rate factors with respect to the P_3 angular model used with the new time discretization model. Generally speaking, the error decreases as the distance between the source area and the detector increases but the shape is similar. Another effect is the presence of material discontinuities that need a higher P_n order. These interface effects may probably explain the greater error in the second detector with respect to the first one in the P_1 analysis (see Figure 10 and 11). Unfortunately the

improvement achieved by the new time scheme, in the P_1 framework, is not apparent (compare Figures 10 and 11), displaying errors of the order of several percents. Such a result is quite undesirable. The old time discretization with P_3 and SP_3 schemes (Figures 12 and 13) shows a good improvement with respect to the P_1 model but still not completely satisfactory. The introduction of the new time scheme for the SP_3 approximation displays results very similar to those of the reference (Figure 14). The computational cost comparison suggests that the introduction of the new time discretization scheme is inexpensive at all or better still it seem to decrease slightly the total computational cost (see Table 1). This effect could be imputed to an improvement of the speed of convergence of the inner iteration of VARIANT due to the different set of time modified cross section (i.e. the different use of the time absorption) between the two (old and new) time scheme. This positive effect result to be dominant with respect the additional computational cost due to the introduction of the odd angular source in the new scheme, the behavior has been detected in all the tests performed comparing the old and new time integration scheme. A last remark about the computation cost is that the introduction of the SP_N method, at least for the P_3/SP_3 set, allows a reduction of a factor two without a strong loss of precision. The conclusions of this test are: higher angular approximations are needed on short time scales such that the behavior of the neutron flux is appropriate. Based upon the current result, the use of the SP_N methodology offers a good compromise between computational costs and precision especially for forecasting future 3D applications.

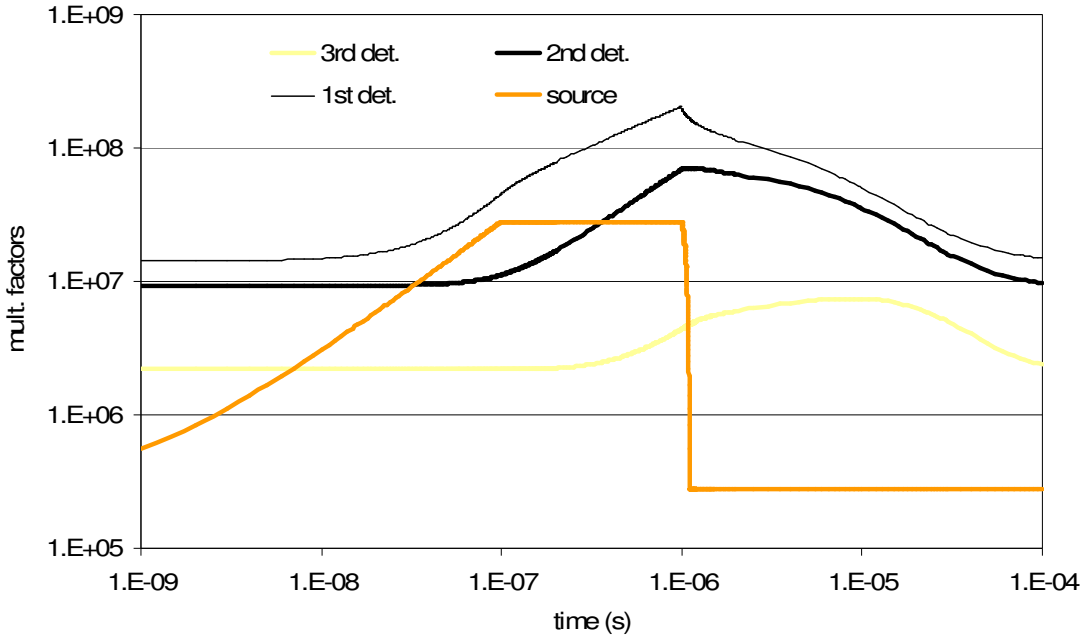

Figure 9: Source and detectors rate multiplication factors.

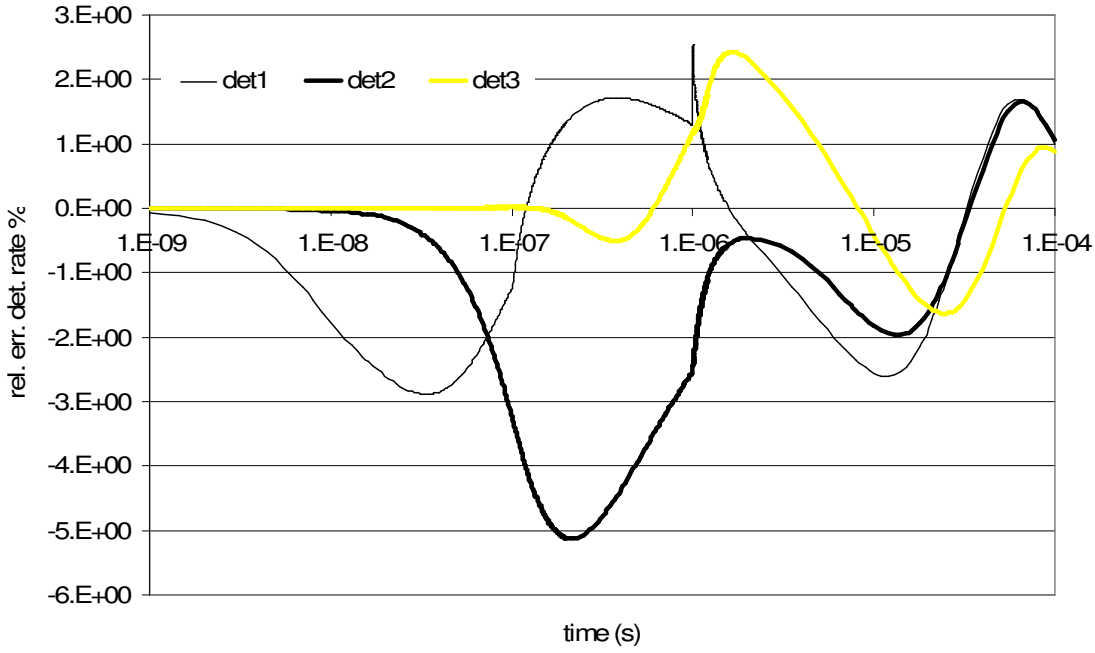

Figure 10: Old time scheme, P_1 angular discretization.

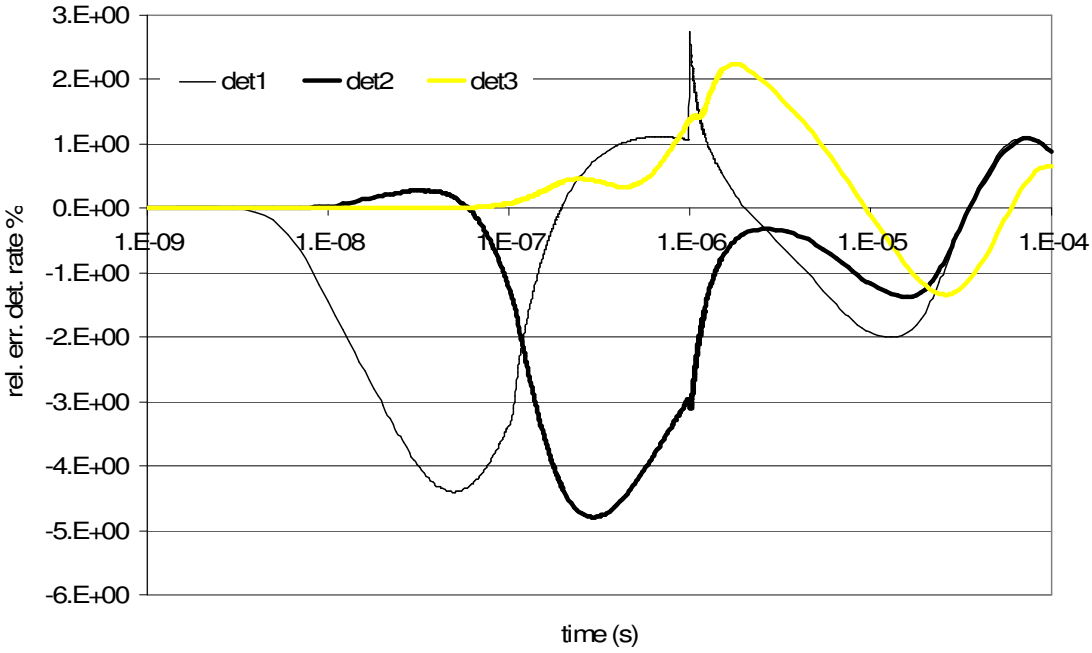

Figure 11: New time scheme, P_1 angular discretization.

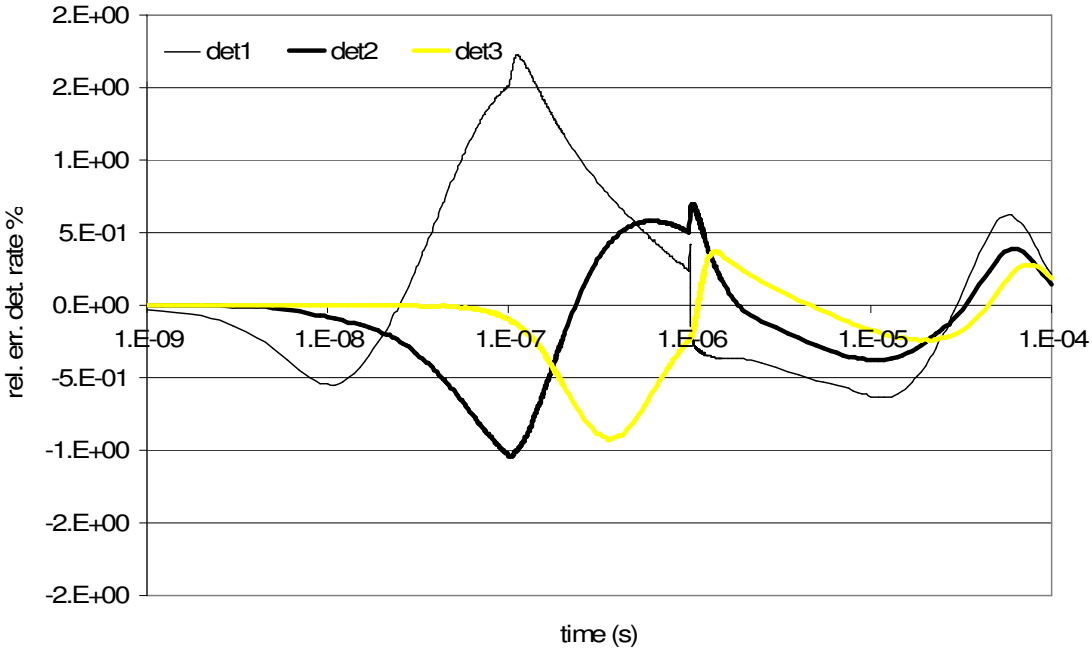

Figure 12: Old time scheme, SP_3 angular discretization.

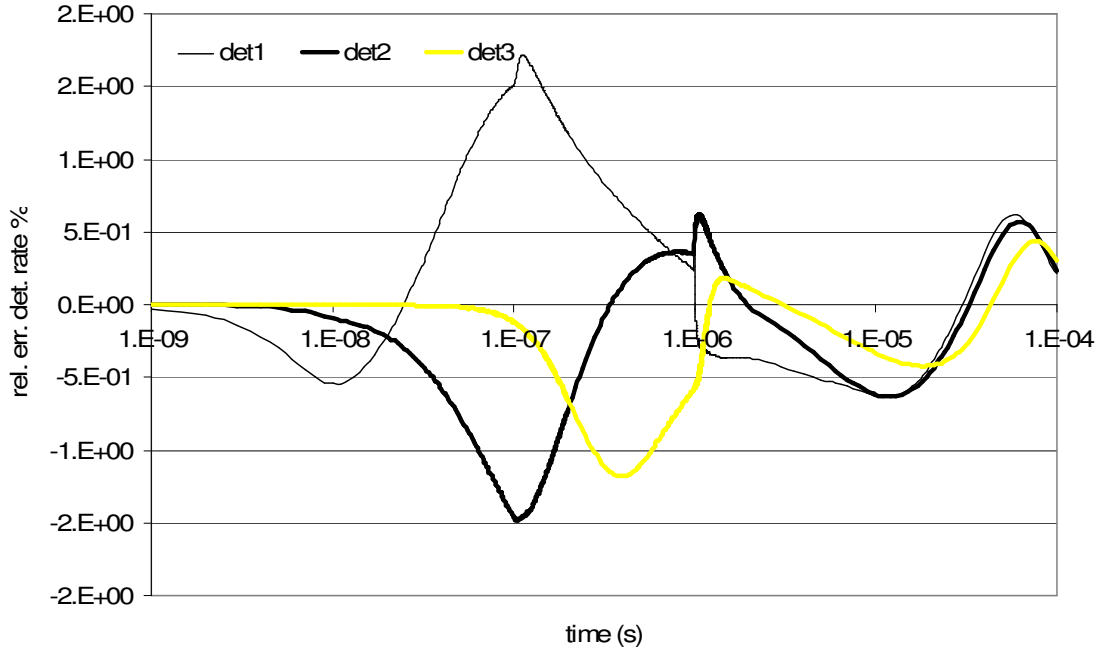

Figure 13: Old time scheme, P_3 angular discretization.

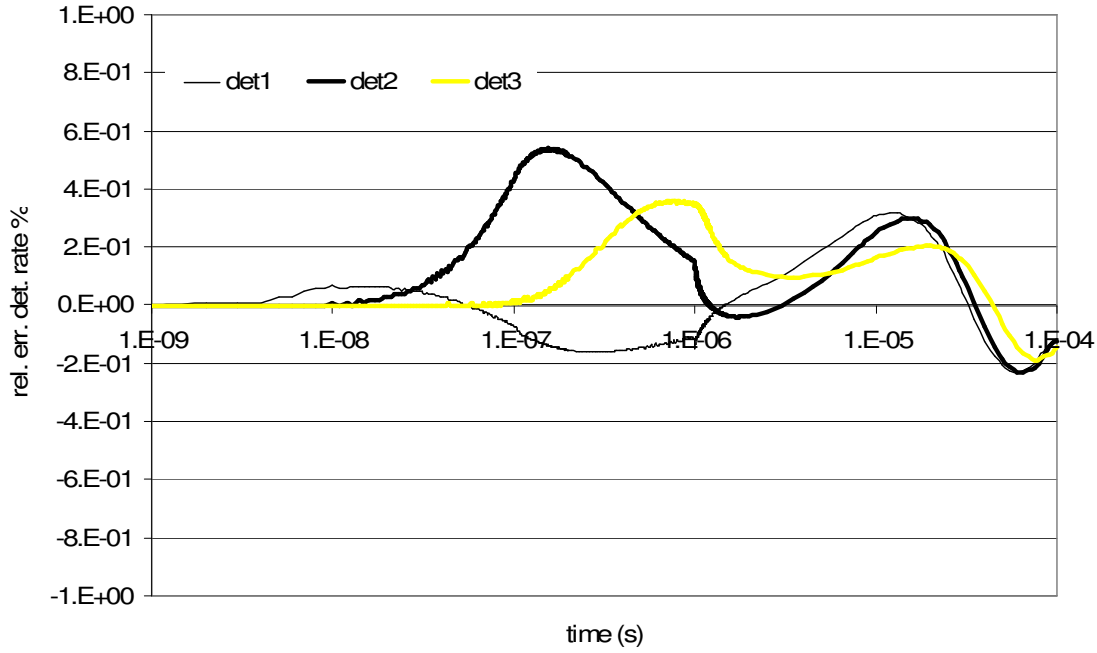

Figure 14: New time scheme, SP_3 angular discretization.

Table 1: Time ratios, k_{eff} values, and relative detector rate errors at t=0.

Angular/time discretization	Computer time ratio with respect to P3new	k_{eff}	Detector rate error at t=0 (%)		
			Detector 1	Detector 2	Detector 3
P1	0.42	0.953451	-1.8	-2.5	13.0
P1new	0.40				
SP3	0.47	0.960459	-0.20	0.06	-0.22
SP3new	0.46				
P3	1.07	0.960116	0	0	0

IV.3. Adaptive Time Step Control Two Dimensional Test

In order to test the time step control scheme, time-dependent analysis of a transient caused by the variation of an external neutron source in a sub-critical core was performed using four energy groups (source spectrum is non-zero in the first energy group only) and a P_1 angular approximation. Figure 15 shows the geometry of this benchmark where the composition of the source and shield region is the same. The spatial grid used by VARIANT is also displayed along with the three regions monitored for the error evaluation (arrows) with respect to a reference result. The fuel and the shield compositions are derived from a fast reactor problem and k_{eff} is equal to 0.97724. The variation of the source is described in Figure 16 (scale indicated on the right axis) and the total transient time analyzed is 100s. This test can also be used to evaluate the influence of the delayed neutron fraction on the transient by performing two different simulations. The first one, referred to as 1 in the following graphs, assumes a negligible delayed neutron fraction, i.e. prompt neutrons only. The second one, referred to as 2 in the following graphs, assumes two families of delayed neutrons each with a fraction ($ß_i$) of 0.5% and with decay constants of $0.1s^{-1}$ and $10s^{-1}$, respectively.

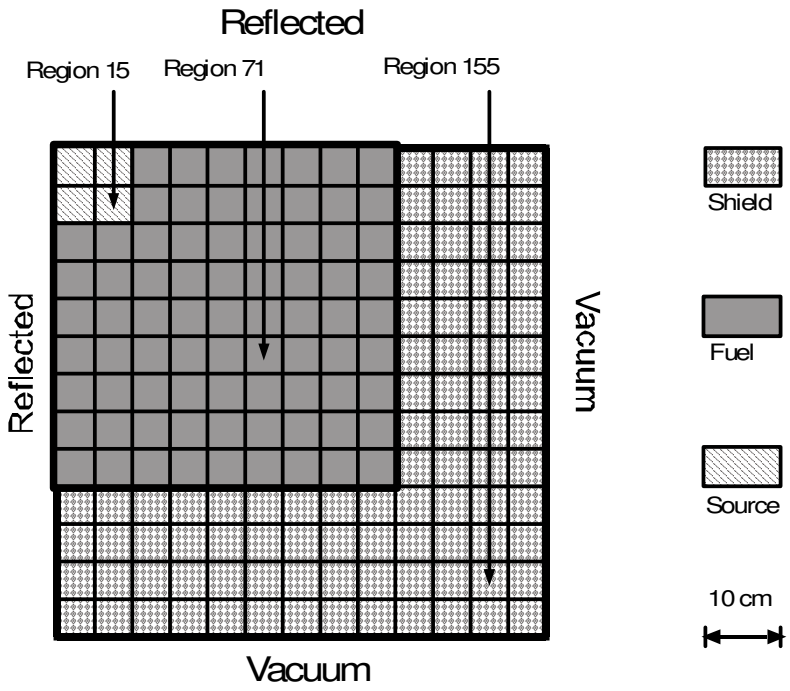

Figure 15: Geometry.

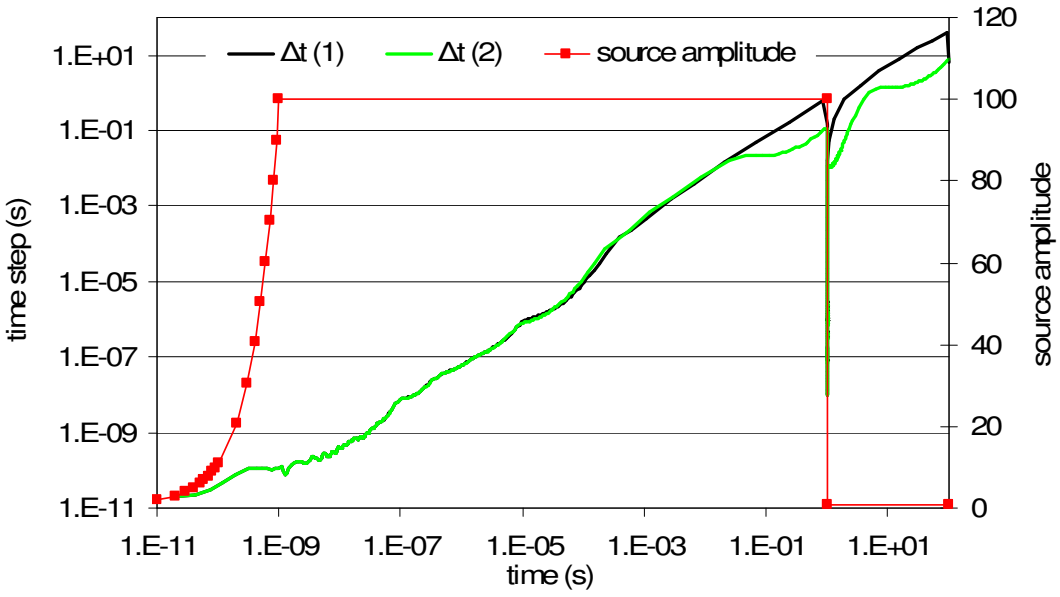

Figure 16: Source amplitude and time steps.

Figure 16 (scale indicated on the left axis) shows the time step (Δt) chosen by the adaptive scheme for the transient simulations. The time step is kept at a very low level until the end of the first part of the source transient ($t=10^{-9}$s), after which it starts to increase rapidly. Already before 0.1s, in the two simulations, $\Delta t(1)$ and $\Delta t(2)$ start to separate from each other. In the reactor with more delayed neutrons, at about $t= 5\cdot10^{-2}$s, the increase of the time step shows a strong degradation. At t= 1s the time step is one order of magnitude smaller compared to the case with almost no delayed neutrons; similar differences are observable in the second part of the transient. The final result is that 431 pseudo-steady-state calculations are needed to reach the end of the transient analysis with delayed neutrons, which is in contrast to the 368 needed for the other case. The physical explanation is that the presence of delayed neutrons slows the reactor in reaching a stable state and thus the time step needs to remain small for a longer period. This difference in the time step choice is even more evident by comparing Figures 17 and 18 where the time step size is plotted (right axis) vs. the time step number.

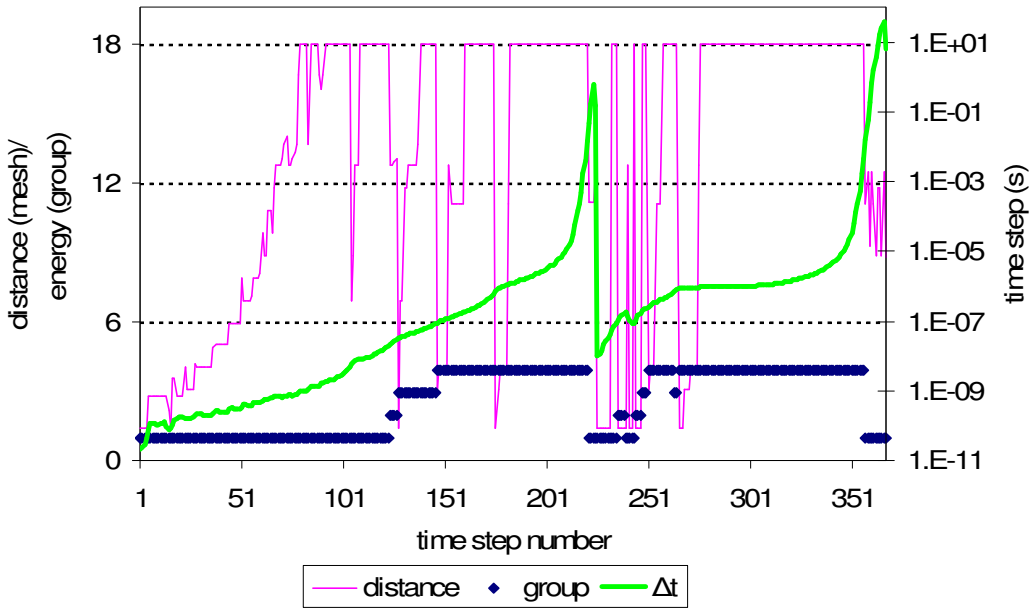

Figure 17: **Position in space and energy of the maximum of the ratio flux third order time derivative over flux (left axis), time step (right axis). Case without delayed neutrons.**

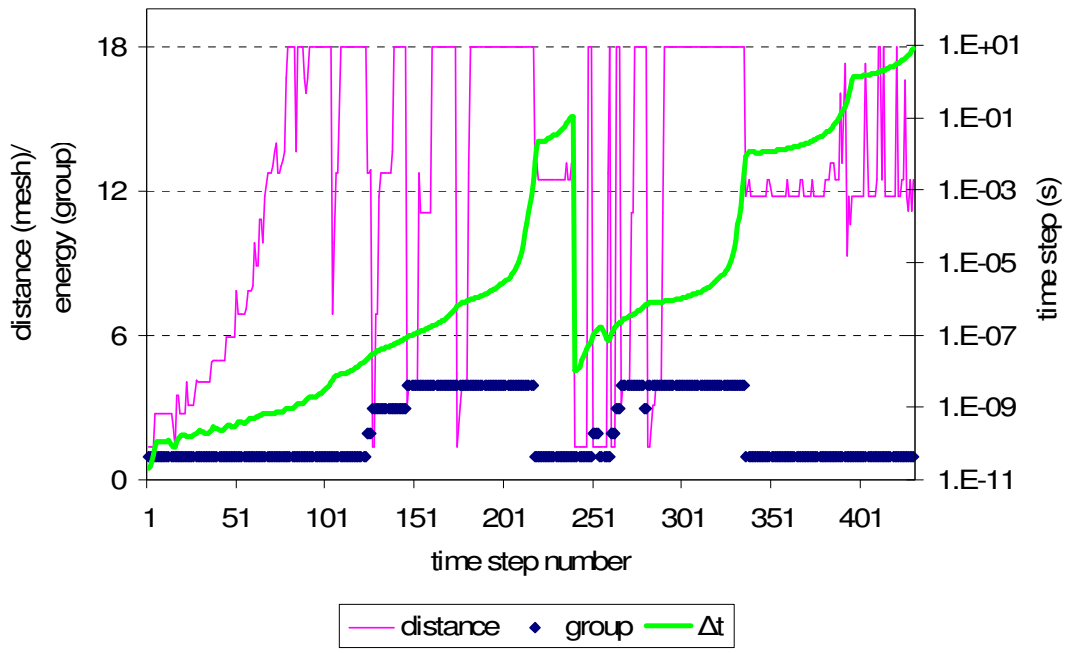

Figure 18: Position in space and energy of the maximum of the ratio flux third order time derivative over flux (left axis), time step (right axis). Case with delayed neutrons.

In Figures 17 and 18, the position in energy (group) and in space (distance in the number of meshes from the center of the core, i.e. from the left upper corner, see Figure 15) is plotted. This characterizes the position where the largest error is observed (see (3.70)) and, thus, the spatial and energy position is used for the time step evaluation. These graphs show that this maximum, at the beginning of the source pulse, is close to the source region and in the first group. After moving through the entire core and reaching the shield, the maximum error returns to the center, but it occurs at a lower energy. It is also interesting to observe that the maximum of the estimated relative error for the second case (the one with delayed neutrons) is situated in the fuel region in the first energy group. This feature is in agreement with the expectation that the delayed neutrons drive the flux during this phase of the transient. As a result, the maximum flux variations are located (in space and energy) where the largest delayed neutron source is present. Figure 17 compared with Figure 18 shows the existence of two additional time scales during the last phase of the transient in the case with delayed neutrons.

This phenomenon, physically, is connected with the presence of the two delayed neutrons families each characterized by a different time scale (decay constants). Figure 19 shows the absolute value of the relative flux error (maximum over energy groups) for the simulation with virtually no delayed neutrons. This error is given with respect to a reference solution obtained with the second order scheme with a constant time step of $2 \cdot 10^{-11}$s. The reference solution is computed until $4 \cdot 10^{-7}$s. Even if this is the steepest part of the transient, for all the three regions, the error is below or hardly exceeds the imposed tolerance that it is of 0.1%. It is also interesting to note how the maximum relative error shows a transition in space and time in accordance with the propagation of the pulse through the core. This simple test shows the potential of the adaptive scheme to use the correct time step in order to achieve a selected precision without any assistance by the user.

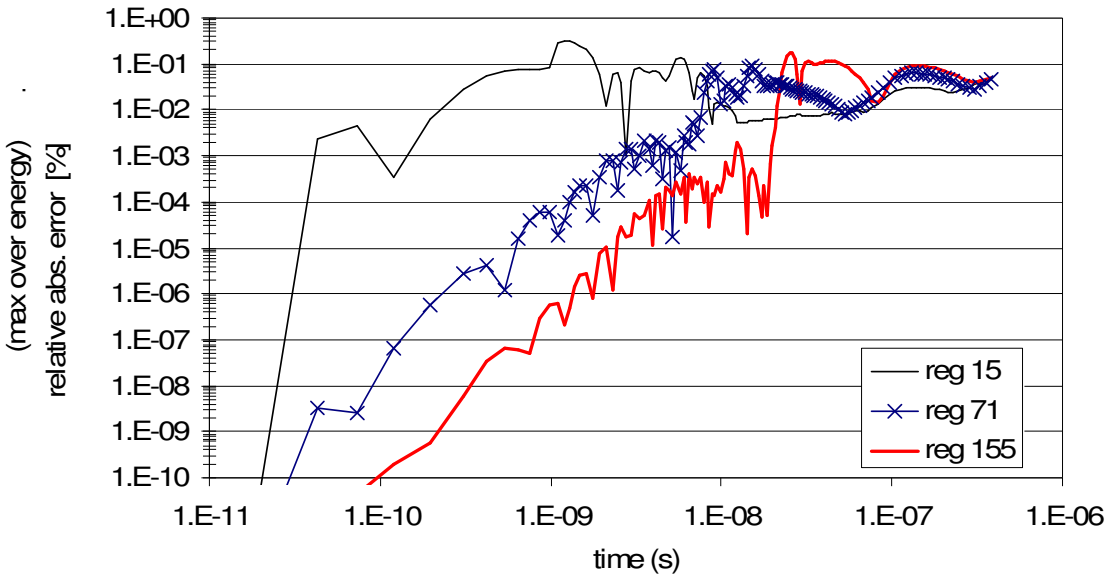

Figure 19: Maximum module of the relative absolute error (over energy) with respect to the reference analysis for meshes 15, 71 end 155.

Note that a small time step must be imposed by the user at the beginning of the transient and in correspondence with the sharp changing of the source. During preliminary tests, the results

have indicated that for small initial time steps, the method adapts such that an increase in the time step by an order of magnitude is possible thereby making the initial time step a relatively inexpensive guess. This geometry and composition were also used for checking less restrictive norms (see(3.85)) for the definition of the error. The tested norms are the following ones:

$$1)\qquad err_{n+2}^{rel} = \frac{\max\limits_{1\le i\le nreg}\max\limits_{1\le j\le ngroup}\left|\partial_t^3\,{}_j^i\overline{\phi}\right|_{n+1}}{\max\limits_{1\le i\le nreg}\max\limits_{1\le j\le ngroup}\left|{}_j^i\overline{\phi}_{n+1}\right|}\frac{\Delta t_{n+2}^3}{6},$$

$$2)\qquad err_{n+2}^{rel} = \max_{1\le i\le nreg}\left|\frac{\max\limits_{1\le j\le ngroup}\left|\partial_t^3\,{}_j^i\overline{\phi}\right|_{n+1}}{\max\limits_{1\le j\le ngroup}\left|{}_j^i\overline{\phi}_{n+1}\right|}\right|\frac{\Delta t_{n+2}^3}{6}, \tag{4.6}$$

$$3)\qquad err_{n+2}^{rel} = \max_{1\le j\le ngroup}\left|\frac{\max\limits_{1\le i\le nreg}\left|\partial_t^3\,{}_j^i\overline{\phi}\right|_{n+1}}{\max\limits_{1\le i\le nreg}\left|{}_j^i\overline{\phi}_{n+1}\right|}\right|\frac{\Delta t_{n+2}^3}{6}.$$

The first one is the weakest while the other two are intermediary with respect to the one originally defined. Figure 20 shows the time step behavior given by the four different error definitions (0 means the original one) for the analysis of the case without delayed neutrons. The use of error definitions 1, 2 and 3 results in almost the same number of time steps to complete the transient (269, 287 and 293), while the original one requires far more with 368 time steps. Even if with different number of time steps, all of the options show the same general behavior. The choice of the error definition is left up to the user who should consider: the type of transient, its computation cost, and the precision required by the calculation.

The same composition, geometry, and transient (without delayed neutrons) was considered for evaluating the need for a damping scheme in the time step control. This possibility should occur such that the oscillations and instabilities of the scheme are avoided. Such phenomena are attributable to the explicit component in the extrapolation of the error at the next time step. Figure 21 shows the time step $\left(\Delta t_{n+2}\right)_D$ behavior obtained by the following damping scheme:

$$
\begin{aligned}
&I && \left(\Delta t_{n+2}\right)_D = \Delta t_{n+2}, \\
&II && \left(\Delta t_{n+2}\right)_D = \frac{\Delta t_{n+1} + \Delta t_{n+2}}{2}, \\
&III && \mathrm{Log}\left[\left(\Delta t_{n+2}\right)_D\right] = \frac{\mathrm{Log}\left[\Delta t_{n+1}\right] + \mathrm{Log}\left[\Delta t_{n+2}\right]}{2},
\end{aligned}
\tag{4.7}
$$

where Δt_{n+2} is the time step computed directly by (3.86). Figure 21 shows that the different damping schemes do not dramatically affect the total number of time steps needed for the transient analysis (348 for the 1st, 368 for the 2nd and 374 for the 3rd). Moreover no instability has been detected in this severe test of a transient analysis.

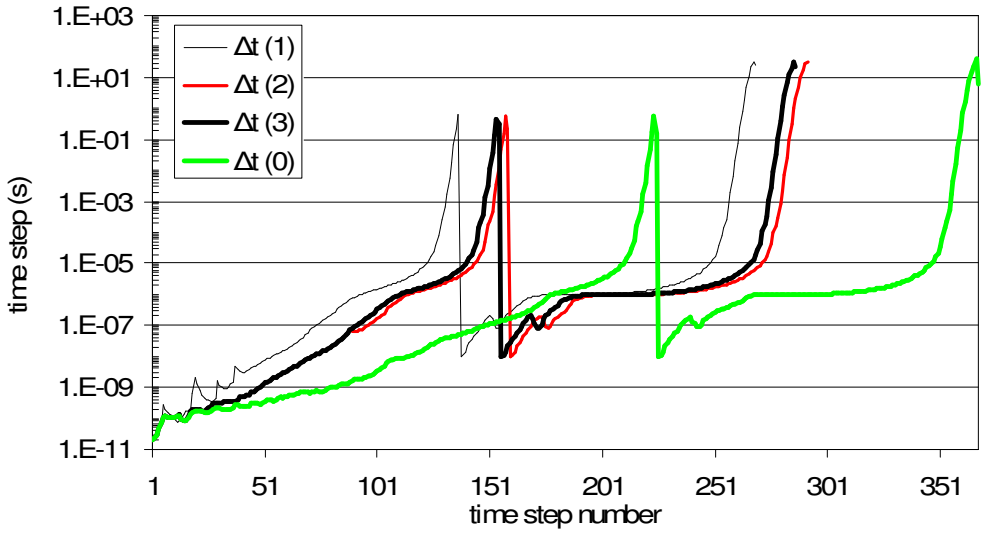

Figure 20: Time step for different error definitions.

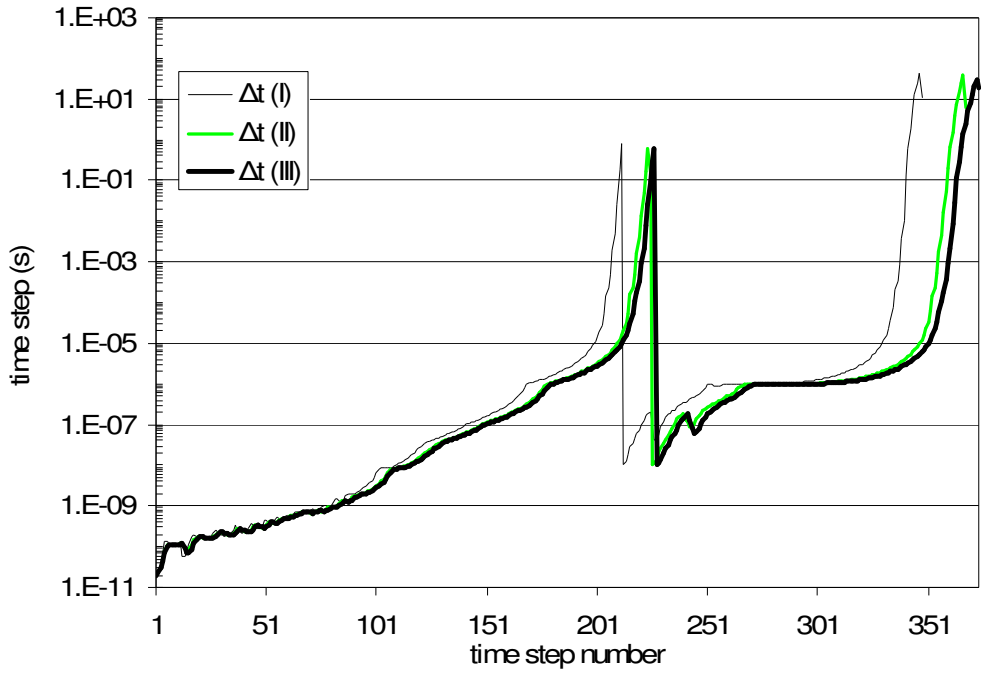

Figure 21: Time step for different damping scheme.

IV.4. PDS-XADS Transient Analysis

The last test performed is based upon a 3D model of an ADS project proposed by ANSALDO [60]. The simulation focuses on three different aspects. First, the old and the new adaptive schemes are compared in the P_1 angular approximation using similar time step structures. Second, the influence on the detector rates and time step size of different angular approximations is examined. Third, the influence of the scattering kernel is examined. In the following, every test performed is identified by, first the angular approximation for the flux and then in brackets, the angular approximation of the scattering kernel. As an example, $P_3(P_2)$ stands for a P_3 spherical harmonics flux approximation and a P_2 scattering kernel.

Model Description:

Figure 22 shows a slice of the reactor core. The fuel assemblies are hexagonal which is characteristic of fast reactor designs. In this problem they are of the same type as those used in the PHENIX reactor [61] and 1/6 radial symmetry is assumed (it is realized by periodic boundary condition between the hexagons on the lower and the upper left side of the geometry shown in Figure 22) in conjunction with vacuum boundary condition on the periphery of the core (upper right side in Figure 22).

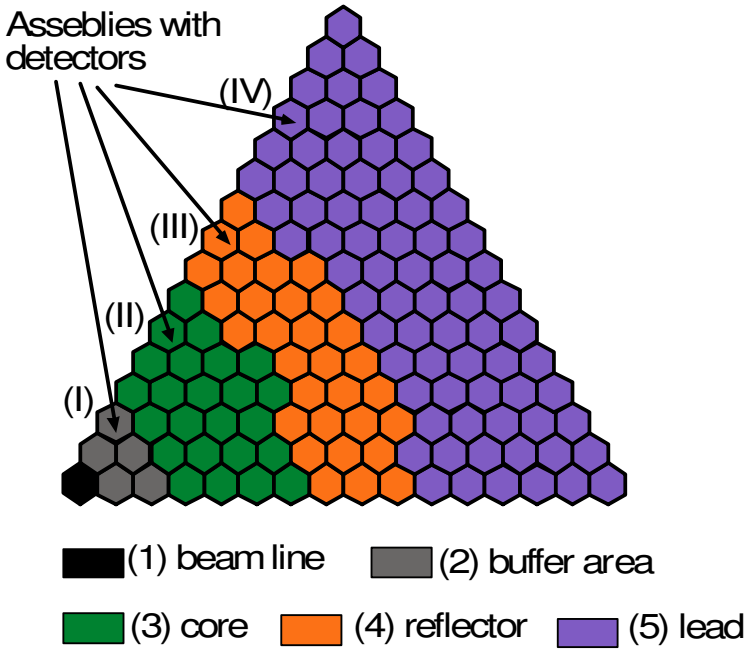

Figure 22: 1/6 slice of core

The number assigned to each assembly type in Figure 22 (1, 2, 3, 4, 5) is used to describe the axial composition given in Figure 23. In the following, roman numbers for the assembly will be used in combination with the indices a/b/c for each plane to denote the detector positions (i. e. the detector II-b is placed in the hexagon marked II in Figure 22 and in section b in Figure 23). The detectors are again U-235 fission chambers. The axial direction is discretized by 16 regions giving a total number of 121x16= 1936 computational regions.

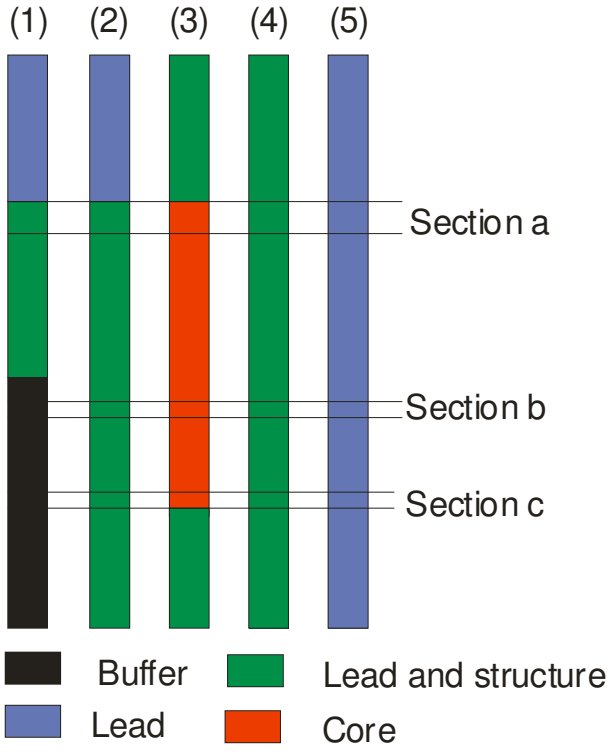

Figure 23: Axial composition.

Neutronic model:

The analysis has been performed using 8 energy groups with 6 families of delayed neutrons. The energy structure is appropriate for a fast spectrum reactor and is described in Table 2.

Table 2: Energy intervals and velocities.

Energy boundary	E (eV)	Energy group	Average velocity (cm/s)
E0	19640300.0000000	1	2232378368.00000
E1	1652990.00000000	2	1479871232.00000
E2	820850.000000000	3	1062186624.00000
E3	407622.000000000	4	622019968.000000
E4	111090.000000000	5	228701056.000000
E5	5004.50976562500	6	70054912.0000000
E6	1010.39001464844	7	33301714.0000000
E7	203.994995117188	8	15590252.0000000
E8	0.00011000000085		

Figure 23 shows the radial flux shape for the b section detectors obtained using a P_3 angular discretization both for the flux and the scattering kernel.

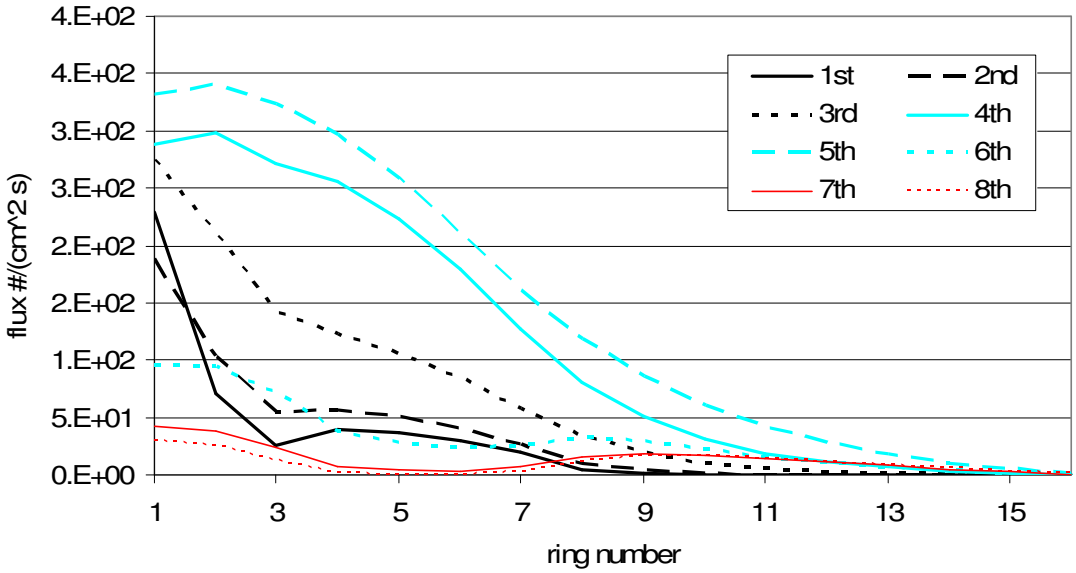

Figure 24: Radial flux shape.

The steady state k_{eff} calculations obviously show differences between the different angular models. Table 3 reports the different values for the sets tested. The average number of neutrons released by each fission, $\bar{\nu}$, as in the MUSE analysis, has been changed in order to have the same k_{eff} for all the angular sets.

Table 3: K_{eff} values before number of secondary renormalization.

Angular model	K_{eff}	Angular model	K_{eff}
$P_1(P_0)$	0.946188	$SP_5(P_0)$	0.950446
$SP_3(P_0)$	0.950341	P_5 (P_0)	0.960502
P_3 (P_0)	0.956482	P_3 (P_3)	0.961202

For the analysis of the results, the response of 5 detectors has been considered: I-c, II-b, II-a, III-b and IV-b. These were chosen for the following reasons:

- I-c is very close to the source and placed in proximity of a composition discontinuity. Moreover, in correspondence with the third ring, Figure 24 shows strong spatial

gradients, thus large differences between the different time angular models are more plausible.

- II-b is placed almost in the middle of the core. Consequently, it will provide a meaningful characterization of the transient inside the active part of the reactor.
- II-a is inside of the active part of the core and should be affected by the material discontinuity. This should show an increasing angular dependence with respect to detector II-b.
- III-b the response of this detector will be driven by the streaming (high angular dependence) into the reflector area coming from the active core (fundamental mode response). At the same time, the high scattering density compared to the absorption leads to a diffusion like behavior of the flux. The response of the detector will tell which one of these phenomena is dominant.
- IV-b this detector is placed almost outside of the core in an area technically easy to access in practice and thus it will be interesting to see its response.

Source and transient description:

The source is spatially located in correspondence with the intersection between section c and the first ring (see Figures 22 and 23). In energy, 55% of the total source spectrum is in the first group, 25% in the second, and 20% in the third. Figure 25 shows the time behavior of the source transient and the multiplication factor for the five detectors obtained by the $P_3(P_3)$ angular model.

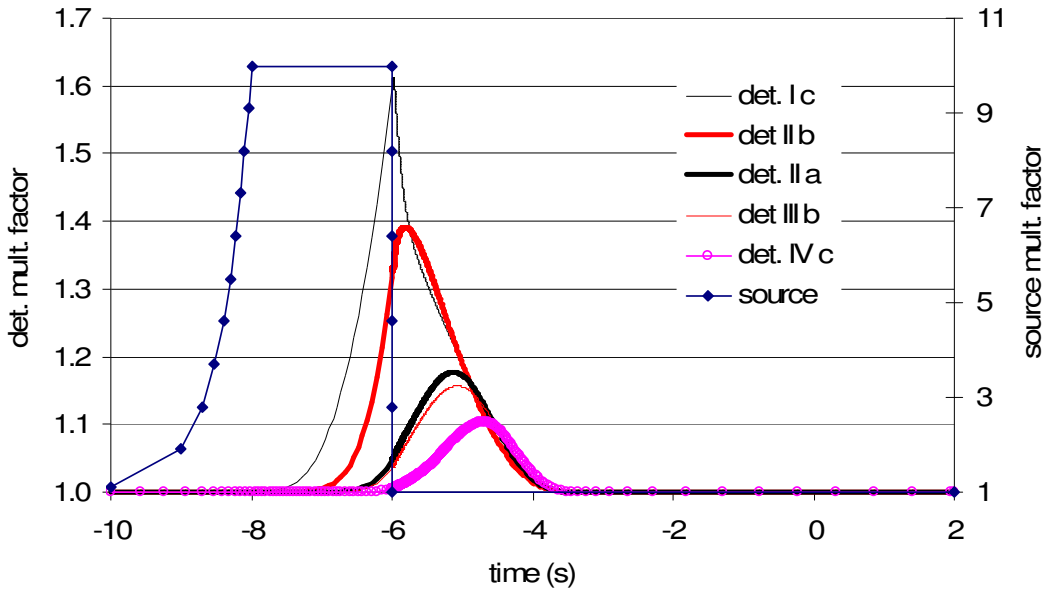

Figure 25: Source and detector responses.

Old scheme comparison:

The comparison with the old scheme is carried out only for the $P_1(P_0)$ angular approximation since the time derivative of the first order angular flux moments (Y_1^0, Y_1^1,Y_1^{-1}) are responsible for the majority of the differences between the old and new scheme. The first considered is the transient analysis using the adaptive time step scheme. The time step behavior created by the adaptive scheme is used to construct a similar sequence of time steps for the old scheme (see Figure 26). Figure 27 shows the detector responses (detector multiplication factor on the left side) obtained by the new $P_1(P_0)$ scheme and the relative differences with respect to the old $P_1(P_0)$ scheme. As expected, the greater difference is shown in the I-c detector which is closer to the source area. In this case, the differences show sharp peaks in correspondence with the discontinuity of the time source derivative. The detector II-b shows almost the same characteristics but with a reduced amplitude. All the other detectors show a very smooth behavior in the response and the relative differences between the models are thus reduced.

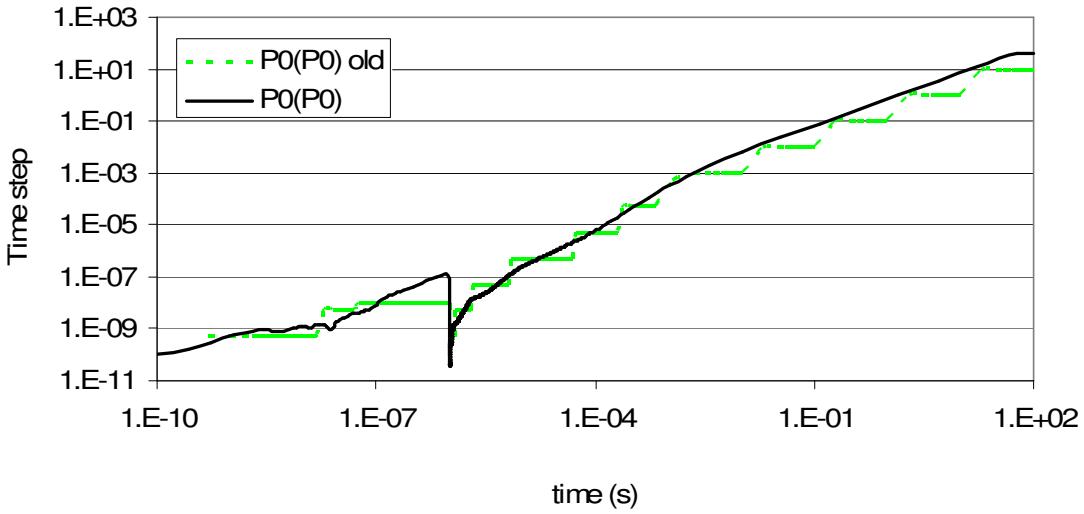

Figure 26: Time step for old and new P0(P0) schemes.

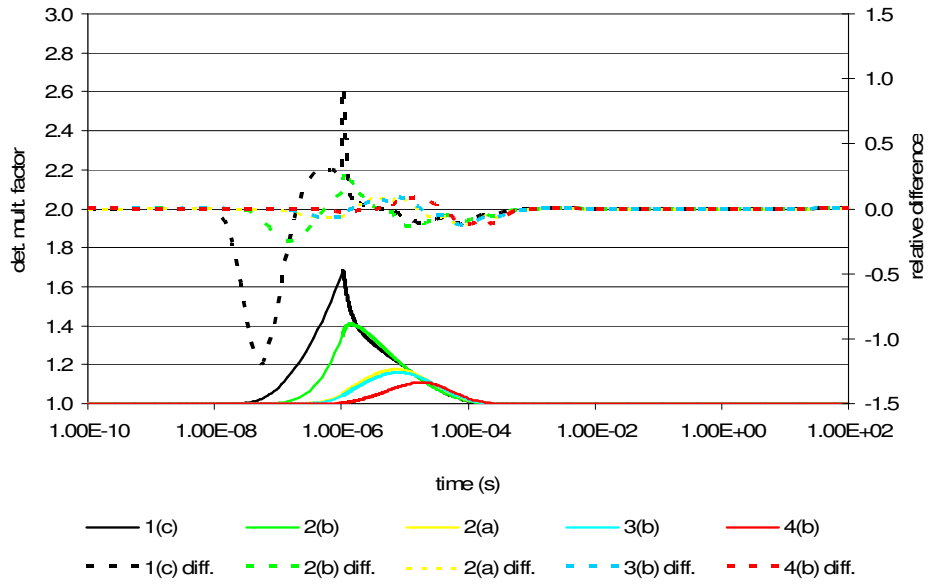

Figure 27: Detector response by new adaptive P1(P0) scheme and relative difference with respect to the old P1(P0) scheme.

Influence of the flux angular discretization:

In order to evaluate the influence of the angular flux approximation over the transient simulation, five different tests ($P_1(P_0)$, SP_3 (P_0), $P_3(P_0)$, SP_5 (P_0), $P_5(P_0)$) were performed where the adaptive time step control was employed. In this case the reference solution is the $P_5(P_0)$ scheme. Table 4 shows the relative difference with respect to the $P_5(P_0)$ steady state calculation in the detector reaction rates. These values have been subtracted from the relative differences plotted in Figures 28 to 32 in order to have a zero error at the steady state. This choice allows focus to be placed only on the different time behaviors of the models.

Table 4: Relative difference in detector reaction rates with respect $P_5(P_0)$ (%).

Angular approximation	Detector				
	I-c	II-b	II-a	III-b	IV-b
$SP_5(P_0)$	-2.68	-0.450	-2.08	-2.28	-2.91
$P_3(P_0)$	-1.23	-0.891	-1.62	-1.64	-1.86
$SP_3(P_0)$	-2.35	-0.051	-1.65	-1.86	-2.49
$P_1(P_0)$	-1.18	-0.457	-2.32	-2.22	3.88

Starting with the results shown in Table 4, some conclusions are already possible. First, the differences should not be considered negligible (more than 1 percent is meaningful for this problem) indicating that the transport effect is important in this core, even after the renormalization of the $\bar{\nu}$. Second, the differences are lower for detector II-b which is placed in the middle of the active part of the core where the large isotropic fission source decreases the angular dependence of the flux. Table 4 also shows very good performance with the lower angular approximations ($P_1(P_0)$), which is probably due to the adjustment of $\bar{\nu}$ (without this process this model is the worst compared to the reference). Figures 28 to 32 show the detector multiplication factors obtained from the reference solution (right axis) and the relative difference with respect to the other schemes (left axis). As expected, the differences reduce from approximately -4% for detector I-c to 0.2% for detector IV-b in the shield zone which is

correlated with an increasing distance from the source area (with regard to the maximum during the transient for the $P_1(P_0)$). The relative differences for detectors I-c, II-b, III-b show a very similar shape that can be qualitatively explained by the physical interpretation of the mathematical models arising by different angular approximations. As described in [58, 59], the time dependent mono-energetic flux, that corresponds to a Dirac delta-function in both time and space for the source $Q_0\delta(x,t)$, is a function that shows a wave front traveling at velocity $v/\sqrt{3}$ and a discontinuity in P_1. This front has the following property:

$$\begin{cases} \phi\left(t, x = tv/\sqrt{3}\right) = C(t)\delta\left(x - tv/\sqrt{3}\right) \\ \lim_{x \to (tv/\sqrt{3})_-} \phi(t,x) = -\infty \end{cases} \tag{4.8}$$

The introduction of additional harmonics in the flux expansion has two main effects. First, additional waves are added to the solution that travel at different velocities with respect to $v/\sqrt{3}$. This enhances the global propagation velocity (for an infinite number of harmonics the solution should travel at a velocity exactly equal to v). Second, the discontinuity is smoothed (physically negative values of the flux are not possible). The relative differences are defined such that positive values mean higher values of the reference with respect to the angular model. After these preliminary considerations, the common behavior of detectors I-c, II-b, III-b may be explained as follows: the low fluctuations in the relative differences at the beginning and end of the transient are connected with small amplitude waves traveling at velocities higher and lower than $v/\sqrt{3}$. The centered negative and positive peaks are due to a smoothing of the Dirac delta-function in the front of the wave and of the $-\infty$ discontinuity in the back of the wave (see (4.8)). The peculiarity shown by detector II-a is likely a result of the vicinity of the reflector which has introduced reflected waves. Differences for the detector IV-b do not show a clear pattern, but they are very low and thus difficult to interpret. An indication that the increase in angular approximation decreases the steepness of the transient flux can also be derived from the fact that the $P_5(P_0)$ option, during the simulation, uses a larger time step with

respect to the other options exactly in correspondence with this part of the transient. When compared with the SP_N method, clearly the same order P_N scheme performs better.

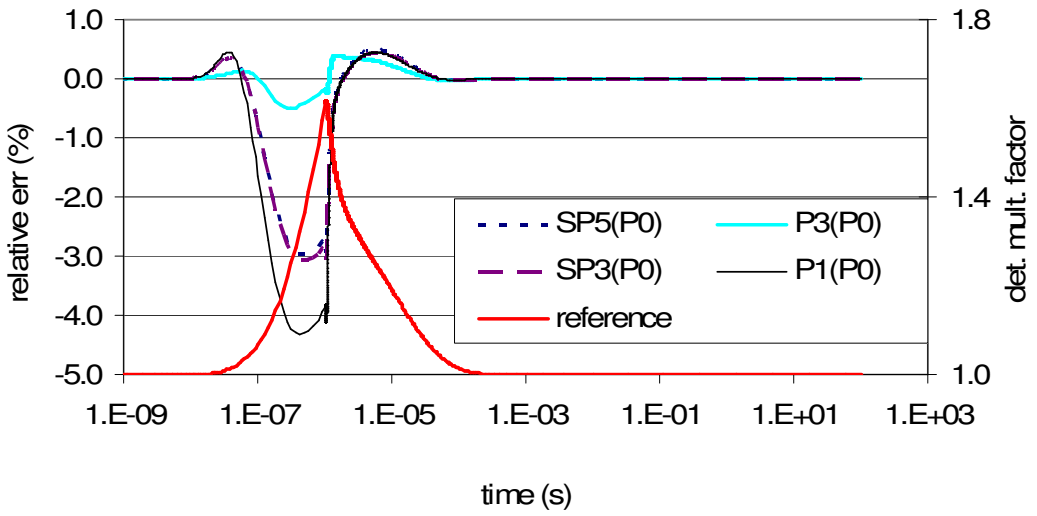

Figure 28: Detector I-c.

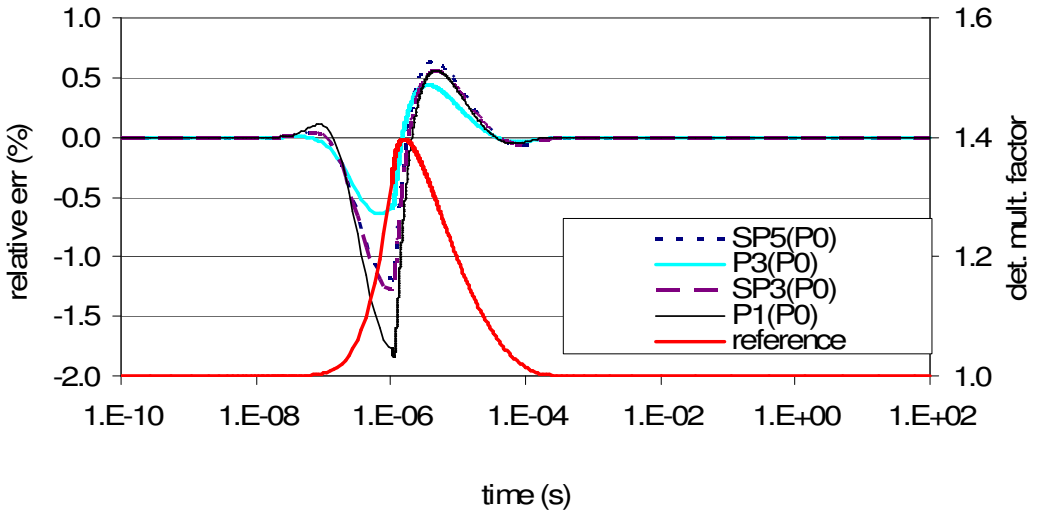

Figure 29: Detector II-b.

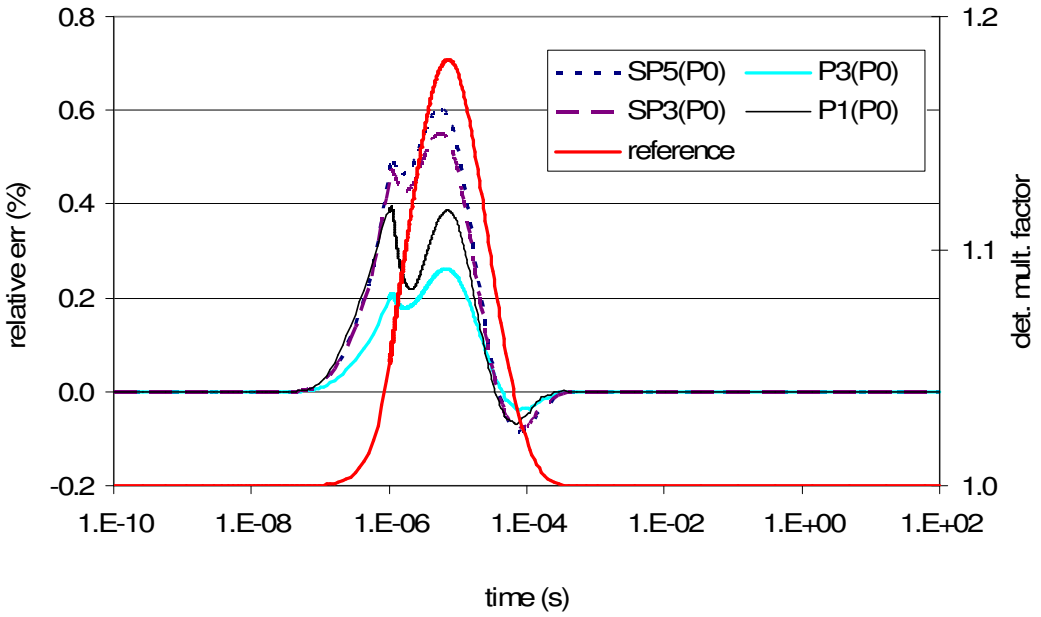

Figure 30: Detector II-a.

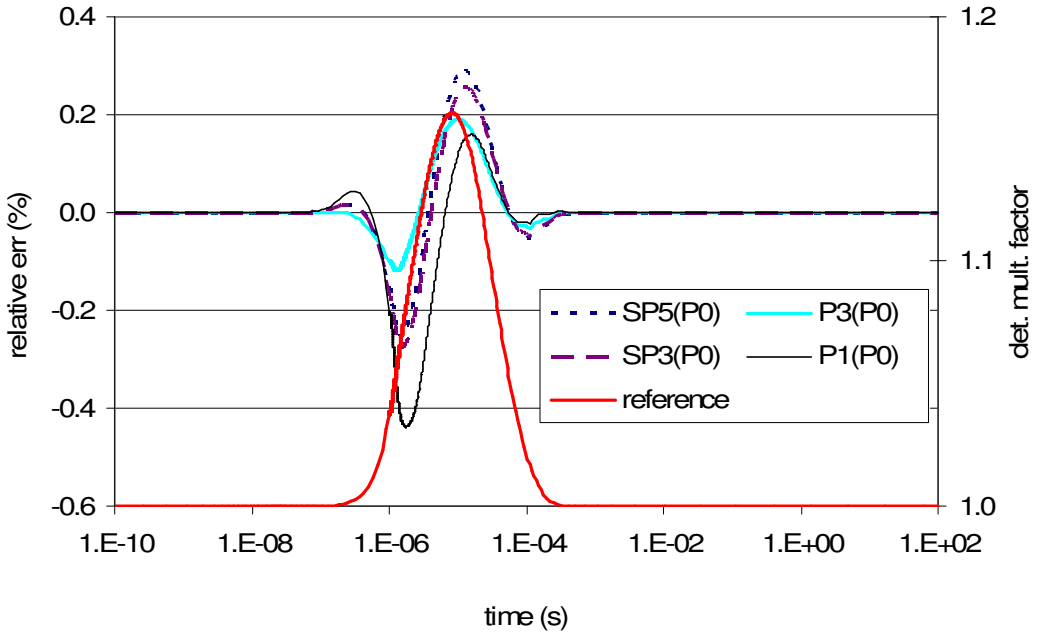

Figure 31: Detector III-b.

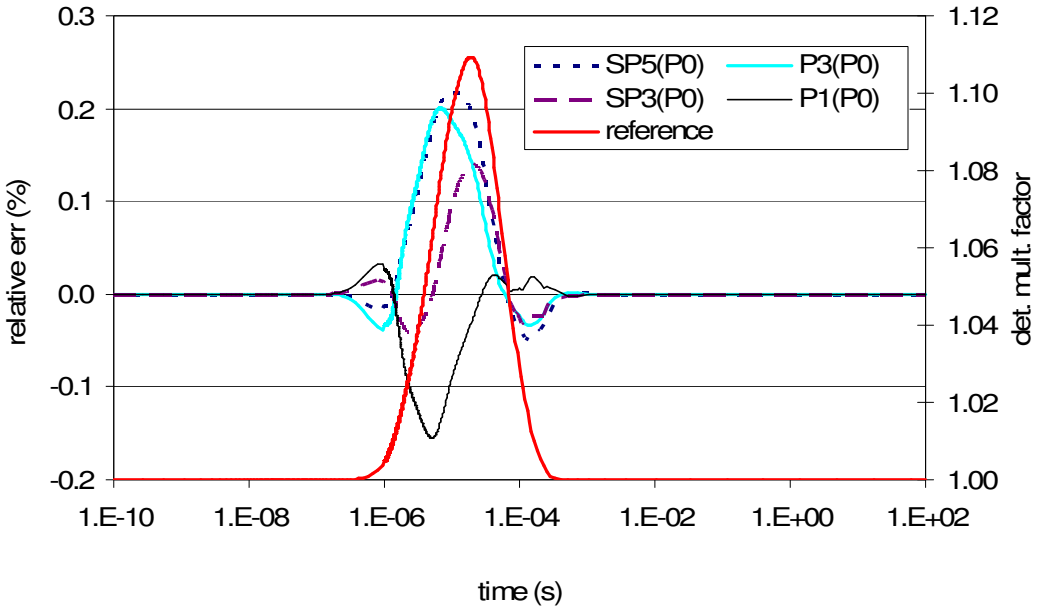

Figure 32: Detector IV-b.

Influence of the scattering kernel angular discretization:

The presence of higher angular terms in the scattering kernel approximation has the effect of decreasing the removal cross section seen by a specific angular flux moment. Consequently, the higher the anisotropic scattering component, the greater the distance in space and time at which the anisotropic flux, created by the localized source, exhibits a diffusion like behavior. Usually the higher angular moments of the scattering kernel are negligible unless low atom mass materials such as hydrogen are present. However, their importance is not only proportional to their absolute value but also to the magnitude of the corresponding angular flux moment. In the reactor considered, although there are no low atom mass materials, the small size of the core and the presence of the source suggests, as confirmed by Figure 24, a strong spatial gradient of the flux and, thus, high amplitude of the higher angular moments of the flux. In such a situation it is not clear what will be the differences due to different approximations of

the scattering kernel. In order to investigate this effect, the results from three different simulations are compared $P_3(P_3)$ (reference), P_3 (P_0), $P_1(P_1)$ and $P_1(P_0)$. Table 5 shows the steady state relative difference with respect to the $P_1(P_3)$ approximation at steady state. It is again surprising how the renormalization process has yielded a result for the $P_1(P_1)$ approximation that is better than the $P_3(P_0)$. The analysis of the time dependent results shows a clear interpretation under the considerations made at the beginning of this section. Close to the source region the difference between the simulations is dominated by the un-collided neutrons thus the $P_3(P_0)$ model is very close to the reference one with respect to the $P_1(P_0)$ or $P_1(P_1)$ models (Figures 33 and 34). Thus, the influence of the higher moments of the scattering kernel remains small close to the source region. As the distance between detectors and the source increases, the perturbation is almost caused by collided neutrons. The ability to preserve the higher angular moments after the scattering process is crucial to preserving the differences between models. As shown in Figures 36 and 37, the $P_1(P_1)$ model improves with respect to the reference as the distance from the source increases.

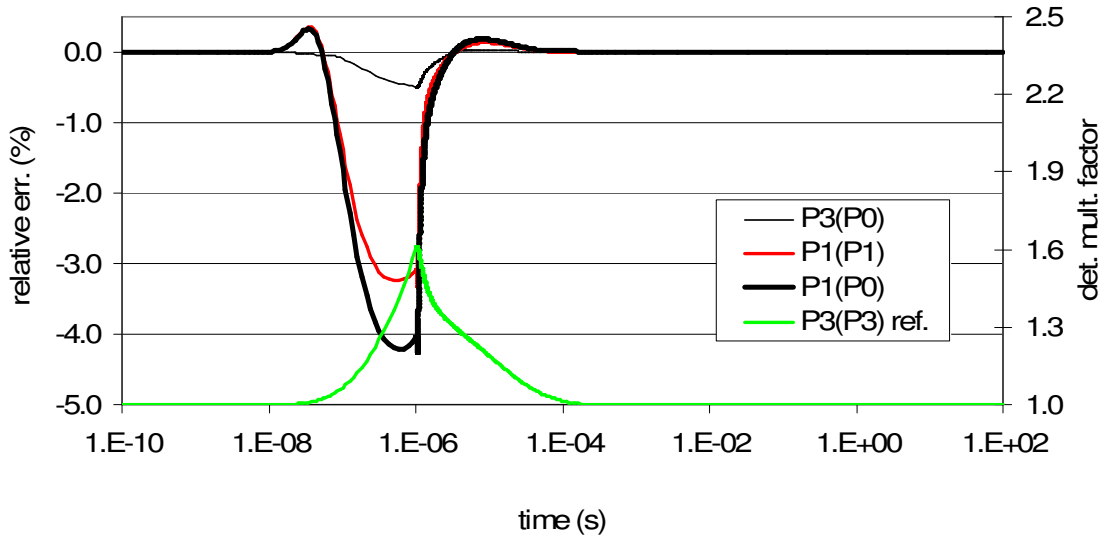

Figure 33: Detector I-c.

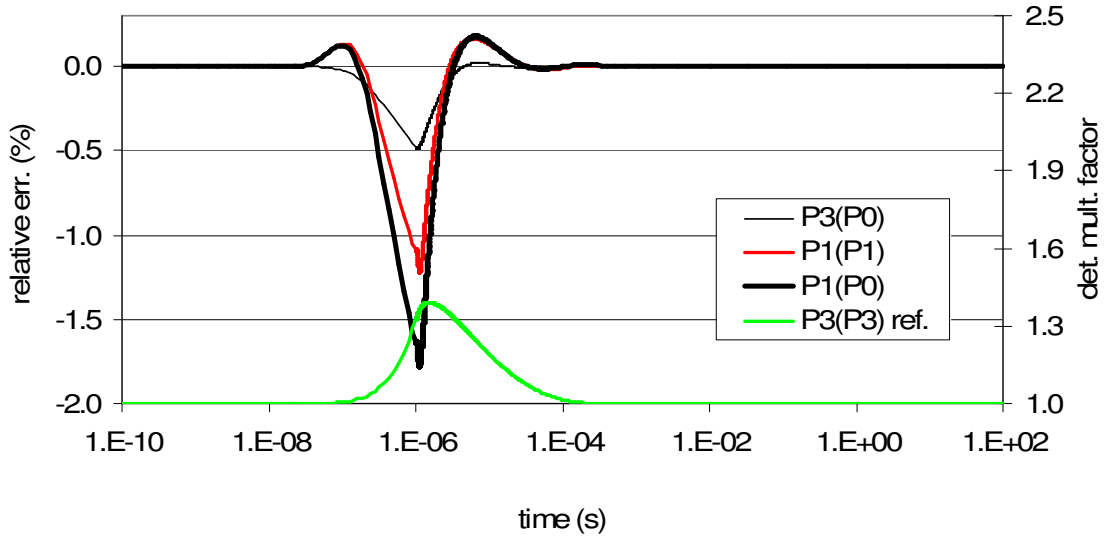

Figure 34: Detector II-b.

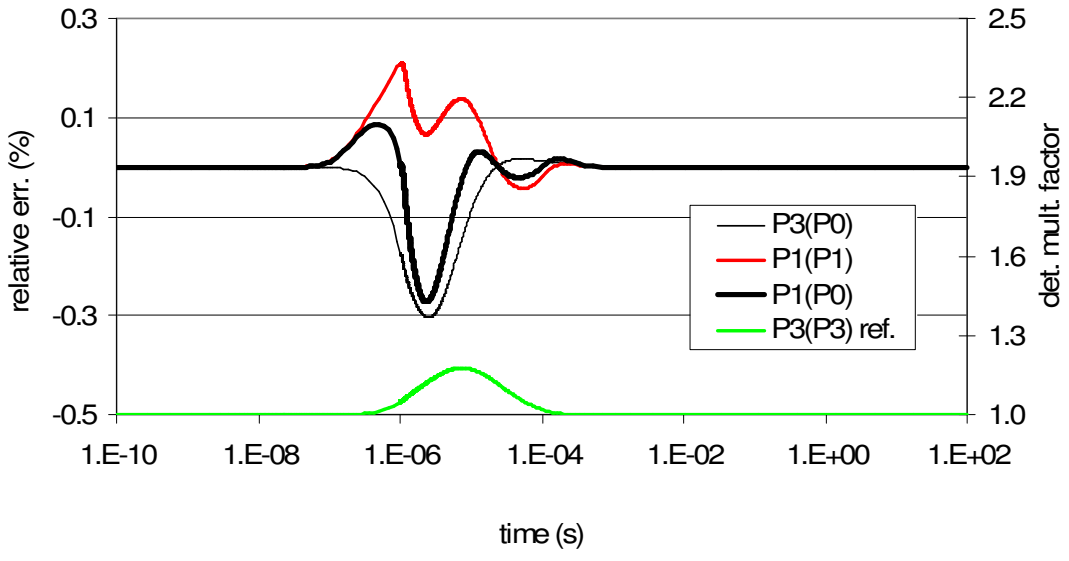

Figure 35: Detector II-a.

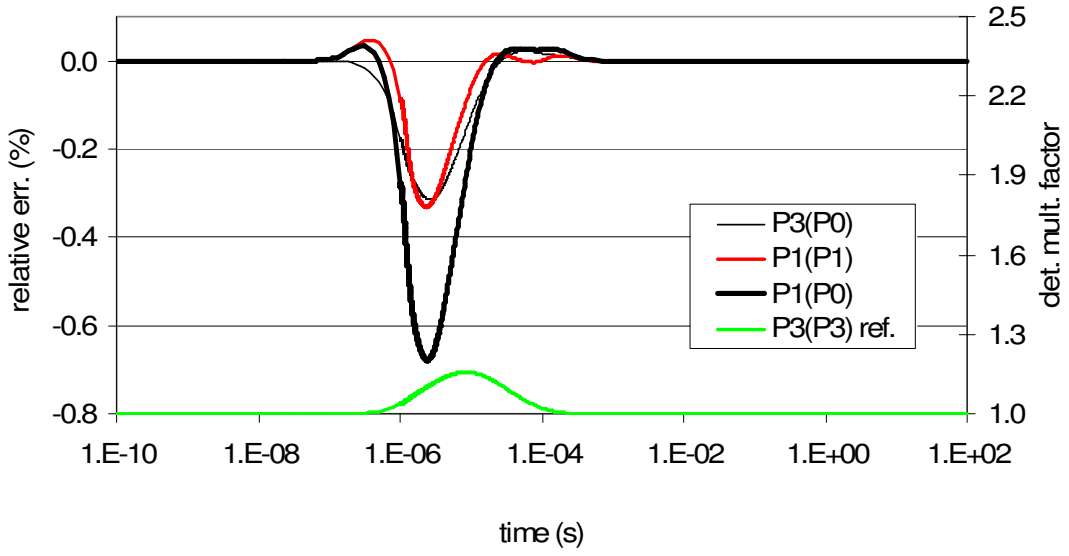

Figure 36: Detector III-b.

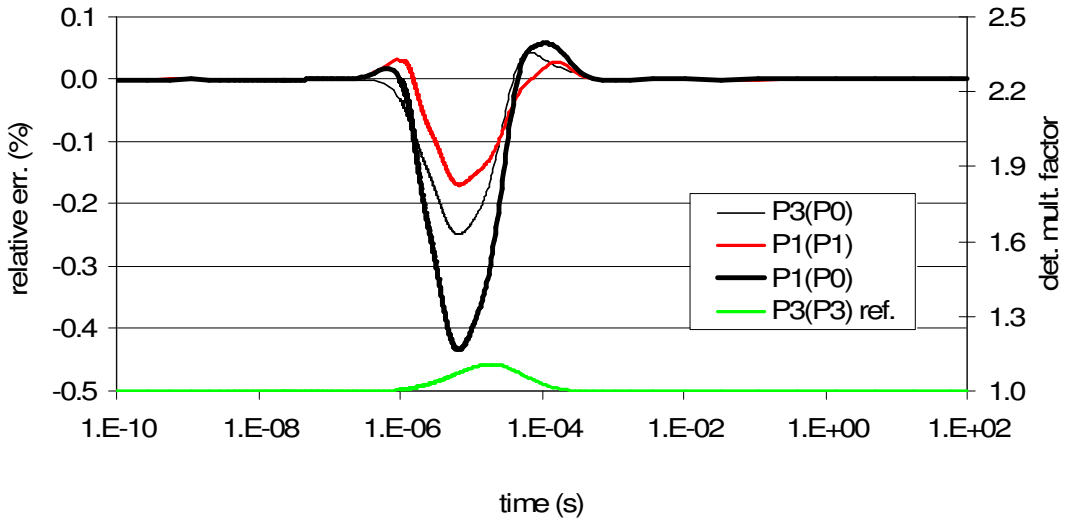

Figure 37: Detector IV-b.

Table 5: Steady state relative difference with respect P3(P3)

Angular scheme	Detector				
	I-c	II-b	II-a	III-b	IV-b
P3(P0)	2.09	1.07	1.11	1.55	1.02
P1(P1)	-0.50	0.18	-0.87	-0.79	1.86
P1(P0)	2.14	1.50	0.42	0.99	3.21

IV.5. Conclusions

The main objective of this work was to provide a new powerful tool for the analysis of neutronic transients in nuclear reactors with special emphasis on application to ADS. In the framework of the even parity second order form of the transport equation solved by VARIANT, a time dependent discretization scheme has been embedded thus making a coherent time discretization of the P_N and SP_N equations available for rectangular and hexagonal meshes in 2D and 3D geometries. The choice of an implicit scheme, for the time discretization, has been carried out in order to eliminate the need for the user to decide the time scale of interest without introducing concerns about the stability of the solution. In order to decrease the computational load typical for an implicit scheme, a time step control has been provided that is able to use larger time steps by maintaining the iteration error (different error norms are available) below a user set maximum value. The scheme has been shown to be accurate by matching analytic results for a simple geometrical configuration along with more realistic cases. The results obtained in this work are all evaluated and discussed to exhibit and explain the relative differences between the different spatial, angular and temporal discretizations available rather than having in mind the goal of a direct comparison with experimental results. The results also focus on physical aspects of the simulation of fast transients in ADS. As already mentioned, several processes affect the final comparison between experiments and code simulations, like multi-group cross-sections preparation, uncertainties in experimental data and nuclear data (microscopic cross-sections). In such a

complex framework, cancellation of errors can easily become the dominant effect with respect to the accuracy of the overall results thereby hiding the accuracy of the method. Comparisons with experiments in such situations can thus be misleading and it is necessary, if possible, to be aware of the error magnitude introduced by the approximations in the numerical treatment. This last point is the main objective of the benchmark problems investigated in the present work. From all the analyses it has been evident that the importance of a higher angular expansion of the flux is fundamental in the short time scale for regions close to the source area (different angular models show differences in the order of several percents). On the other hand on these conditions the importance of the scattering kernel expansion order seems to be negligible. For very small size reactors, the importance of the flux expansion order is relevant (see chapter IV.2) for all of the locations and persists longer after the sharp peak of the detector responses. Physically this is due to a direct coupling between the source region and the external boundary of the reactor, thus the expansion order of the flux affects the number of source neutrons present in the fissionable part of the core. When the reactor size is large enough to ensure a spatial decoupling, a larger angular representation of the perturbation is not needed since the size of the reactor allows the perturbation to exhibit diffusion like behavior before reaching the detector locations. In these cases it is anyway necessary to carefully evaluate the influence of the introduction of higher order expansions of the scattering kernel which increase the spatial coupling (see chapter IV.4). During the simulation performed in chapter IV.4, the relative difference between two consecutive angular approximations decreases with respect to an increase of the order (i.e. P_1 vs. P_3, P_3 vs. P_5) as expected. A general overview of all of the results suggests that for very small experimental reactors, a P_5 flux expansion order will be necessary. For medium-sized reactors a P_3 expansion should be satisfactory. The time step control has shown its ability to deal with different types of transients and thus its use is always suggested to the user in order to optimize the computational cost. Hopefully this methodology will offer researchers an additional tool in order to clarify discrepancies between experimental

and simulation results with the final goal of decreasing the need for expensive experimental tests. Such ability will also allow researchers to better predict the behavior of new reactor concepts such as an ADS. The variations of the external source considered in this study are typical examples for an initiating transient in such a type of reactor. The presented results and their discussions illustrate the importance of various phenomena and approximations and their relevance e.g. with respect to reactor size or detector position. The detailed understanding of the implemented new time step control feature will help in applying this concept and the associated option in the used tool, the VARIANT and KIN3D codes, also for different types of transients, e.g. those induced by relocation of material. Unfortunately it was not possible for all the tests performed to provide a comparison of the computation cost between the old and the new direct scheme because different computers were used for the simulations. Nevertheless, generally, the impression about the slight reduction of the time consumption described in Section IV.2, due to a change in the convergence speed of the iterative solution of the pseudo steady state transport problem performed by the VARIANT code, were generally confirmed.

BIBLIOGRAPHY

1. J. R. Lamarsh: **Introduction to nuclear reactor theory,** Reading, Mass., Addison-Wesley Pub. Co., 1966.
2. K. O. Ott and W. A. Bezella: **Introductory nuclear reactor statics**, La Grange Park, Ill., USA: American Nuclear Society, 1983.
3. G. I. Bell and S. Glasstone: **Nuclear reactor theory**, New York, Van Nostrand Reinhold Co., 1970.
4. J. J. Duderstadt, J. L. Hamilton, J. Louis: **Nuclear reactor analysis**, New York : Wiley, 1976.
5. A. M. Weinberg, E. P. Wigner: **The Physical Theory of Neutron Chain Reactors**, The University of Chicago Press, 1958.
6. H. A. Bethe, J. H. Tait: "An Estimate of the Order of Magnitude of the Explosion when the Core of a Fast Reactor Collapses", British Report UKAEA-RHM (56)/113, 1956.
7. C. Rubbia, J. A Rubio, S, Buono, F. Carminati, N. Fiétier, J. Galvez, C. Gelès, Y. Kadi, R. Klapisch, P. Mandrillon, J. P. Revol, and Ch. Roche: "Conceptual Design of a Fast Neutron Operated High Power Energy Amplifier". European Organization for Nuclear Research CERN/AT/95-44(ET), 1995.
8. J. Tommasi, S. Massara: "LMFR Dedicated Core for transmutation, Critical versus Subcritical Comparison" GLOBAL99, Jackson Hole, USA, 1999.
9. W. Maschek, A. Rineiski, K. Morita, G. Mühling, M. Flad, R.J.M. Konings: "Safety Analyses for ADS Cores with Dedicated Fuel and Proposals for Safety Improvements" Technical Committee Meeting of IAEA, Argonne, USA, 2000.

10. W. Maschek, X.-N. Chen, T. Suzuki, A. Rineiski, C. Matzerath Boccaccini, Mg. Mori, K. Morita: "Review on Safety Issues and Analysis Tools for Accelerator Driven Systems and Transmuters", ICONE - 13, Beijing, China, 2005.
11. T. Suzuki, X.-N. Chen, C. Matzerath Boccaccini, A. Rineiski, W. Maschek, K. Morita: "Safety Analyses in the Framework of an Accelerator-Driven-Transmuter Benchmark", Annual Meeting of Nuclear Technology /JK2005/, Nürnberg, Germany, 2005.
12. K. Tsujimoto, et al.: "Neutronics Design for Lead-Bismuth Cooled Accelerator- Driven System for Transmutation of Minor Actinide", *J. Nucl. Sci. Technol*., **41**, 21, 2004.
13. B. E. Simmons and J. S. King: "A Pulsed Neutron Technique for Reactivity Determination", *Nucl. Sci. Eng.*, 3, 1958.
14. K. O. Ott, and R. J. Neuhold: "**Introductory Nuclear reactor Dynamics**", La Grange Park, Ill., USA: American Nuclear Society, 1985.
15. J. Y. Doriath, C. W. McCallien, E. Kiefhaber, U. Wehmann, J. M. Rieunier: "ERANOS: The Advanced European System of Codes for Reactor Physics Calculation", Proceedings of *International Conference on Mathematical Methods and Supercomputing in Nuclear Applications*, Karlsruhe, Germany, 1993.
16. A. Rineiski, J. Y. Doriath: "Time Dependent Neutron Transport with Variational Nodal Method", *proc. Joint Int. Conf. on Math. Methods and Supercomputing for Nuclear Applications*, Saratoga, USA, 1997.
17. G. Aliberti, G. Imel, G. Palmiotti: "MUSE-4 Experiment Measurement and Analysis", technical note Argonne National Laboratory, ANL-AFCI-092, 2003.
18. R. Soule, E. Gonzalez-Romero: " The MUSE Experiment for the Sub-Critical Neutronics Validation and Proposal for a Computer Benchmark on Simulation of MASURCA Critical and Sub-Critical Experiments", proc. 6th *Information and Exchange Meeting on Actinide and Fission Product Partition and Transmutation*, Madrid, Spain, 2000.

19. G. Aliberti, G. Imel, G. Palmiotti, M. Salvatores: "Dynamic Analysis of Source Driven Fast Neutron Systems for Experimental Techniques of Subcritical Reactivity Measurement", *Trans. ANS Annual Meeting*, 89, 641, November 2003, New Orleans, Louisiana
20. R. T. Ackroyd: "The Finite Element Method for the Neutron Transport. I. The Even Parity Equation for Neutron Transport and its Maximum and Minimum Variational Principles", UKAEA TRG Report 2705(R), 1975.
21. R. T. Ackroyd: A Finite Element Method for Neutron Transport-I. Some Theoretical Considerations", *Annals of Nuclear Energy*, 5, 1978.
22. E. W. Larsen: "A Homogenized Multigroup Diffusion Theory for the Neutron transport Equation", **Computing Methods in Applied Science and Engineering**, 1997, I, *Lecture notes in Mathematic*, 704, R. Glowinski and J. L. Lions, editors., Springer-Verlag, Berlin 357, 1979.
23. E. W. Larsen and R. P. Hughes: "Homogenized Diffusion Approximation to the Neutron Transport Equation", *Nucl. Sci. Eng*., 73, 1980.
24. J. E. Roberts, J. M. Thomas: " Mixed and Hybrid Methods", **Handbook of Numerical Analysis**, P. G. Ciarlet, J. L. Lions, editors, Vol II, North Holland, Amsterdam, 1991.
25. F. Brezzi, M. Fortin: "Mixed and Hybrid Finite Element Methods", **Springer Series in Computational Mathematics**, no. 15, Springer-Verlag, New York, 1991.
26. E. E. Lewis: " Primal, Mixed and Hybrid Finite Elements for Neutronics Computations", Proc. *Int. Conf. Mathematics and Computation, Reactor Physics and Environmental Analysis of Nuclear Systems*, Madrid, Spain, 1999.
27. P. V. Girault: **Finite Element Methods for Navier-Stokes equations**, Springer-Verlag, Berlin Heidelberg, p. 62, 1986.
28. R. Courant, D. Hilbert: **Methods of Mathematical Physics**, Vol. 1, Interscience Publisher, Inc. N. Y. 1973.

29. Dilbert and E. E. Lewis: "Variational Nodal Methods for Neutron Transport", *Nucl. Sci. Eng.,* 91, 1985.

30. E. E. Lewis: "Interface Coupling Reductions in Variational Nodal Methods for Neutron Transport", *Nucl. Sci. Eng.,* 102, 1989.

31. C. B. Carrico, E. E. Lewis, and G. Palmiotti: "Three-Dimensional Variational Nodal Transport Methods for Cartesian, Triangular and Hexagonal Criticality Calculations", *Nuc. Sci. Eng.,* 111, 1992.

32. Babuska, J. T. Oden, J. Lee: "Mixed-Hybrid Finite Element Approximations of Second Order Elliptic Boundary-Value Problems", *Computer Methods in Applied Mechanics and Engineering,* 11, 1977.

33. B. Carrico, E. E. Lewis, and G.Palmiotti: "Matrix Rank in the Variational Nodal Method", *Trans. Am. Nucl*. Soc., 67, 1994.

34. E. E. Lewis, W. S. Yang, M. A. Smith, and G. Palmiotti: "Interface Conditions for Spherical Harmonics Methods," *Nucl. Sci. Eng*., 150, 2005.

35. G. Y. Rumyantsev, "Boundary Conditions in the Spherical Harmonic Method: " *J. Nucl. Energy*, 16, 1962.

36. B. Carrico, and E. E. Lewis: "Generalization of the Variational Nodal Method to Include Anisotropic Scattering", *Trans. Am. Nucl*. Soc., 66, 1992.

37. G. Palmiotti, C. B. Carrico, and E.E. Lewis: "Variational Nodal Methods with Anisotropic Scattering", *Nucl. Sci. Eng.*, 115, 1993.

38. W. S. Yang, M. A. Smith, G. Palmiotti, and E. E. Lewis: "Interface Conditions for Spherical Harmonics Methods," *Nucl. Sci. Eng.*, 150, 259, 2005

39. E. Lewis, C. B. Carrico and G. Palmiotti: "Variational Nodal Formulation for the Spherical Harmonics Equations", *Nucl. Sci. Eng.,* 122, 1996 .

40. C. B. Carrico, U. R. Hanebutte, and E. E. Lewis: "Comparison of Space-Angle Approximations in Response Matrix Algorithms", Proc. of *Mathematical Methods and Supercomputing in Nuclear Applications*, Karlsruhe, Germany, I-58, 1993.

41. J.Y. Doriath, F. Malvagi, G. Palmiotti, J. M.Ruggieri, C. B. Carrico, E. E. Lewis, and G. Gastaldo: "Variational Nodal Method (VNM) to Solve 3D Transport Equation: Applications to EFR Design", proceedings of *Mathematical Methods and Supercomputing in Nuclear Applications*, Karlsruhe, Germany, I-571, 1993.

42. C. B. Carrico and E. E. Lewis: "Nodal Variational Transport Solutions of Multigroup Criticality Problems", *Progress in Nuclear Energy*, 25, V2-3, 1991.

43. C. B. Carrico and E.E. Lewis: "Variational Nodal Solution Algorithms for Multigroup Criticality Problems", proc. *Int.Topl. Mtg. Advances in Mathematics, Computations and Reactor Physics*, Pittsburgh, USA, 1991.

44. E. M. Gelbard: "Application of the Simplified Spherical Harmonics Equations in Spherical Geometry", WAPD-TM-294, Bettis Atomic Power Laboratory, 1962.

45. D. S. Selengut: "A New Form of the P_3 Approximation", *Trans. Am. Nucl. Soc.*, 13, 1970.

46. Y. H. Liu and E. M. Gelbard: "Accuracy of Nodal Transport Using the Simplified P_3 Fluxes in Benchmark Test", *Trans. Am. Nucl. Soc.*, 52, 1986.

47. E. E. Lewis and G. Palmiotti: "Comparison of Simplified and Standard Spherical Harmonics in the Variational Nodal Method", *Trans. Am. Nucl. Soc.*, 73, 1995.

48. G. Thömmes, R. Pinnau, M. Seäid, T. Götz, and A. Klar: "Numerical Methods and Optimal Control for Glass Cooling Processes", *Transp. Theory Stat. Phys.*, 31:513–529, 2002.

49. M. Seäid, M. Frank, A. Klar, R. Pinnau, and G. Thömmes: "Efficient Numerical Methods for Radiation in Gas Turbines", *J. Comp. Applied Math.*, 170:217–239, 2004.

50. M. Seäid and A. Klar: “Generalized Numerical Approximations for the Radiative Heat Transfer Problems in Two Space Dimensions”, In P. Lybaert, V. Feldheim, D. Lemonnier, and N. Selcuk, editors, Computational Thermal Radiation in Participating Media, pages 419–429. Elsevier, 2003.
51. E. W. Larsen, J. M. McGhee, and J. E. Morel: “Asymptotic Derivations of the Simplified P_N Equations”, proceedings of *Mathematical Methods and Supercomputing in Nuclear Applications,* Karlsruhe, 1993.
52. E. Larsen, G. Thömmes, A. Klar, M. Seäid, and T. Götz: “Simplified PN Approximations to the Equations of Radiative Heat Transfer and Applications”, J. Comp. Phys., 183:652–675, 2002.
53. E. Schneider, M. Seaïd, J. Janicka, A. Klar: “Validation of simplified PN models for radiative transfer in combustion systems”, to be published.
54. E. E. Lewis and G. Palmiotti: “Simplified Spherical Harmonics in the Variational Nodal Method”, *Nucl. Sci. Eng.*,126, 1997.
55. A. Rineiski: “KIN3D: Module de cinétique spatiale et de perturbations pour TGV2”, note technique SPRC/LEPh 97-203, CEA, 1997.
56. F. Di Pasquantonio: “Propagation of monokinetic neutron waves in dissipative media”, Energia Nucleare, vol. 11, no. 9, 1964.
57. H. Krainer, N. Pucker: “Propagation of neutron pulses according to the time dependent P1-approximation”, Atomkernenergie (ATKE), 14-4, pp. 11, 1969.
58. R. McClarren, J.P. Holloway: “An Implicit Riemann Solver for the Time-Dependent Pn Equations”, International Topical Meeting on Mathematics and Computation, Supercomputing, Reactor Physics and Nuclear and Biological Application, Avignon, France, 12-15 September, 2005.

59. T. A. Brunner, J. P. Holloway: "Two Dimensional Time Dependent Riemann Solvers for Neutron Transport," *2001 ANS International Meeting on Mathematical Methods for Nuclear Applications*, Salt Lake City, USA, September 2001.

60. (PDS-XADS) EU Contract No. FIKW-CT-2001-00179.

61. A. D'Angelo, F. Cleri, P. Marimbeau, M. Salvatores, and J. P. Grouiller: "Analysis of Sample and Fuel Pin Irradiation in PHENIX for Basic Nuclear Data Validation", *Nucl. Sci. and Eng.,* 105, 1990.